NOVEL METHODOLOGY FOR SPATIAL RISK ANALYSIS OF OVERHEAD TRANSMISSION LINES SUBJECT TO WILDFIRES

by

Alessandro C. S. Berredo

A thesis submitted to the faculty of
The University of North Carolina at Charlotte
in partial fulfillment of the requirements
for the degree of Master of Science in
Applied Energy and Electromechanical Engineering

Charlotte

2023

Approved by:

Dr. Michael Smith

Dr. Wesley Williams

Dr. Maciej Noras

ABSTRACT

ALESSANDRO C. S. BERREDO. Novel Methodology for Spatial Risk Analysis of Overhead Transmission Lines subject to Wildfires. (Under the direction of DR. MICHAEL SMITH)

Wildfires are one of the main threats to overhead power lines worldwide, causing permanent damages and interruptions. Wildfires represent the second leading cause of outages in the Brazilian Interconnected Grid and the fourth leading cause in the North American bulk grid. It is estimated that 4.8 thousand momentary and permanent failures in the North American bulk grid from 2008 to 2019 were caused by wildfires [1]. Among the operational impacts to the power grid, this particular type of event may result in significant physical damages, such as burning support structures and conductors, and contamination of the insulation system. In addition, wildfires under conductors can cause the degradation of the insulation medium resulting in phase-to-ground and phase-to-phase wildfire-induced flashovers.

Preventing transmission lines from fire-induced flashovers is a challenging task. While engineers have the opportunity to design new transmission lines to prevent this type of failure mode, modifying the clearance distances of existing lines may be economically unfeasible. Consequently, vegetation management, fire prevention campaigns, and firefighting strategies are the only options to prevent damage and line outages. The environment in which the asset is installed and the characteristics of the transmission line may impact the reliability of the installation in different ways as the insulating performances of overhead transmission lines for steady-state and transient operating conditions are affected by the clearance distances adopted. Nevertheless, current overhead transmission line standards do not establish design or operation and maintenance protocols to evaluate and address risks, impacts, and mitigation methods of wildfire. This design shortcoming very often results in impacts on the grid.

This research proposes a novel data-driven methodology to estimate the risks of wildfire and outage of overhead transmission lines (OHTLs) due to fire-induced flashovers. Publicly available remote sensing data and geoprocessing techniques are applied in a case study of a compact 500 kV OHTL installed in the Brazilian tropical savanna to estimate the risk of wildfire and the insulation performance of the OHTL.

In addition, the research proposes an empirical model to determine the minimum vegetation clearance distance (MVCD) in order to prevent fire-induced flashovers in OHTL installed in that particular biome. The research evaluates the results of six different calculation methods and clearance distances of line spans identified in 108 wildfire-related outage events.

The outcomes from this research may be used as decision-making tools for a) route optimization of new overhead transmission lines, identifying crossed regions with higher exposure to wildfires; b) determining minimum clearance distance for new transmission lines to prevent fire-induced flashover; and c) Vegetation management prioritization for existing assets, identifying and providing specific clearance distances to prevent critical spans from outage due to fire-induced flashovers as well as providing information for firefighting strategies.

ACKNOWLEDGEMENTS

I want to acknowledge and express my special thanks to my advisor Dr. Michael Smith who guided and advised me through the steps of this project. I would also like to thank my committee members for trusting in the potential and importance of this research.

This work would not have been accomplished without the support of the Brazilian electric transmission utility Transmissora Aliança de Energia Elétrica - TAESA. I am specially indebted to Mr. Marco Antonio de Faria, Technical Director, who has been supportive and worked actively to provide me with the necessary resources for this scientific research.

I would also like to give special thanks to my wife and my family for their continuous support when undertaking this graduation.

Finally, I would like to thank God for leading me through all challenges.

TABLE OF CONTENTS

LIST OF TABLES

LIST OF FIGURES

LIST OF ABBREVIATIONS

ANEEL Brazilian Agency of Electric Energy.

BSA Electrical Breakdown Strength of Air.

CFO Critical Flashover Voltage.

CQFS Criticality of wildfires in Rights of Way

ERP Enterprise Resource Planning.

GIS Geographic Information System.

GNDVI Green Normalized Difference Vegetation Index

HSIL High Surge Impedance Loading.

IBAMA Brazilian Institute of the Environment and Renewable Natural Resources.

K Kelvin.

kPA Kilopascal.

kV Kilovolts.

LiDAR Light detection and ranging.

MVCD Minimum Vegetation Clearance Distance.

NDVI Normalized Difference Vegetation Index

NERC North American Electric Reliability Corporation.

NESC National Electrical Safety Code.

OHTL Overhead Transmission Line.

ONS Brazilian National System Operator.

PU Per Unit.

RGB Red, green and blue.

ROW Right of Way.

SCADA supervisory control and data acquisition.

SIL Surge Impedance Loading.

SIRGAS Geocentric Reference System for South America.

TAESA Brazilian electric transmission utility Transmissora Aliança de Energia Elétrica.

TOV Transient Overvoltage.

UID Unique Identity Number.

US United States.

UTM Universal Transverse Mercator.

VIIRS Visible Infrared Imaging Radiometer Suite.

CHAPTER 1: INTRODUCTION

Wildfires are one of the most prevalent originators of both momentary and sustained transmission line outages worldwide. It is estimated that 2.7 thousand momentary and permanent failures in the North American bulk grid from 2008 to 2019 were initiated or sustained by wildfires (see Figure 1.3) [1]. Associated with these wildfires, there are three well-known failure and degradation modes of overhead lines that need to be considered, as listed below:

- Degradation of the dielectric strength of air between conductors and the ground.

  Flames between the conductors and conductors to ground, high temperatures in the air gap, and airborne particles and gases from burnt fuel in the smoke plume can degrade the dielectric properties of air and result in phase-to-ground or phase-to-phase flashovers.

- Damages to conductors and support structures can result in equipment failure (e.g., breaking of conductors or burning of wood poles) and sustained outages.

- Damages to the grounding system and insulators of support structures can degrade the insulating performance. Soot in the smoke can contaminate the surface of the insulators, degrading their insulating performance over time.

There is not currently much work regarding the impact of heat from wildfires on the aging of insulators. However, although not strongly related to impacts of wildfires on line components, investigations performed by Mehmood, Bashrat, et al. [9] and Shaik, Mohamed Ghouse, and Vijayarekha Karuppaiyan [10] indicate that the combined effect of electrical and environmental stresses including heat and contamination may play a significant role in the aging performance of composite insulators.

In order to prevent negative impacts from vegetation encroachment and wildfires on power transmission infrastructure, electric utilities apply significant resources (e.g., time and financial capital) annually on hardening and vegetation management in the surrounding of the existing infrastructure [11]. For instance, Eskom [12], the state-owned utility in South Africa, mentions the importance of managing the fuel (i.e., vegetation) that could ignite and propagate fires in addition to managing the growth of trees posing risks of approximation or contact with the energized conductors. Eskom's infrastructure is also exposed to tropical savanna wildfires.

Despite engineers estimating long-term climatic events to design more reliable and resilient overhead transmission lines, the minimum vegetation clearance distances (MVCD) to prevent the risks of wildfire-induced flashovers are very often neglected by line designers. Current standards and guidance in overhead line design used in North America and Brazil do not address the impacts of wildfires in establishing compatible clearance distances. Although current technology allows elimination of where and when these events will likely occur, as designing "wildfire-proof" installations can be cost-prohibitive. Thus, utilities rely on social-environmental campaigns and vegetation management practices to prevent the occurrence and consequences of wildfires.

Many studies have been carried out to predict the mechanisms of ignition and propagation of wildfires and how they impact overhead lines. One of the main contributions, published by Frank A. Albini [13] in 1976, describes computational models for predicting fire behaviors (i.e., ignition and spreading) to aid decision-making on prevention actions. Long-term historical data of wildfires are "post-fire events" and alone might possibly enable a relatively accurate estimation of where and when these events occur, thus providing a straightforward tool to estimate the risk of wildfires. In addition, results can be used in many applications, such as planning and designing "wildfire-compatible" overhead transmission lines or for vegetation and risk management of overhead lines in operation.

The motivation for this research lies in the fact that a) current efforts of vegetation management are not sufficient to prevent overhead transmission lines from multiple events of fire-induced flashover, b) vegetation management represents the greatest operational expenditure costs in many Brazilian utilities, c) environmental impacts associated to vegetation management require the selection of the most critical locations along the line right of way and d) current line design guides to determine minimum clearance distance to vegetation do not address the risk of fire-induced flashovers.

The proposed new approach for estimating the risk of outage of overhead transmission lines uses historical data of wildfires obtained via satellite imagery, post-processed using the Getis-Ord Gi* spatial analysis to classify the risk of wildfires. The Getis-Ord Gi* model is further explained in Section 1.3 and Subsection 4.3.2.

1.1 Problem Statement Overview and Discussion

While fire represents the eighth major cause of outages in the North American transmission grid, wildfire is the second major cause of outages in the Brazilian interconnected grid. Weather-related events, including lightning, lead the statistics of outages (see Figure 1.1).

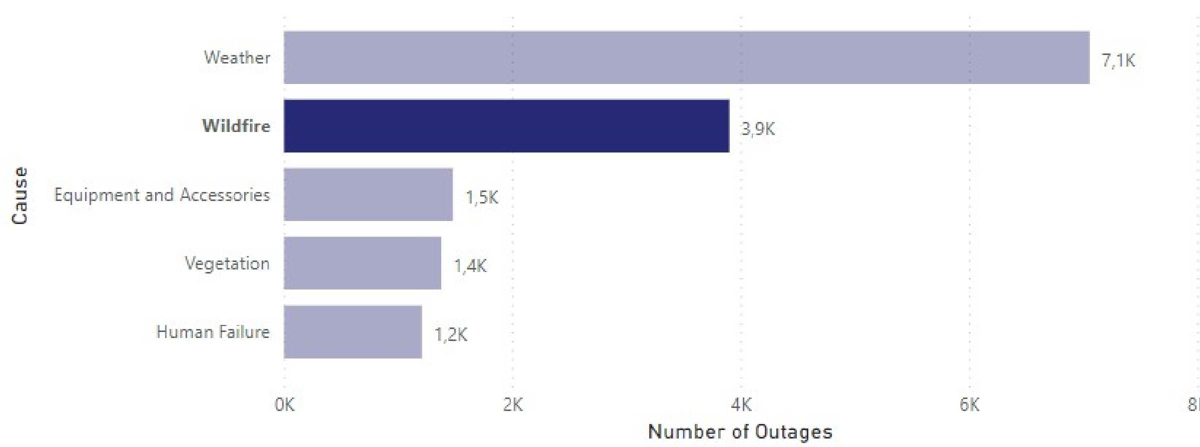

Figure 1.1: Outages by year (2012-2022) in the Brazilian Interconnected Grid.[4]

Besides the risk of significant physical damage to transmission components (e.g., structural and conductor burning), wildfires under conductors can cause degradation of the insulating medium, and result in phase-to-ground and phase-to-phase flashovers. Figure 1.2 shows an example of a fire-induced flashover, which occurred in the 500 kV OHTL Colinas - Miracema C1, in Brazil. In that particular case, vegetation management had been performed in the right of way (ROW). However, the remaining vegetation on the side boundaries of the ROW provided the conditions that resulted in the flashover.

On March 23$^{\text{rd}}$ of 2013, two important 500 kV transmission lines interconnecting north and northeast Brazil failed due to a large wildfire event that resulted in three hours of power interruption in the northeast region and loss of 10,900 MW [15]. The case study focuses on one of the transmission lines involved in this blackout event, a 500 kV single-circuit transmission line located in northern Brazil. Curiously, the vegetation at the line span where the failure occurred had been managed by the utility following the Brazilian standard protocols days before the event, raising questions about why a fire-induced flashover would have occurred. The investigated OHTL, parallel with another 500 kV line with the same design characteristics but operated by another utility, provides the strategical function of interconnecting two bulk grid subsystems (i.e., North and Northeast) that are notably impacted by wildfires. According to [16], three mechanisms may lead transmission lines to outages due to fire-induced flashover events:

- Degradation of the dielectric strength caused by the reduction of the air density.
- Influence of suspended particles (flame and thick smoke).
- Flame conductivity.

This research aims to determine the risk of outage of the above-mentioned transmission line due to wildfire-induced flashover. Besides the risk of wildfire, it is necessary to

(a) Wildfire under a 500 kV line in Brazil; before flashover event

(b) Wildfire under a 500 kV line in Brazil; flashover event

Figure 1.2: Flashover event caused by wildfire under a 500 kV Transmission Line in the Brazilian Cerrado [14]

classify the vulnerability of the installation to the failure mode (i.e., wildfire-induced flashovers). Therefore, failure details and clearance distances of the line spans involved in wildfire-induced flashovers were obtained from design and outage reports and compared with the calculation results from six different methods to determine the minimum vegetation clearance distance to vegetation. Both risks of wildfire and outage were further validated by statistical correlation with the historical failure data of the transmission line presented in the case study.

The research outcome compares the results of the new method of classification of the risk of wildfire with the method proposed in Berredo et al. [17] for a particular line section. In addition, the research proposes a new method to calculate the MVCD for lines exposed to tropical savanna wildfires. The MVCD result is compared with models proposed in West & McMullan [18], J.R. Fonseca et al. [2], Lanoie & Mercure [19], and Berredo A. et al. [17].

Results are also compared with the existing minimum vegetation clearance distances practices established in NERC FAC-003-4 (Transmission Vegetation Management) [20] and adopted in the US Bulk Grid and with the current Brazilian standard NBR 5422 [21]. Most of the 108 outages analyzed in this research occurred in line spans where vegetation management had been performed. Only 18% of the outages occurred in spans where vegetation management had not been performed for justified reasons, such as locations with very high clearance distances to the ground (e.g, valley crossings or rugged relief).

Whereas many past pieces of research present significant contributions to understanding and estimating the behavior of vegetation fire and how it affects the electrical performance of overhead transmission lines, a few authors suggest practical approaches in the design stage to cost-effectively identify the risk of wildfires and prevent flashovers associated with the degradation of the breakdown strength of air. Existing standards typically address the minimum clearance distances required for safety and for live working maintenance capabilities, but also for the operational performance of the installation, such as to prevent short circuits caused by lightning, transient overvoltages, and vegetation encroachment. However, these standards do not address insulating issues caused by wildfires, such as when conductors are engulfed by flames.

The main objective of this thesis is to propose a novel methodology to address the impacts of wildfire-induced flashovers in overhead transmission lines. The proposed methodology comprises two approaches (i.e., two risk pillars) to identify the risk of outage of OHTL caused by wildfire-induced flashovers:

- Risk of wildfire: The risk of wildfire-related flashover can exist only if a source of fire exists. For example, the probability of a flashover in a span crossing a lake is remote. Conversely, spans crossing a forest can be subject to wildfire, resulting in flashover events.

  This risk pillar addresses identifying the source of risk in critical locations to prevent exposure of the transmission line to wildfires. For example, a geographical location frequently associated with wildfire will increase the risk of damages and outages simply because wildfires are frequent in that location. Rerouting the line or managing the vegetation in the right of way can reduce exposure to the risk of wildfire.

- Risk of wildfire-related flashover: The source of risk exists. However, the route cannot be modified to avoid it. For example, a new transmission line with its right of way legally established or limited by environmental constraints may not be allowed to deviate from regions with a higher risk of wildfire exposure. Existing transmission lines in operation may not have the option to prevent wildfire-related outages other than performing vegetation management. In some cases, environmental permits of the existing transmission lines will constrain the method and the footprint of vegetation management, as in the case study presented in this research.

This risk pillar addresses the minimum clearance distance required to withstand the degradation of the breakdown strength of air caused by wildfires. This pillar also approaches vegetation management techniques to reduce the exposure of the installation to wildfires.

Knowing these two risks, engineers should be able to:

- Identify less vulnerable routes for new OHTL.
- Design OHTLs resilient to wildfires.
- Establish appropriate preventive maintenance actions to mitigate outages and damages caused by wildfires.

To this end, the study is organized into two parts:

- Development of a methodology to classify the risk of occurrence of wildfires to avoid the exposure of the installation.

  This part proposes a data-driven approach based on geographic information systems (GIS) to identify and classify the risk of wildfire along the transmission line.

- Development of a methodology to estimate minimum clearance distances to prevent the line from flashover when wildfires cannot be avoided.

  This part seeks to establish a calculation method to estimate the minimum vegetation clearance distance to prevent fire-induced flashovers in overhead lines crossing the Brazilian savanna biome. This work uses the line design and outage information from a case study to identify the threshold distance to prevent wildfire-induced flashovers and compares this threshold distance with results from six MVCD calculation methods.

The key research questions addressed in this thesis are listed below:

- Questions regarding Risk of wildfire:
  - What are the wildfire components that contribute to the degradation of the breakdown strength of air?
  - Can wildfire models proposed in the literature be simplified using existing remote sensing data for transmission line planning and designing applications?
  - How can remote sensing contribute to estimating wildfire risks?
  - What vegetation management practices can be effectively adopted to mitigate wildfires in existing transmission lines?
- Questions regarding Risk of wildfire-related flashover:
  - How do wildfires affect the insulation strength of overhead transmission lines?
  - What insulation coordination studies can be used to establish the MVCD options based on other vegetation fires?
  - What are the overall economic and environmental impacts of wildfire-proofing a transmission line? Can wildfire-proofing design result in a lower life-cycle total cost than vegetation management?

Results from this research may be used to estimate effective minimum clearance distances to mitigate fire-induced flashovers, to improve line routing and design to reduce the impacts of wildfires on new transmission lines, to identify what sections of the right of way are potentially critical for fire-induced flashovers and, finally, to determine how the vegetation management should be done in order to reduce the risk of outages.

1.2 Power Grid Infrastructure and Environment Characteristics

Before discussing the current work (see Section 1.3) and challenges (see Section 1.4), to help establish the foundational information needed in this focus area, this section and the subsections below discuss power grid outage statistics, wildfire-related outages in Brazil, the influence of the biome on outages, the Brazilian power grid infrastructure, environment (e.g., biome influence), and the focus area considered in this study.

1.2.1 Statistics of Outages of OHTL in the North American Bulk Grid

The wildfire phenomenon represents the eighth leading cause in the North American bulk grid, with 520 momentary outage events and 2.18 thousand sustained outage events between 2008 and 2019 [1] (see Figure 1.4).

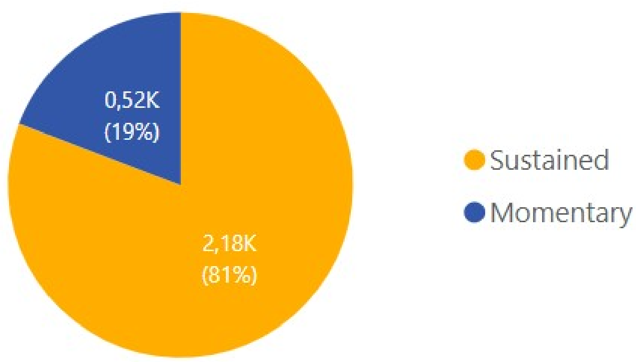

Figure 1.3: Percentage of sustained and permanent outages due to fire in the North American bulk grid (2008-2019) [1].

Despite the low contribution to outage statistics in the North American bulk grid, wildfires are intrinsically related to circuit failure. Thus, in addition to the impacts of outages, damages to circuit equipment (e.g., burning structures and conductors) often result in sustained outages. Figure 1.4 shows the main causes of outages in the North American bulk grid between 2008 and 2019. Note that although fire has a low contribution to the total outages with 2.7 thousand events, failure of circuit equipment is the second leading cause of outages in the North American bulk grid with 18.5 thousand events.

NERC [22] classifies failure causes into two types: a) initiated cause and b) sustained cause. The initiated cause, as the name self explains, is the cause that initiates the outage. The initiated cause can result in a momentary outage or evolve into a sustained outage resulting from permanent damages to the circuit equipment. The failure cause can be the same for the whole outage, initiated and sustained, or the outage can have distinct initiated and sustained causes. For example, a momentary outage occurs due to a fire-induced flashover in a given span. In sequence, the wildfire burns down and leads to the failure of one of the wood structures supporting the conductors resulting in a sustained outage. In this example, the initiating cause of the outage is distinct from the sustained cause. Note that the outage would have two causes; the initiation cause (fire) and the sustained cause (equipment failure). It means that although the fire has its own classification, the consequences of wildfire events can evolve into equipment failure, thus another outage class.

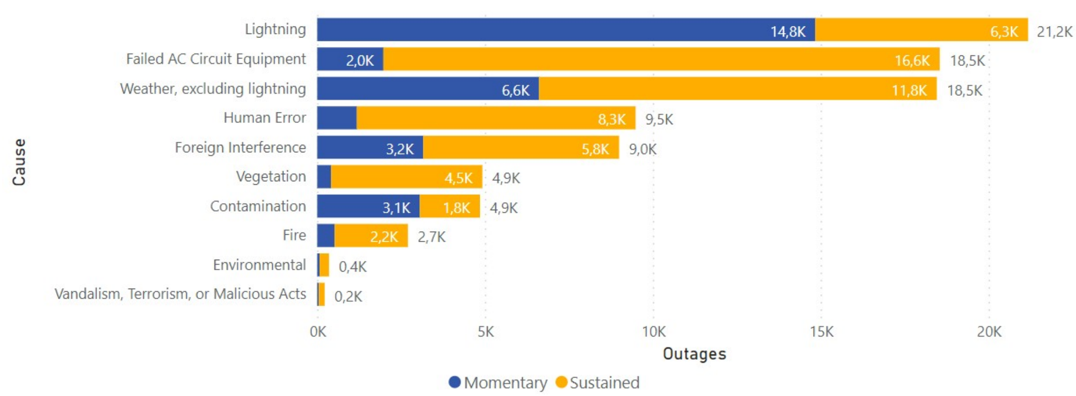

Figure 1.4: Number of momentary and permanent outages by cause in the North American bulk grid (2008-2019).

Figure 1.5 shows the distribution of momentary and permanent outages between 2008 and 2019, initiated or sustained by fire, in the North American bulk grid. Note that the majority of the outages are permanent. According to NERC[1], momentary outages are those in which the line can successfully re-energize in less than one minute, and sustained outages are those with a duration of more than one minute.

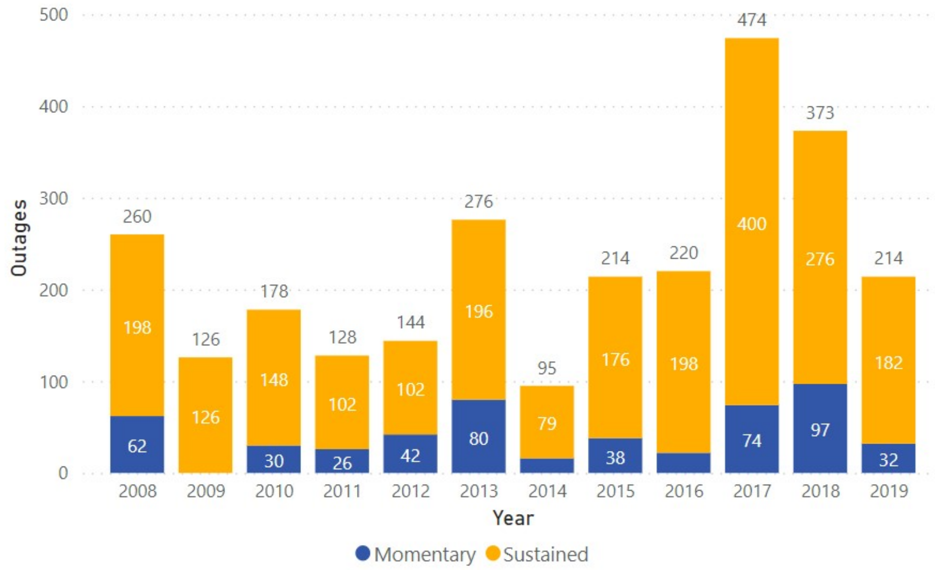

Figure 1.5: Outages by year (2008-2019) due to fire in the North American bulk grid.

1.2.2 The Wildfire-related Line Outages in Brazil

According to the Brazilian National System Operator (ONS), wildfires represent the second highest cause of outages in the interconnected grid [4], with 3.9 thousand outages from 2002 to 2022. Outages caused by weather conditions include inclement weather and lightning.

Despite the high capital required to deploy wildfire-proof OHTLs, current technology, such as spatial analysis of historical wildfire data obtained via satellite remote sensing, available free of cost, may enable routing optimization of new lines in order to prevent exposure to locations with an active history of fire. In addition, when re-routing is not an option, the same spatial analysis can be used as a risk management tool to identify critical locations with higher densities of wildfire occurrence. Therefore, the technology may empower engineers with decision-making tools to address the consequences of wildfires, such as damages to components or outages due to wildfire-induced flashovers.

In Brazil, most line outages resulting from fire-related flashovers are associated with native vegetation in the Cerrado biome or with the burning of sugarcane. Fonseca et al. [2] performed extensive research on the impacts of the burning of sugarcane plantations under overhead transmission lines. The ATE II OHTL, for example, was exposed to 8,137 hotspots between 2012 and 2022. The rate of hotspots per length of line section is shown in Figure 1.6. Note that the rates of hotspots for the line sections between Colinas (CO) and São João do Piauí (SJI) are 10 times higher than for the line section between São João do Piauí (SJI) and Sobradinho (SOB).

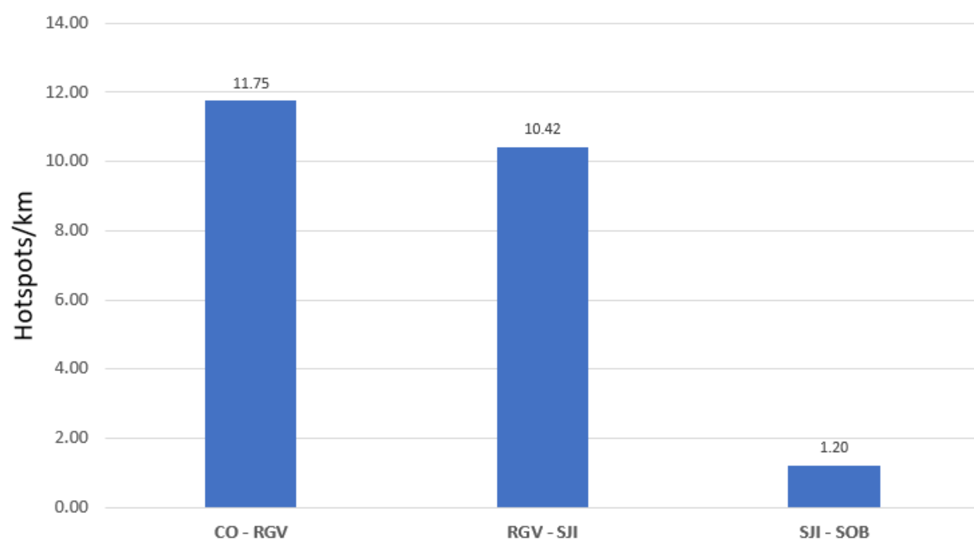

Figure 1.6: Number of hotspots per length of line section between 2012 and 2022

Analyzing the Technical Report 31/2008-SFE/ANEEL [14] published by the Brazilian National Electric Power Agency (ANEEL), it is clear that 500kV lines account for most of the wildfire-related outages involving native vegetation. Considering the top 20 OHTL in terms of outages due to fires, 500 kV lines (see Figure 1.7a) account for 90% of the total outages, while sugarcane-related fires impact lines operating at all voltage levels from 230 to 500 kV, with outages concentrated in northeastern Brazil and northern Sao Paulo State in southeastern Brazil (see Figure 1.7b).

Figure 1.8 shows outage information from overhead transmission lines operating between 138 and 800 kV in the Brazilian bulk grid between 2017 and 2021. The top chart shows the frequency of outages by voltage level, and the bottom chart shows the outage rate by voltage level.

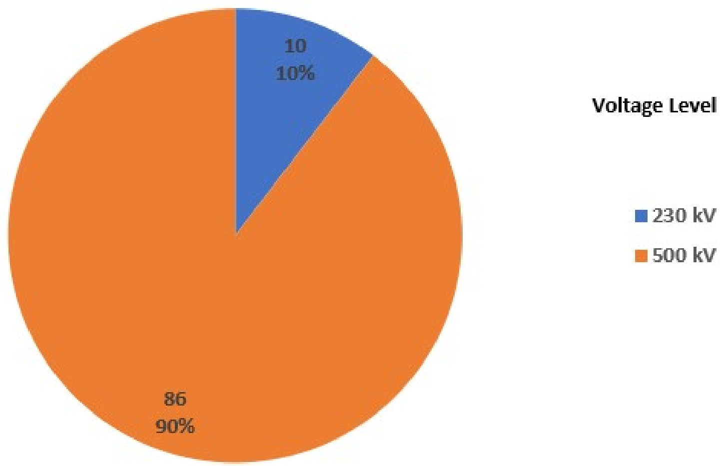

(a) Line outages involving wildfire of native vegetation by voltage level

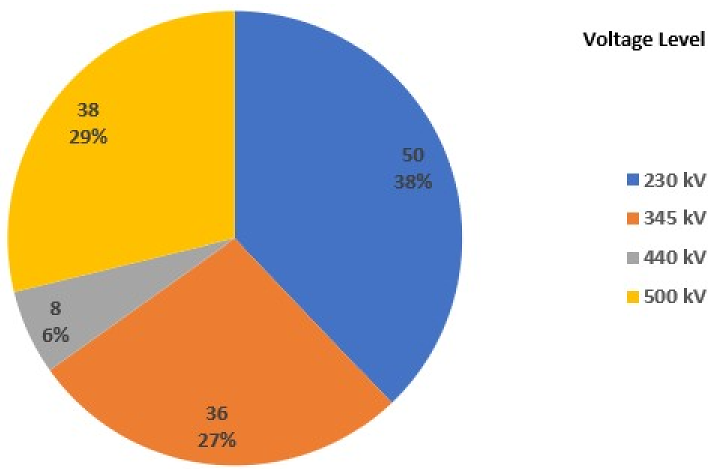

(b) Line outages involving sugarcane burning by voltage level

Figure 1.7: Number of Outages per overall length of the top 20 OHTL due to wildfire and sugarcane burning in the Brazilian bulk grid from 2014 to 2016 [14]

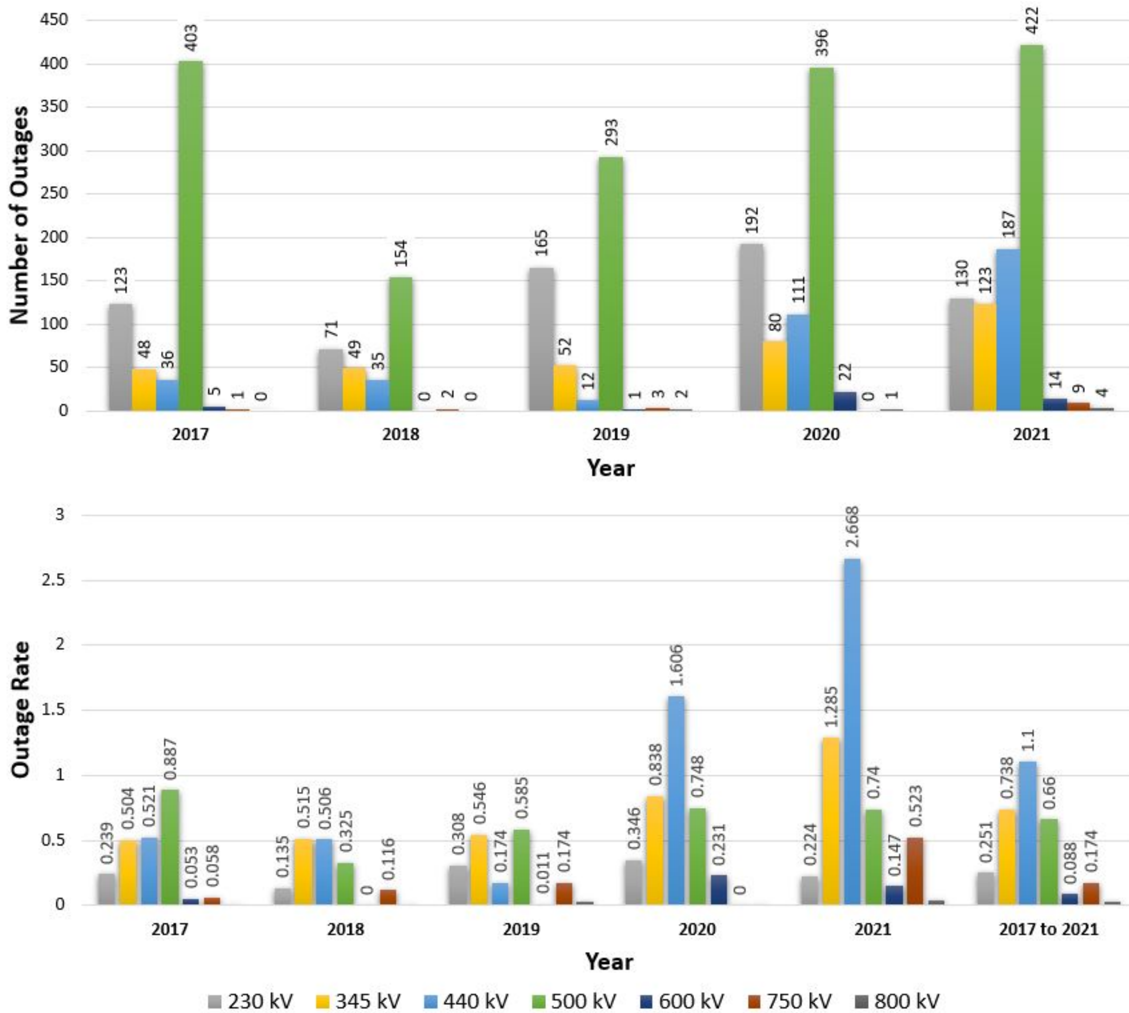

Figure 1.8: Frequency and Outage rate due to wildfires across the Brazilian grid between 2017 and 2021 [5].

Presently, remote sensing and geoprocessing technologies provide relatively accurate data for predicting weather and wildfire events and for many other data-driven applications. These data sources became popular in the past years and are used daily to substitute in-field surveys and assessments with accurate results in many fields of science and engineering. The definition of what data variables should be used for a given data-driven decision-making application usually relies on those variables that strongly correlate with the physical event. A model with poor or insufficient variables may produce very low-accurate predictions. Conversely, a model with excessive variables may result in better event prediction but may also make the application unfeasible for daily work.

Geoprocessing-related studies have been proposed to predict the risks of ignition and propagation of wildfires and to predict how they impact overhead lines. Two relevant contributions, Albini [13] and Chuvieco et al. [23], describe computational models for predicting fire behaviors (i.e., ignition and propagation) to aid decision-making on prevention actions.

1.2.3 Influence of Biome

The Brazilian territory is classified into 6 land biomes, as described below and seen in Figure 1.10.

- Amazon: The Amazon rainforest is the world's largest tropical rainforest, occupying the Amazon River's drainage basin and its tributaries in northern South America, ranging from the eastern slope of the Andes mountains to the Atlantic Ocean. Its vegetation types include rainforests, seasonal forests, deciduous forests, flooded forests, bamboo stands, palm forests, savannas, dry forests, and cloud forests [24].

- Cerrado: The Cerrado biome is the largest savanna region in South America, located between the Amazon, Atlantic Forests, and Pantanal biomes. It is mostly located on large plateaus ranging in elevation from 500 to 1,700 m. The vegetation types are dominated by savanna-like vegetation varying from open fields to tall closed forests [25].

- Caatinga: The Caatinga is a uniquely Brazilian semi-arid biome that consists primarily of small, thorny trees that shed their leaves seasonally, covering the greatest semiarid region in Northeast Brazil. The name "Caatinga" is a Tupi word meaning "white forest" or "white vegetation" [26, 27].
- Atlantic Forest (Rain Forest): According to [28], the Atlantic Rain Forest is one of the seven moist forest areas of the Neotropics and the second largest after the Amazonian rain forest. It covers 3,000 km along the Atlantic Coast and 17 different Brazilian states. The vegetation is associated with secondary forests, in which only 10% of the original vegetation remains preserved.
- Pantanal: The Pantanal Biome is present in the States of Mato Grosso, Mato Grosso do Sul, and Goiás and includes one of the most extensive wetlands in the world. Its ecosystem includes flood plains, grasslands and highland cerrado, seasonally flooded cerrado, seasonally flooded grasslands, forest-like cerrado, deciduous forests, gallery forests, Buriti palm stands, Amazon like-forest, Atlantic Forest influenced forest, Chaco and Chaco Forest [29].
- Pampa: The Pampa biome is located in the southernmost state of Brazil, Rio Grande do Sul, within the South Temperate Zone, where grasslands scattered with shrubs and trees are the dominant vegetation [30].

Approximately 46.6% of the Brazilian transmission system is concentrated in the Brazilian savanna (i.e., Cerrado and Caatinga). These two biomes have in common the characteristic of frequent wildfire occurrences. Overhead lines installed in those biomes are frequently exposed to wildfires. Consequently, these lines are subjected to more frequent fire-induced flashover events.

According to Frost Robertson [31], the regular occurrence of fire in the tropical savanna is more frequent in the dry season, mainly caused by people hunting, preparing land for cultivation, improving the quality of grazing for livestock, and controlling the spread of woody plants, while lightning contributes mainly at the beginning of the rainy season. Figure 1.9 shows a landowner performing prescribed burning in the grassland of the Cerrado vegetation, supervised by technical staff from the Brazilian Institute of the Environment and Renewable Natural Resources (IBAMA), in the Municipality of Serra da Mesa, State of Goiás.

Figure 1.9: Land owner in Brazil performing prescribed burning in the Cerrado vegetation.[6]

The Cerrado biome characteristics are cited in [32] as a mixture of open grasslands, shrublands, open woodland, and closed canopy woodlands. It is the focal region for the expansion of Brazilian agriculture. Frost and Robertson [31] mentions that regular fires are one of the characteristic features of tropical savannas.

Also, according to Frost and Robertson [31], the intensity of the wildfire in the tropical savanna will depend on the amount and type of fuel, its moisture content, and prevailing climatic conditions, principally air temperature and relative humidity. Most wildfire events in the Brazilian savanna occur in winter, in the dry season.

Therefore, electric utilities execute their annual vegetation management tasks before that season. The spread rate will depend on wind speed, topography, and the fuel's moisture content. Wildfires in tropical savannas are surface fires, with average flame heights of 2.8m varying from 0.5m to 5m considering both back and head fires [31].

The flame characteristics are significant for this research since the proposed equation to calculate the minimum vegetation clearance distance for vegetation subject to wildfire considers the flame height as a potential reducer of the clearance distance. Lanoie & Mercure [19] estimated that flames from wildfires can reach temperatures of about 1000 °C. However, Lanoie & Mercure studied a particular vegetation species (i.e., spruce trees) not present in Tropical Savannas. In addition, Sukhnandan [16] proposes that the high density of ions in the flame, due to fuel oxidation reaction and thermal ionization of the gas, turns it into a very conductive channel between conductors and ground that will result in sustained corona and subsequent flashover across the air gap. Flame conductivity is the base for the model proposed in Lanoie & Mercure. The model is further explained in Subsection 2.4.6.

The Cerrado and Caatinga biomes are the second and third in terms of density of wildfires in the Brazilian territory, with 2.45 hotspots/km^2 and 1.16 hotspots/km^2 events, respectively, in the analyzed period (see Figure 1.10)[33].

Regarding installation presence, around 31.4% and 15.2% of the transmission system is installed in the Cerrado and Caatinga biomes, respectively. However, overhead lines installed in those biomes are frequently exposed to wildfires and, consequently, more frequently associated with fire-induced flashover events, which highlights the need for attention in this area. Figure 1.11 shows the percentage of the length of overhead transmission line by biome.

According to the work in [32, 34], the Cerrado and Caatinga biomes (i.e., biomes that are classified as tropical and steppe savannas) represent 24% and 9.74% of the Brazilian territory, respectively. A GIS map generated with official data for this

Figure 1.10: Number of wildfire events per squared km per Biome.

research shows that Cerrado is present in 31.4% of the Brazilian territory, while Caatinga is present in 15.2% (see Figure 1.11).

Figure 1.12 shows the relationship between the number of fire events per area (orange column) and the territory area (gray column) for each biome in the period of analysis. The chart is sorted by territory size. It is interesting to highlight that the largest density wildfires, 3.44 hotspots per km^2, occurred in the Pantanal biome for the analyzed period despite the smallest territory area. Only 0.2% of the total length of the bulk grid is currently installed in that biome. Figure 1.13 shows the percentage of total length OHTLs per biome in Brazil. The largest percentage in the Atlantic Forest is due to the highest concentration of people in the southeast region, in the States of Rio de Janeiro and São Paulo.

Regarding the current vegetation management practices performed by utilities with lines exposed to tropical savanna biomes, Eskom, the South African electric utility

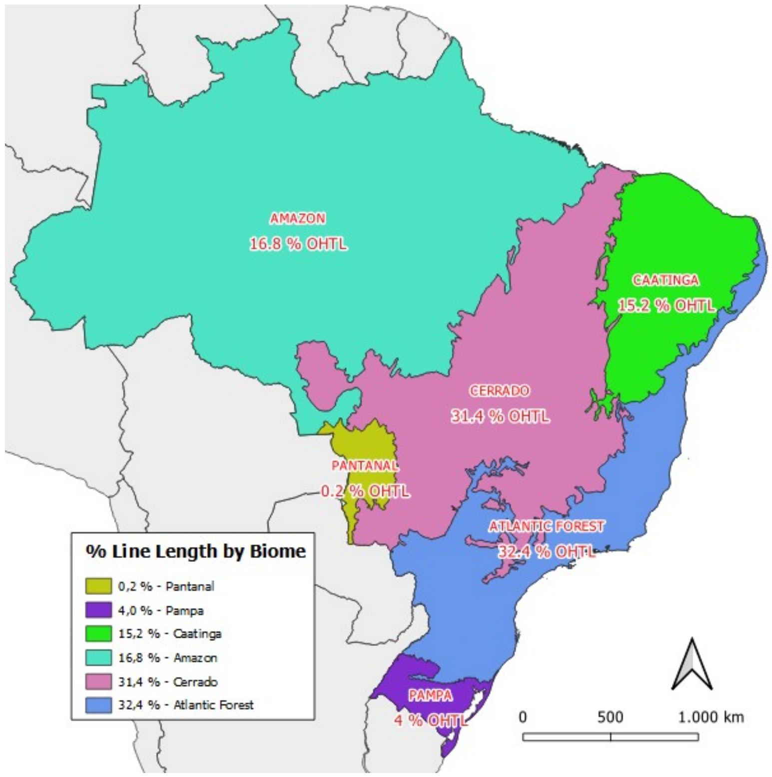

Figure 1.11: Percentage of length of overhead lines per biome

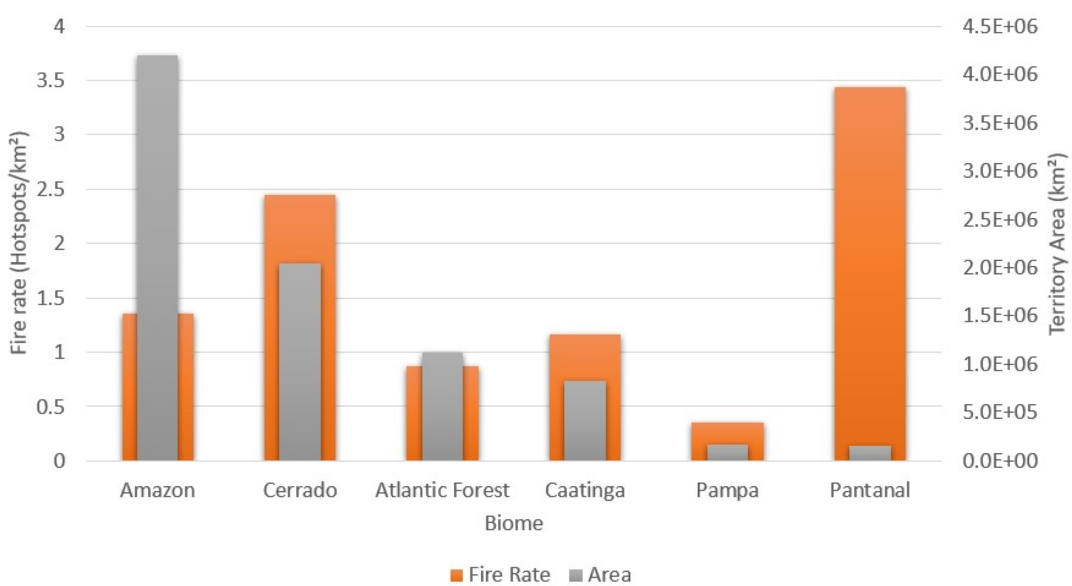

Figure 1.12: Fire Rate vs Territory Area.

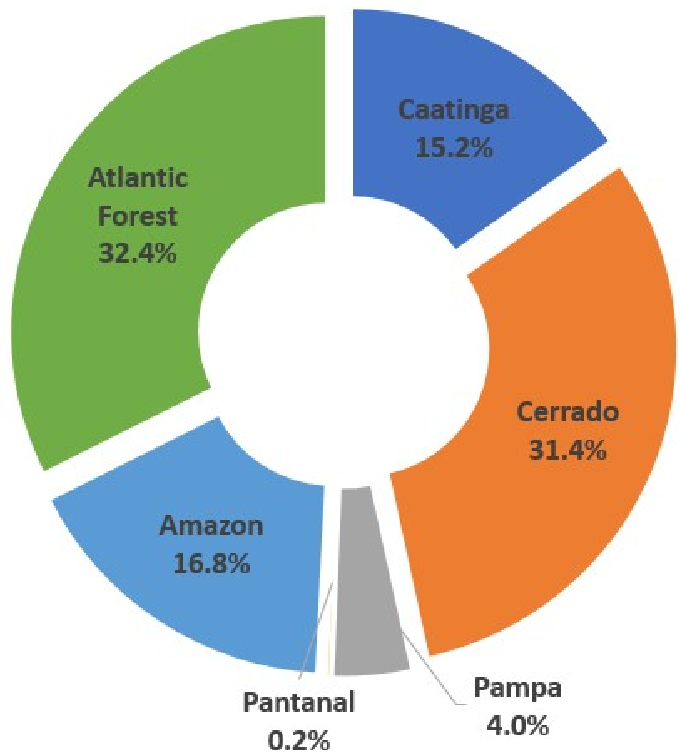

Figure 1.13: Distribution of line length per biome in Brazil.

[12], mentions the importance of managing the fuel (i.e., vegetation) that could ignite and propagate fires in addition to managing the growth of trees posing risks of approximation or contact with the energized conductors.

1.2.4 The Brazilian Bulk Grid

Brazil is the largest electricity market in Latin America and the 7$^{\text{th}}$ largest in electricity generation capacity in the world, generating and distributing electricity to more than all the combined power produced by other South American nations. Over 50% of the produced energy is consumed in the country's Southeast region [35].

In terms of transmission grid size, Brazil has a country-wide 99% interconnected system (i.e., 1% of the system is still isolated) of over 175,000 kilometers (108,000 miles) of OHTL with nominal voltage ranging from 230 kV a.c. up to 800 kV d.c., with a predominance of 500 kV and 230 kV lines, interconnecting four subsystems (see Figure 1.15) [4]. The system configuration facilitates the power flow through subsystems, allows synergistic gains between subsystems, and explores the diversity of hydrological regimes of the 16 available basins. Figure 1.14 shows the footprint of the OHTL interconnected system.

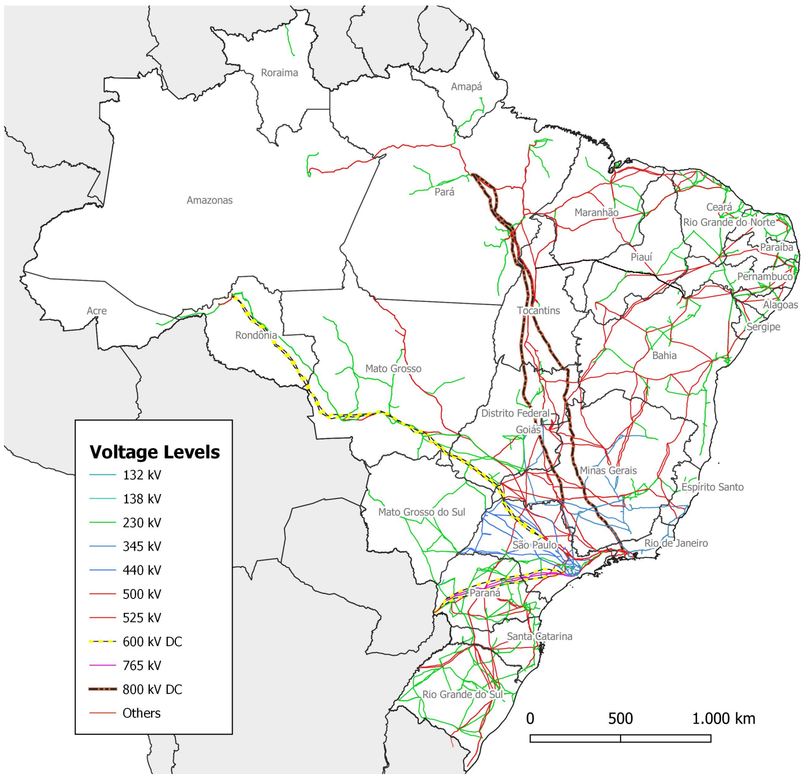

Figure 1.14: Brazilian Interconnected Grid.

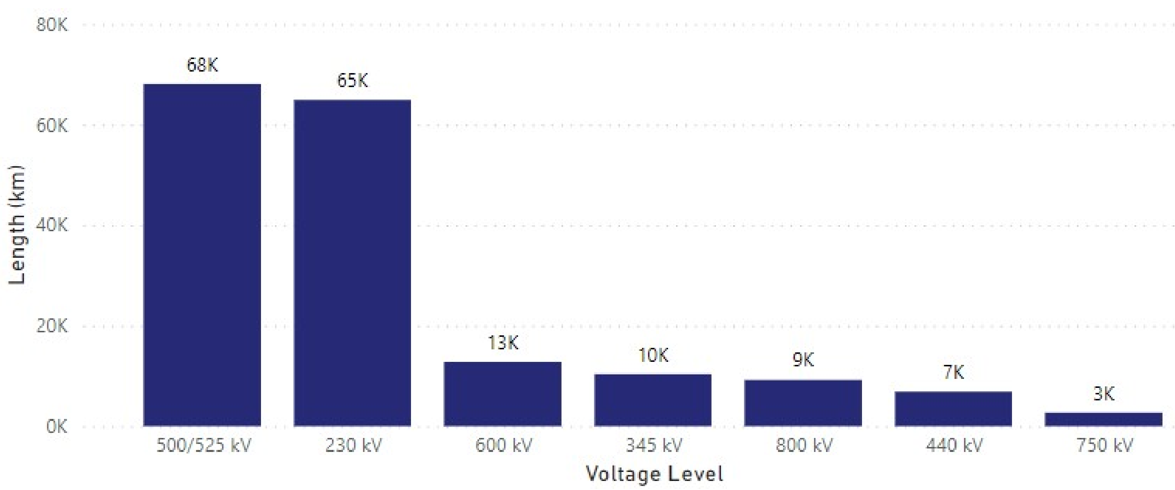

Figure 1.15: Total Length of OHTL in the Brazilian Interconnected Grid (2022).[4]

1.2.5 Infrastructure Focus Area for this Study

The infrastructure focus area for this study is a 500 kV compact overhead transmission line, entitled ATE II, that interconnects four substations: Colinas (CO), Ribeiro Gonçalves (RGV), São João do Piauí (SJI) and Sobradinho (SOB). This circuit is a strategic asset in the grid since (together with a second line with the same design characteristics but operated by another agent) it has the function of interconnecting two subsystems (i.e., North and Northeast) that are notably impacted by wildfires (see Figure 1.16).

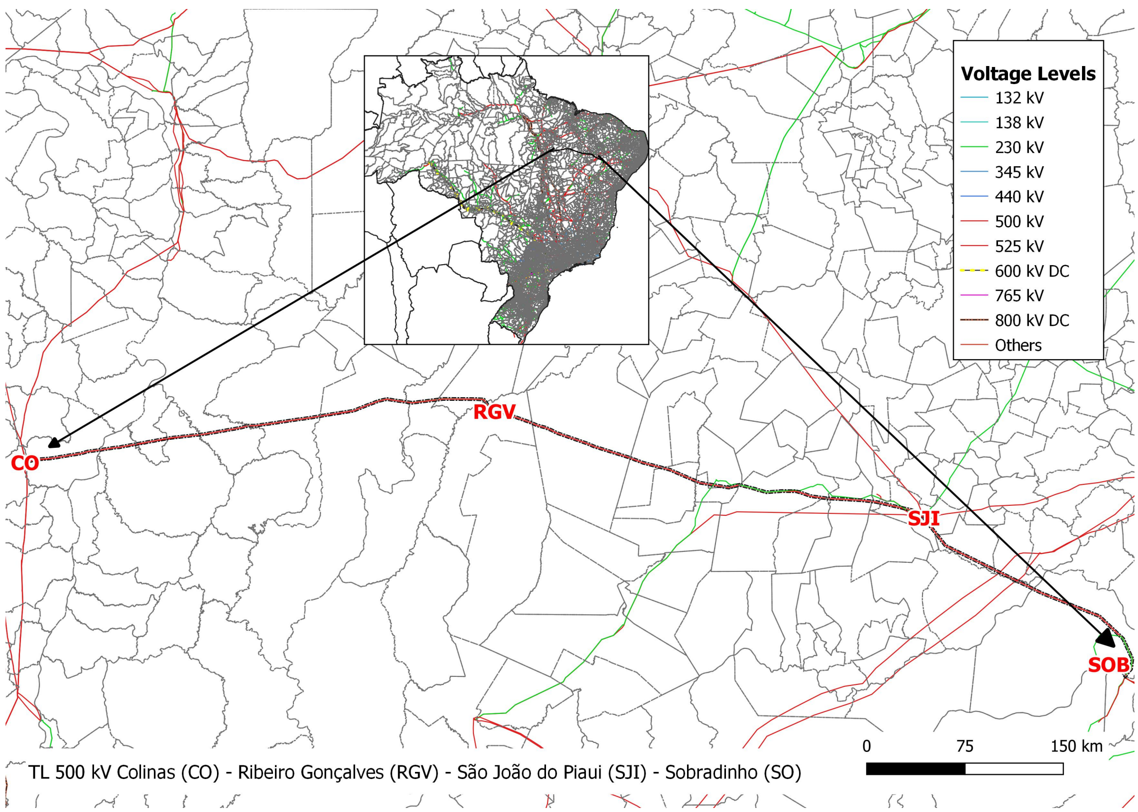

Figure 1.16: Detailed Map of the 500 kV Overhead Transmission Line.

This backbone was selected for the focus area of this study based on its compact design characteristics and singular exposure to both biomes (i.e., Cerrado and Caatinga) that will contribute to different reliability performances. Between 2013 and 2021, this line segment accounted for 108 outages associated with fire-induced flashovers, all in the Cerrado biome portion.

The line has a total length of 923,432 km of bare conductors. It is supported by 1,871 structures, mainly compact cross-rope latticed steel structures with 5 meters of electrical clearance distance (i.e., spacing) between phase conductors. Table 1.1 shows the main characteristics of the OHTL.

Table 1.1: Overhead Transmission Line - Main Characteristics

Characteristic	**Value**
Nominal Voltage	500 kV
Total Length	923.432 km
CO - RGV Length	366.67 km
RGV - SJI Length	342.95 km
SJI - SOB Length	212.45 km
Circuit Configuration	Horizontal
Minimum Vegetation Clearance Distance (MVCD)	9.5m
Phase spacing	5m
Conductor type	ACSR 954 kcmil Rail
Phase Conductor configuration	4-symmetrical bundle
Current	2,736 A per phase
Operating Temperature -Long Duration	60°C
Surge Impedance Loading (SIL)	2,369 MVA

1.3 Overview of Current Work

Since wildfires are one of the most prevalent originators of momentary and permanent outages of transmission lines worldwide, many studies have been carried out to predict where wildfires occur, how they propagate, and how they impact the performance of overhead lines. For example, Berredo A. et al. [17] proposed adapted methodologies to estimate fire ignition and spreading based on remote sensing, tabular, and in-field data. Berredo A. et al. [17] adapted the models proposed in Chuvieco et al. [23] and Frank A. Albini [13] to predict the ignition and propagation of wildfires in two specific Brazilian land biomes, Cerrado and Caatinga, aiming to address the criticality of outages of line sections exposed to wildfires. However, the practi-

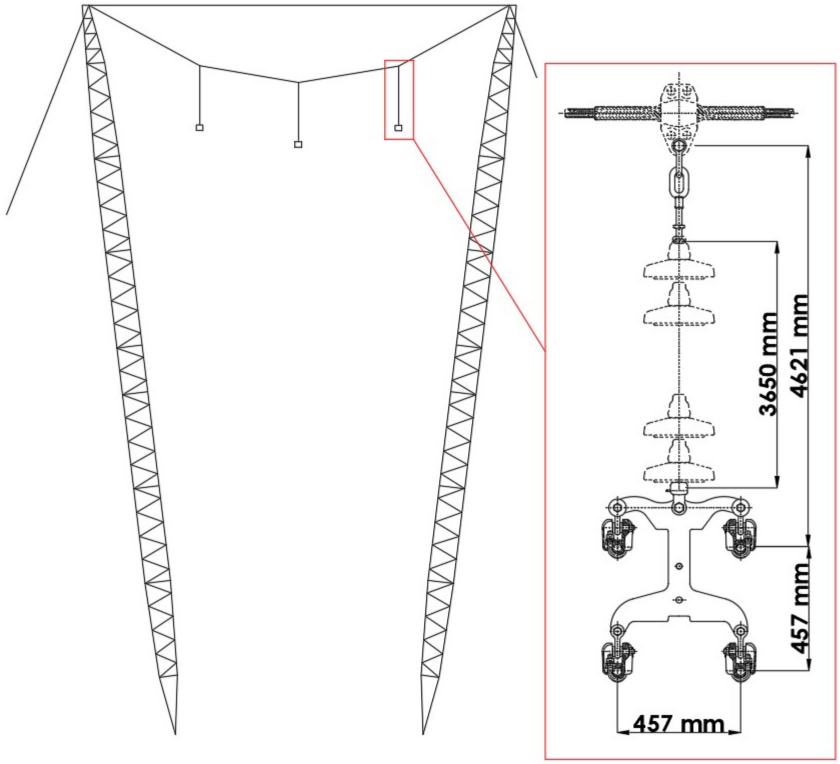

Figure 1.17: Crossrope structure and insulator string details.[7]

cal application of those models to the work routine of electrical utilities resulted in time and resource-consuming as they require the acquisition and intense processing of bulk satellite imagery and in-situ survey data from multiple sources. Subsection 2.3.1 presents a detailed explanation of the application of the model of risk of wildfire proposed in Berredo et al.

As mentioned in Section 1.2.5, the proposed novel approach for estimating the risk of wildfire uses Getis-Ord Gi* spatial statistic analysis of historical data of wildfires. The Getis-Ord Gi* is a spatial statistics method that resolves the standard deviation (z-score) and the probability (p-values) of a given pattern occurring for a population of spatial data. It shows where events with either high or low values cluster spatially by looking at each location within neighboring events. A particular event with a high value is interesting but may not be a statistically significant hotspot. A statistically significant event should have a high value and be surrounded by other events with high values. The Getis-Ord Gi* method proportionally compares the local sum for a hotspot and its neighbors to the sum of all events. When the local sum is very different from the expected local sum, and when that difference is too significant to be the result of random chance, a statistically significant z-score results.

Oxoli et al. (2017) [36] applied Getis-Ord Gi* statistics to detect significant variations in soil consumption for the Lombardy Region in northern Italy and correlation analysis of performance indicators characterizing Airbnb lodgings for the city of Venice in Italy. Daniel Paül i Agustí (2021) [37] used Getis-Ord Gi* to analyze the spatial distribution of tourism interest by comparing projected images from the Instagram social network. Pal et al. (2023) [38] applied Getis-Ord Gi* statistics and optimized hotspot analysis, to detect hotspot and coldspot zones of global earthquakes. Khan et al. (2022) [39] adopted various hotspot spatial analysis techniques such as Getis-Ord Gi*, Global Moran's I, Local Moran's I, Kernel density estimation, and emerging hotspot analysis to prioritize locations for road safety actions by indicating and quantifying the existence of single-vehicle lane departure crashes. Geoprocessing software such as ESRI's ArcGIS [40] and QGIS [41] provide spatial analysis tools to calculate all the above-mentioned methods of spatial analysis, including the Getis-Ord Gi* statistics.

Regarding the consequences of OHTLs exposed to wildfires, West & McMullan (1979) [18], J.R. Fonseca et al. (1990) [2], Lanoie & Mercure (1997)[19] and Berredo A. et al. (2019) [17] studied the impacts of wildfire-induced flashovers on overhead lines and proposed equations for estimating the breakdown strength of air based on the burning temperature and other characteristics of different species of vegetation. These equations allow for estimating the minimum vegetation clearance distances in order to prevent flashovers associated with wildfires. However, the effectiveness of each of the evaluated models is conditioned to the type of vegetation exposed to fire. The studies suggest that the burning characteristics of different vegetation species can influence the breakdown strength of air, therefore impacting the risk of outages. The investigated models are further explained in Section 2.4.

Some of these equations propose minimum vegetation clearance distances required to mitigate the risk of flashover events when overhead transmission lines, conditioned to specific land biomes, are exposed to wildfires. The current Brazilian NBR 5422 [21] and the North American NERC FAC-003-4 (Transmission Vegetation Management) [20], standards that establish protocols to determine the minimum vegetation clearance distances for overhead transmission lines, are also investigated in this research.

1.4 Current Challenges

Numerical models have been proposed to estimate the risks of wildfires and to understand what degradation mechanisms influence the insulation strength of air exposed to wildfire. However, to predict the ignition and propagation of wildfires, the existing models require a large amount of GIS data from multiple sources and heavy computational processing, which results in time-consuming and costly implementation. In addition, part of the required data should be collected in field inventory campaigns. For instance, to obtain the risk of wildfire proposed in Berredo et al., a dataset with 17 different geospatial data layers should be collected and processed to enable the analysis of criticality to wildfire-induced flashover. In the US, the software Flammap, developed by the US Forest Service [42], is supported by an organized repository that contains all required geospatial data layers. However, the repository covers data from the continental United States, Alaska, and Hawaii only. Thus, using the software Flammap for fire prediction in any other location would require gathering and processing massive spatial data.

In the ambit of insulation coordination, empirical equations have been proposed to estimate the degradation of the dielectric strength of air based on the reduction of the air density, the influence of suspended particles present in the flame and smoke, and the electrical conductivity of the flame. The evaluated models are empirical and were proposed based on laboratory experiments where specific types of fuel were burned to simulate fire characteristics in the studied locations. Since biomes and vegetation species may present different burning characteristics, every biome interacting with the transmission line may pose a different thread. It means that all models (i.e., risk of fire, vulnerability, and criticality) should be re-evaluated for application in a land biome other than those related to Tropical Savannas such as Cerrado or Caatinga.

1.5 Thesis Statement and Research Contributions

Vegetation fire is one of the biggest threats to electric bulk power systems worldwide, causing momentary and permanent outages of transmission lines and substantial damage to line components. Therefore, accurate methods for analyzing the spatial risk of overhead transmission lines subject to wildfires are necessary to improve system reliability cost-effectively. The proposed <u>new contributions</u> obtained from this thesis include the following items:

- The study highlights the fragility of the current Brazilian standard in determining safe clearance distances to prevent wildfire-induced flashovers in overhead lines.

- The substantial number of outages associated with compact lines due to phase-to-phase flashovers highlights the need to adopt higher phase-to-ground clearance distances to compensate for the elevated temperatures in the air gap between phases.

- Analysis of existing MVCD calculation methods applied to 108 outages is presented, which shows that these methods are insufficient to prevent wildfire-induced flashovers.

- The existing clearance distances adopted in ATE II show that results from different MVCD calculation approaches are insufficient to prevent wildfire-induced flashovers.

1.6 Thesis Organization

The thesis chapters are organized as follows:

- CHAPTER 1 provides an introduction to the topic. The objectives, motivation, and contribution of the thesis are presented in this chapter. It also introduces the challenges associated with risk classification of ignition of wildfires and the establishment of minimum OHTL design conditions to prevent outages due to wildfire-induced flashovers, based on work in the existing literature.

- CHAPTER 2 discusses the existing methods for risk assessment of wildfires, vulnerability to wildfire-induced flashovers, the criticality of outage, and existing models to determine the minimum clearance distance to prevent OHTL from flashing over when exposed to wildfire events.

- CHAPTER 3 discusses the methodology and considerations for representing the overhead transmission system via a GIS-based spatial model.

- CHAPTER 4 proposes a new method for risk assessment of wildfires and the vulnerability and criticality to wildfire-induced flashover based on an adapted minimum vegetation clearance distance model for lines installed in the Cerrado and Caatinga biomes and validated by statistical investigation of line outages.

- CHAPTER 5 presents the test scenarios for validation of the proposed methodology, presents the test results, and discusses the performance, including the comparison of the results.

- CHAPTER 6 discusses the conclusions and offers suggestions for future work.

- APPENDIX A provides the outage data.

- APPENDIX B provides the results regarding the risk of wildfire.

- APPENDIX C provides the results of the vulnerability of the overhead line to wildfire-induced flashover.
- APPENDIX D provides the results of the outage criticality of the overhead line.

CHAPTER 2: EXISTING METHODOLOGY

2.1 Chapter Introduction

An explanation of the current standards and guidelines regarding the overhead line designs used in North America and Brazil are detailed in this chapter, as they are a fundamental piece of this research and relate to the overall contributions of the thesis, with a particular focus on addressing the minimum clearance distances practiced in those countries, respectively. The chapter also includes a detailed explanation of the existing models of risk of wildfire, vulnerability of OHTLs to wildfire-induced flashover, criticality to outages, and calculation procedures of minimum vegetation clearance distance proposed per standards and on other technical publications.

2.2 Current Standards and Guidelines

Preventing transmission lines from fire-induced flashovers is a complex and costly task. For instance, vegetation management is one of the top operational expenses in Brazilian utilities operating OHTLs installed in the Cerrado and Caatinga biomes. The environment in which the asset is installed and the transmission line characteristics play different and important roles in the mode of failure. A typical transmission line relies on its designed clearance distances to provide reliable insulating performance for steady-state and transient operating conditions. While the reduction in the clearance distance and the degradation of the dielectric properties of air may result in flashovers, in the absence of wildfire, the principal failure mode, no fire-induced flashovers shall occur.

This research did not find any technical standard for the design of overhead transmission lines explicitly proposing calculation procedures for minimum clearance distance regarding the impacts of wildfires. However, this chapter identifies and discusses many technical research publications addressing the problem. Current standards and guidelines on overhead line design used in North America and Brazil, the National Electrical Safety Code (NESC) [43] and NBR 5422 [21], do not establish procedures to determine compatible clearance distances to prevent the impacts of fire-induced flashovers.

Fire-induced flashovers can be caused by three mechanisms. As mentioned, according to [16], the mechanisms that may lead transmission lines to fire-induced flashover events are:

- Degradation of the dielectric strength of air caused by the reduction of the air density. In the event of a fire, the high temperature in the vicinity of the conductors will reduce the air density and, consequently, the dielectric strength of the air gap. If the dielectric breakdown strength of air is reduced to a value below the electric field strength imposed by the energized line between conductor and ground or between conductors, a condition to occur the flashover is established.

- Influence of airborne particles (flame and thick smoke). Vegetation species may present different burning characteristics, moisture content, and suspended ash particles in the air may increase or decrease the contribution to triggering the flashover [16] [19].

- Flame conductivity. Studies have demonstrated the effects of the flame on the dielectric strength of the air gap. Fire flames have a very low electrical resistance, characteristic of the vegetation type being burned [19].

The North American Electric Reliability Corporation (NERC) published the standard entitled “FAC-003-4 Transmission Vegetation Management” aiming to maintain a high level of reliability in the North American electric transmission system by regulating minimum requirements for vegetation management and minimizing encroachments from vegetation located adjacent to the ROW of overhead transmission lines operated at 200 kV or higher voltage. The main objective is to prevent the risk of those vegetation-related outages that could lead to cascading failure events[20]. FAC-003-4 provides minimum vegetation clearance distances for lines at a voltage of 200 kV and above but is not intended to address wildfire-related outages.

NBR 5422 is the Brazilian standard for the design of overhead transmission lines [21]. The document has never been updated since 1985. NBR 5422 provides a two-part equation for calculating the minimum clearance distance to various types of obstacles. The obstacle options include:

- Accessible locations exclusive to pedestrian
- Locations with the presence of agricultural machinery
- Roads, streets, and avenues
- Unelectrified railroads
- Navigable waters
- Non-navigable waters
- Roofs and terraces
- Walls
- Power lines
- Telecommunication lines
- vegetation

The calculation approach to address vegetation aims to prevent outages due to the proximity between energized conductors and vegetation. It does not specify whether the minimum distance from vegetation would be sufficient to prevent wildfire-induced flashovers.

2.3 Models of Risk of Wildfire

Overhead lines must be exposed to wildfire (cause) to exist the risk of fire-induced flashover (consequence). If there is no exposure to wildfire, there should not exist the correlated risk of outage. There is only one scenario where this hypothesis can exist: when there is no fuel. This hypothesis is unlikely to occur with overhead lines since even water bodies such as lakes and rivers may present some species of vegetation. However, riparian zones where vegetation is present alongside water bodies may be protected by environmental laws and therefore preserved. In consequence, if exposed to wildfires, line spans crossing these particular environments may be exposed to outages.

Where the ignition of wildfire exists, propagation may or not occur. For example, the use of controlled fire is a common practice of vegetation management to control the spread of wildfires in parks and forests. Overhead line rights of way (ROW) subjected to vegetation management (removal of the fuel) may work as firebreaks if the management is sufficiently wide to isolate the two sides of the ROW where the vegetation is not managed. If the remains of the removed vegetation are disposed of on the right of way, the risk of ignition and propagation will exist.

This section approaches one existing model to determine the risk of wildfire, used as a reference in this research. Berredo et al. [17] proposed a model in 2016 to classify the risk of wildfire based on Albini[13], Rothermel[44] and Chuvieco [23] ignition and propagation models. A new approach to establishing the risk of wildfire proposed in this thesis aims to provide electric utilities with a GIS tool to classify the risk of wildfires by a different approach as a means of reducing the resources and efforts required to obtain the results of the probability of occurrence of wildfires. The new methodology focuses exclusively on a large database of detection of wildfires (spotting) to determine the risk of wildfire. The justification relies on the fact that if wildfire events are detected in a given location over time, it may be sufficient to establish the current probability of occurrence of wildfires. Propagation (spreading) in this research is also considered a detected hotspot on a 2 km buffer zone around the transmission line. Therefore, a model to determine the risk of propagation of wildfire is ignored. The new model uses QGIS GIS processing tools [45] to establish the probability of occurrence of wildfires, but the process can be performed in any GIS with spatial processing and analysis capabilities (e.g., ESRI ArcGIS).

2.3.1 Risk of Wildfire based on Berredo et al.

As introduced in 1, Berredo et al. proposed a complete methodology to classify the risk of outage of overhead lines due to fire-induced flashovers. The methodology is organized in three risk models (i.e., risk of ignition of fire, risk of propagation of fire, and risk of vulnerability to flashover), that will compose the classification of risk of criticality to the outage (i.e., flashover) if exposed to wildfire (see Figure 2.1). This Subsection 2.3.1 explains the models related to the risk of wildfire, ignition, and propagation, while Subsection 2.4.3 explains the mechanisms that may lead the transmission line to flashover if exposed to wildfires. The MVCD adopted in Berredo et al. results in the classification of vulnerability to wildfire-induced flashover by line span.

As Albini and Rothermel's models are implemented into modules of the FlamMap GIS software [42], Berredo et al. is implemented into a plugin for the QGIS software [45] to perform the spatial analysis. The QGIS plugin developed to support the methodology provides four results:

- Map of risk of fire ignition
- Map of risk of fire propagation
- Map or risk of fire (ignition and propagation)

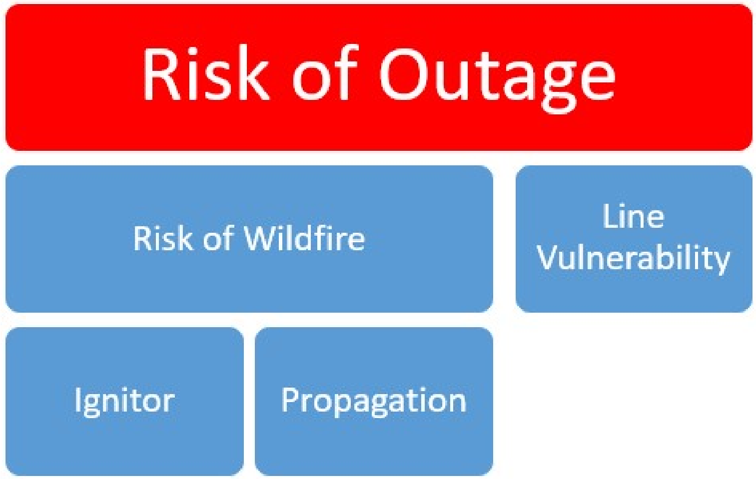

Figure 2.1: Risk Model of Berredo et al.

- Map of vulnerability to flashover
- Map of criticality (fire and vulnerability to flashover)

Mapping the risk of outages is the ultimate goal of the methodology. The researchers envisioned a GIS tool called CQFS (Criticidade a Queimadas em Faixa de Servidão - *Criticality of wildfires in Rights of Way*) to identify line spans located in the Brazilian savanna likely to flashover in the scenario of a wildfire.

The risk of wildfire is the outcome of the matrix containing the results of risks of ignition and propagation. Berredo et al. used Albini's spotting model [13], Rothermel's surface fire spread model [46][44], and Chuvieco [23] to classify the risks of ignition and propagation (spreading) of wildfire, tailored for the Brazilian tropical savannas (i.e., Cerrado and Caatinga biomes).

Tables 2.1 and 2.2 show the input data required to determine the risk of ignition and propagation of wildfire, respectively.

Table 2.1: Variables used in the Model of Ignition of Wildfire.

Begin of Table 2.1		
Input Data	**Type**	**Description**
Transmission Line	Line Vector	Path of the overhead transmission line.
Sun Irradiance	Raster	Small Sun irradiance in kJ/m^2.
Maximum Temperature	Raster	Maximum temperature registered in °C.
Average Wind Speed Census	Raster Raster	Average wind speed recorded in m/s. Census - population counting, extracted from the IBGE source.
Land Use	Raster	22 classes of land use.
GNDVI	Raster	Green Normalized Difference Vegetation Index is the index of the vegetation "greenness," obtained from an arithmetic raster function using Near-Infrared and Green bands of a multiband image.
NDVI	Raster	Normalized Difference Vegetation Index is the index of the relative biomass obtained from an arithmetic raster function using Near-Infrared and red bands of a multiband image.
Basal Area	Raster	Average area (m^2/ha) occupied by tree stems - obtained from field survey and correlated with LiDAR and Stereoscopic Airborne Radar imagery.
Density	Raster	Estimation of vegetation density (species/ha) - obtained from field survey, LiDAR, and Stereoscopic Airborne Radar imagery.
Volume	Raster	Volume of biomass (kg/ha) obtained from field survey, LiDAR, and Stereoscopic Airborne Radar imagery.
Hotspots	Raster	Records of wildfire obtained from several satellites (i.e., NOAA-15, NOAA-18, NOAA-19, METOP-B, MODIS (TERRA and AQUA), VIIRS (NPP-Suomi), GOES-13 and MSG-3).
Altitude	Raster	Vertical elevation of the crossed area in meters.

Continuation of Table 2.1		
Input Data	**Type**	**Description**
End of Table		

Table 2.3: Variables used in the Model of Propagation of Wildfire.

Input Data	Type	Description
Transmission Line	Line Vector	Path of the overhead transmission line
Slope Orientation	Raster	Orientation of slope measured clockwise in degrees from 0 to 360 in five categories
Hypsometric Curve	Raster	Elevation
Clinographic Curve	Raster	Slope steepness in degrees
Land Use	Raster	22 classes of land use
Highway	Raster	Identification of highways and roads along the transmission line buffer

2.4 Calculation Methods for MVCD

Wildfires may cause an increase in temperature in the vicinity of the transmission line resulting in the reduction of the density of air, consequently reducing the dielectric strength of the medium. Flames may channel the air gap between the ground and the conductors resulting in lower clearance distances. In addition, smoke may also carry potentially conductive airborne particles that could degrade the insulation strength of air. Therefore, clearance distances compatible with these variables of influence should be maintained in order to prevent lines from flashing over in the event of wildfires. This section presents six different approaches (NBR 5422 [21], FAC-003-4 [20], Berredo et al. [17], Fonseca et al. [2], FAC-003-4 corrected by West & McMullan [18] and Lanoie & Mercure [19]) to determine the minimum clearance distance to vegetation (MVCD).

In practice, important environmental wildfire-influencing factors such as wind speed and direction, vegetation characteristics, height and moisture, and calorific power are dynamic and discrete. Therefore, determining the risk of flashover can be very difficult and time-consuming as it would require extrapolations and assumptions based on literature. In order to address uncertainties, this study adopted a data-driven approach based on 108 outage events to estimate the probability of flashover. The obvious disadvantage of this approach is that changing the location of the installation may affect parameters associated with the biome. In other words, lines installed in biomes other than Cerrado or Caatinga may require adjusting the estimated minimum clearance distance based on a new dataset of wildfire-related outages. Also, line-to-line outages are influenced by the line-to-line clearance distance. Compact lines may present higher line-to-line failure rates in comparison to conventional overhead line clearance distances. For instance, the phase-to-phase clearance distance of the OHTL investigated in this research is half of that adopted in conventional 500kV OHTLne designs.

2.4.1 ABNT NBR 5422:1985

NBR 5422 [21] provides a two-part equation for calculating the minimum clearance distance to obstacles: the first part is a constant value or base distance (a) referent to the type of obstacle. The second part of the equation calculates the parcel of the distance that varies with the nominal voltage of the transmission line, as seen in (2.1),

$$D = a + 0.01 \cdot \left(\frac{Du}{\sqrt{3}} - 50 \right) \tag{2.1}$$

where, a is the basic distance in meters and Du is the maximum operating line voltage (phase-to-phase) in kV. The standard adopts a basic distance (a) of 4 meters for vegetation obstacles and 6.5 for locations with traffic of agricultural machinery.

Despite the objective of preventing air gap flashovers due to the proximity between energized conductors and vegetation, the current NBR 5422 standard does not specify whether the minimum distance from vegetation would be sufficient to prevent wildfire-induced flashovers.

2.4.2 NERC FAC-003-4 (Gallet Equation)

NERC FAC-003-4 [20] establishes the applicable minimum clearance distance to vegetation in North America. This standard adopts the Gallet equation, which calculates the insulation coordination in OHTL design (see Algorithm 1). The approach calculates the voltage crest of a given line, estimates the initial minimum clearance distance, then calculates the critical flashover voltage, corrects the results to a specific atmospheric pressure, and calculates the withstand voltage at the same atmospheric pressure. This method requires a few iterations to identify the minimum dielectric strength required to withstand the critical flashover voltage.

NERC FAC-003-4 does not apply to MVCD to prevent fire-induced flashovers but only to prevent flashovers due to the approximation of vegetation to line conductors. However, in the West & McMullan approach, as further explained in [18], this study adjusted the critical flashover voltage from FAC-003-4 to reflect the air density corresponding to the temperature of 250°C due to fire under the transmission line.

2.4.3 Berredo et al. MVCD Calculation Method

Berredo et al. [17] proposed a method of calculating the MVCD subject to elevated temperatures derived from the calculation of the breakdown voltage of the air between sphere electrodes. However, instead of assuming a fixed temperature, Berredo et al. used an approximation to estimate the average temperature in the air gap (see Algorithm 2). Berredo et al. assumes two hypothetical values of flame temperature in the air gaps between ground and conductors and between conductors to represent the fire characteristics of the Brazilian savanna, 300°C and 100°C, respectively.

The model is intended to determine whether a wildfire can result in the flashover of the energized circuit (vulnerability). The vulnerability to flashover will be low for those line spans exposed to wildfire, with sufficient clearance distance to provide the required insulation strength. Spans with short clearance distances will result in a

Algorithm 1 NERC FAC-003-4 algorithm

1: Calculate the voltage crest V_m via (2.2), where TOV is the transient overvoltage factor in pu and V is the nominal voltage (kV).

$$V_m = TOV \cdot V \cdot \sqrt{\frac{2}{3}} \tag{2.2}$$

2: Compute the initial clearance distance D_i per (2.3), where K_w is the wet/dry conditions factor and K_g is the gap factor.

$$D_i = \frac{8}{\frac{3400 \cdot K_w \times K_g}{\left(\frac{V_m}{0.85}\right)} - 1} \tag{2.3}$$

3: Calculate the Critical Flashover Voltage (CFO) for D_i at standard atmospheric conditions CFO_s via (2.4), where D is the air gap distance.

$$CFO_s = K_w \cdot K_g \cdot \frac{3400}{1 + \frac{8}{D}} \tag{2.4}$$

4: Calculate the CFO at a specific height above sea level CFO_A by applying the atmospheric correction factor via (2.5), where A is the altitude (km).

$$\begin{aligned} CFO_A &= CFO_s \cdot \exp\left(-m \cdot \frac{A}{8.6}\right) \\ m &= 0.125 \cdot G_0 \cdot (G_0 - 0.2) \\ G_0 &= \frac{CFO_s}{500 \cdot D} \end{aligned} \tag{2.5}$$

5: Calculate the withstand voltage of the gap at a given height above sea level via (2.6), where σ = standard deviation.

$$V_{m(3\sigma)} = CFO_A \cdot \left(1 - 3\frac{\sigma}{CFO_A}\right) \tag{2.6}$$

higher flashover vulnerability than line spans with larger clearance distances.

Algorithm 2 Berredo et al. (2019) [17] - Calculation Steps

1: Calculate the Air Density via (2.7).

$$\delta = \frac{\rho T_0}{\rho_0 \cdot \left(273 + \frac{\left(\sum_{n=1}^{h}\right) \cdot T_s \cdot (h^{-0.992})}{h}\right)} \tag{2.7}$$

2: Calculate the Breakdown Strength of Air (2.8).

$$V_{r(rms)} = \frac{22.7 \cdot \delta \cdot 0.125 \cdot \left(1 + \frac{0.54}{\sqrt{\delta \cdot 0.125}}\right) \cdot \frac{h}{0.125}}{0.25 \cdot \left(\frac{h}{0.125} + 1 + \sqrt{\left(\frac{h}{0.125} + 1\right)^2 + 8}\right)} \tag{2.8}$$

In (2.7): δ is the air density correction factor, ρ is the atmospheric pressure on place (mm/HG), ρ_0 is the reference atmosphere pressure (760mm/HG), T_0 is the reference temperature (293 K), T_s is the temperature at the ground fire, and h is the clearance between the conductor and the top of the vegetation. Instead of using a fixed temperature, Berredo et al. adopted an average temperature of 300°C in the air gap between the conductor and ground and 100°C in the air gap between conductors resulting in the air density correction factor of 0.474 and 0.729, respectively. In (2.8): $V_{r(rms)}$ is rms voltage associated with the breakdown strength of air, ρ_0 is the reference atmosphere pressure (760mm/HG), T_0 is the reference temperature (293 K), and h is the clearance distance between the conductor and the top of the vegetation.

Berredo et al. classified the vulnerability to flashover by comparing the results of the breakdown strength of air in kV rms presented in 2.8 with the existing clearance distance found in the assessed line spans. The criterion to determine the phase-to-ground and phase-to-phase vulnerabilities are listed as follows:

- **Phase-to-Ground Vulnerability**
  - Low Vulnerability - Dielectric Strength above 380 kV rms

  - Medium Vulnerability - Dielectric Strength between 348 kV and 380 kV rms
  - High Vulnerability - Dielectric Strength below 348 kV rms

- **Phase-to-Phase Vulnerability**
  - Low Vulnerability - Dielectric Strength above 650 kV rms
  - Medium Vulnerability - Dielectric Strength between 600 kV and 650 kV rms
  - High Vulnerability - Dielectric Strength between below 600 kV rms

2.4.4 Fonseca et al. MVCD Calculation Method

Fonseca et al. [2] investigated the insulation requirements for overhead transmission lines subjected to the burning of sugarcane under conductors in order to reduce the outages to a minimum. Since different vegetation species may release different substances and quantities of floating particles, the specimen plays an important role in the breakdown strength of air and, therefore, in the risk of outages. According to Fonseca et al., floating particles are responsible for the greatest reduction of the breakdown voltage in the burning of sugarcane [2].

Results and statistics obtained from Fonseca et al. show that the analyzed faults were caused by phase-to-ground and phase-to-phase flashovers in mid-span, depending on the line configuration. The predominance of phase-to-phase events occurred in circuits operating at 138 kV, whereas phase-to-ground events occurred at higher voltage levels. All of the analyzed circuits are located in Southeastern Brazil, and the analyzed outages were all caused by the burning of sugarcane plantations. Electrical tests in Brazil, via conductor-conductor and conductor-plane electrode configurations subjected to the burning of sugarcane, resulted in a dielectric strength of 35 kV/m. In addition to the laboratory experiment, Fonseca et al. investigated the performance of two transmission lines operating at 138 kV. The study also investigated the sag increasing due to the high temperature under the conductors. It was noticed that the burning of sugarcane 5 m high resulted in flames of up to 1 m high.

Based on the investigation performed, Fonseca et al. proposed the following equations to determine the minimum vegetation clearance distance,

$$D = D_{basic} + D_{el} + D_{sag} \tag{2.9}$$

where D_{basic} is assumed 5 m for OHTL crossing sugarcane plantations, D_{el} is the electrical distance corresponding to (2.10) for lines with phase-to-ground voltage up to 245 kV, (2.11) for lines with phase-to-ground voltage above 245 kV, and D_{sag} is the vertical distance to compensate for the additional sag due to the heating of the conductors.

$$D_{el<245kV} = \frac{U}{35} kV/m \tag{2.10}$$

$$D_{el>245kV} = 7 + \frac{U - 245}{150} kV/m \tag{2.11}$$

Fonseca et al. considered two electric distances (i.e., $D_{el<245kV}$ and $D_{el>245kV}$) to distinguish between the influence of the flame (i.e., the flame either partially or completely fills the air gap). Table 2.4 shows the results of the dielectric strength of air for different percentages of air gap flame bridging. Table 2.5 shows the results of MVCD calculations for OHTL operating at different voltage levels.

2.4.5 West & McMullan - Temperature vs. Breakdown Strength Strength of Air

West & McMullan [18] proposed a relationship between the rise in temperature and the degradation of the dielectric strength in the air gap based on laboratory experiments. The study demonstrated the reduction in the dielectric strength of air by increasing the temperature in the air gap. According to the experiment, the

Table 2.4: Fonseca et al. % of gap bridging vs dielectric strength [2]

% of gap bridging	Dielectric Strength (kV rms/m)
100	35.0
90	46.5
80	58.0
70	69.5
60	81.0
50	92.5

Table 2.5: Fonseca et al. MVCD by voltage level [2]

Nominal Voltage (kV)	Span Length (m)	Conductor (kcmil)	D_{el} (m)	D_{sag} (m)	MVCD (m)
138	300	336.4	2.4	1.0	8.4
230	350	795.0	4.0	1.0	10.0
440	400	954.0	7.2	1.1	13.3
500	400	954.0	7.4	1.1	13.5
750	450	1113.0	8.4	1.1	14.5

dielectric strength of air was reduced to less than half with temperatures exceeding 350°C, and to one-third of the original strength when exposed to around 700°C.

Based on (2.12), where V_t is flashover voltage under current conditions, V_s is flashover voltage under standard conditions, p is barometric pressure (kPa), and T is the temperature (K) if the air gap is exposed to 250°C, the dielectric strength across 500 kV, voltage peak phase-to-ground (408.25 kV), would be reduced to 228.62 kV (45.7% of the nominal voltage) as shown in Figure 2.2.

$$V_t = V_s \cdot \frac{2.892 \cdot p}{T} \tag{2.12}$$

2.4.6 Lanoie & Mercure - Minimum Clearance Distance to Wildfire based on Flame Resistivity

Lanoie & Mercure [19] proposed a minimum clearance distance to spruce tree fires based on measurements of the electrical resistivity of flames during the burning of

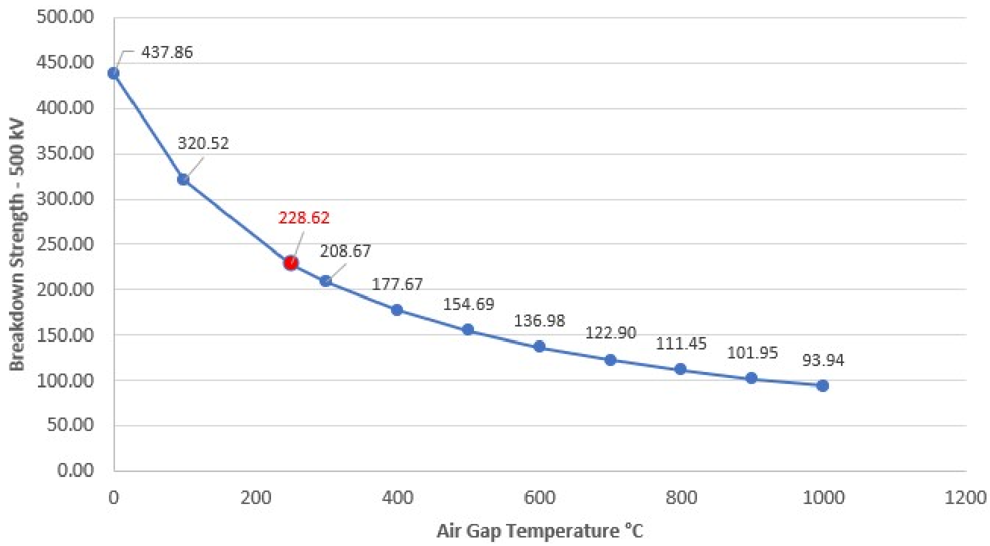

Figure 2.2: Breakdown strength of air across 500 kV vs. temperature.

living spruce trees in Canada. According to the authors, the reduction of the air density alone could not explain the 90% of loss of insulating strength identified on their tests. Based on IEEE Std 4 [47], exposing the air gap to 1000 °C would result in 50% of loss of insulating strength due to the reduction in the air density. The authors found the minimum critical electric field (E_c) of 12 kV RMS/m when flames of burning spruce trees spanned the air gap. Nevertheless, according to Lanoie & Mercure, the chemical characteristics of the flame, rich in minerals such as dissolved salts, would facilitate the occurrence of flashovers.

This aspect reiterates the proposal that the vegetation characteristics would play a significant role in the risk of wildfire-induced flashovers. For instance, line sections exposed to Cerrado and Caatinga resulted in a very different risk of wildfire and vulnerability to flashover. Only 30 of the 108 investigated outages (27.7%) occurred in the Caatinga biome. The Cerrado biome responded for 72.3% of the outages. However, as mentioned in 1.2.2, from 8,137 wildfire events contained in the ATE II buffer between 2012 and 2022, only 255 events occurred in the line section between São João do Piauí (SJI) and Sobradinho (SOB). In addition, none of the outage events occurred in the section between substations São João do Piauí (SJI) and Sobradinho

(SOB), which represents 23% of the total line length.

2.5 Chapter Summary

This chapter presents and provide details of six methods to calculate the minimum approach distance to vegetation. Three methods, Berredo et al., Fonseca et al., and Lanoie & Mercure aim to determine the minimum clearance distances to prevent fire-induced flashovers. However, they were developed for different types of vegetation. While Berredo et al. focuses on mixed grassland and bushes present in the Brazilian savanna, Fonseca et al. established clearance distances for burning of sugarcane, and Lanoie & Mercure for spruce trees. The other methods presented in this thesis do not consider changes in the insulating medium caused by wildfires and are intended only to prevent outages caused by approximation with energized circuits.

CHAPTER 3: GIS-BASED SPACIAL MODELING OF TRANSMISSION SYSTEM

3.1 Chapter Introduction

This chapter includes concepts and information on Geographic Information Systems (GIS), and how GIS and remote sensing data empowered this research with spatial analysis of vegetation and wildfires. It highlights the key contributions, as they relate to the overall contributions of the thesis.

According to [48], a geographic information system (GIS) is used to simulate complex patterns, visualize and analyze real-world situations, management, and support decision. Among the applications, GIS is intensively used as a decision-making tool in a vast number of fields, including energy, natural resources management, transportation, environment, marketing, real estate, tourism, and public safety. GIS enables the visualization and analytics of the interrelations of social, environmental, climate, geological, infrastructure, and any other information that can be distributed in space. Due to the spatial-temporal and multi-variable characteristics, GIS offers a unique opportunity to identify, display and analyze threats that may impact energy infrastructure.

Geospatial data can be obtained in many ways. GPS-enabled mobile devices can collect geographic locations, photographs, manually-entered descriptive information, and data from other embedded sensors. Aircraft and satellites collect bulk aerial photographs and remote sensing data from extensive areas.

Geospatial data is organized into the following (two) categories [48]:

- Vector Data
  - Points: represent discrete objects such as structures of overhead lines.

Points are mapped with a single pair of x-y coordinates.

  - Lines: represent linear features such as transmission line conductors, rivers, or roads. Lines are represented by a sequence of x-y coordinates
  - Polygons: represent closed areas such as political boundaries. Like lines, polygons are also represented by a sequence of x-y coordinates. However, they make up their boundaries.

- Raster Data
  - Raster data is represented by image sources such as aerial photographs and satellite images. Images are divided into a matrix of rows and columns regularly spaced. A single matrix cell is known as a picture element (pixel). Each pixel is identified by its location in the matrix (row and column number), which includes a digital number (or pixel value) of radiometric data that can be classified as an attribute of interest. Radiometric data are obtained from sensors that will collect the intensity of electromagnetic radiation of a portion of the electromagnetic spectrum. The visual portion of the electromagnetic spectrum is characterized by the red, green, and blue wavelength bands (RGB). More advanced sensors can collect a broader fraction of the electromagnetic spectrum (multi-spectral and hyper-spectral bands), which will enable the acquisition of a such as infrared. The Landsat8 satellite, for example, can collect information in 11 different bands from 0.433 to 12.5 μm.
  - The pixel resolution is very important for remote sensing since the pixel value will give the results for that geographic area. For example, if the infrared pattern of wildfire is the information of interest, a resolution of 300 m/pixel means that the smaller classification area will be 90,000 m^2. Thus, the minimum size of a wildfire will be an area of 300 m x 300 m.

A variety of GIS software is available commercially and free of cost. Options vary from enterprise solutions, including toolboxes for geoprocessing analysis of every need, focusing on specific niches such as applications for digital twins, asset management, infrastructure operation, or image processing. Some GIS software are listed below.

- ESRI ArcGIS —Proprietary [49]
- QGIS —Open-Source [45]
- Hexagon Geomedia —Open-Source [50]
- MapInfo —Open-Source [51]
- Global Mapper —Open-Source [52]
- Grass GIS —Open-Source [53]
- GE Smallworld GIS —Open-Source [54]
- SAGA GIS —Open-Source [55]
- Bentley MAP —Proprietary [56]

This research adopted the software application QGIS to perform the spatial analysis of the risk of wildfires, vulnerability to wildfire-induced flashovers and outages. QGIS is a free and open-source geographic information system licensed under the GNU General Public License, with development led by the Open Source Geospatial Foundation (OSGeo)[57]. Many other GIS-related software are fostered by OSGeo, including PostGIS, the spatial database extension for the PostgreSQL DBMS.

Some benefits considered for choosing QGIS include the fact that Academia and researchers around the world contribute with information and the development of plugins and tools to address the demands of many areas of science and engineering. Currently, QGIS 3 offers more than 900 tools, 25 toolboxes, and 1742 Python plugins.

3.2 GIS-Based Model of Overhead Transmission Lines

GIS is intensively used in a vast number of fields, including asset management of energy infrastructure. Public agencies and utilities worldwide have adopted GIS tools to manage energy infrastructure assets for quite some time. In many cases, these systems are linked to sensors, supervisory control and data acquisition (SCADA), and Enterprise Resource Planning (ERP) systems to include real-time or near real-time operational information to empower spatial analysis and decision-making [48]. The GIS interface developed in the context of this research used and generated the following spatial layers:

- **GIS layers consumed from other sources:**
  - ESRI basemap (satellite)
  - Country boundaries
  - State boundaries
  - Brazilian biomes
  - Brazilian bulk power grid (Existing base from EPE)
  - Substations
  - Line route
  - Support structures
  - Line spans
  - Conductors
  - Right of Way
  - TAESA outage data
  - OHTL wildfire footprint buffer
  - Line span wildfire footprint buffer

  - Fire Archive (hotspots) from SV-C2-250344 VIIRS C2 BR
  - Average wind velocity
  - Sun irradiance
  - Maximum temperature
  - Altitude
  - Census (Population counting) Hypsometric item curve
  - Clinogaphic curve
  - Slope orientation
  - Highways
  - Landsat 8 imagery
  - Stereoscopic Airborne Radar imagery
  - LiDAR points cloud

- **GIS layers generated from spatial analyses:**
  - GNDVI (Green Normalized Density Vegetation Index)
  - NDVI (Normalized Density Vegetation Index)
  - Basal area
  - Vegetation density
  - Vegetation volume
  - Land use
  - Risk of ignition (Berredo et al.)
  - Risk of propagation (Berredo et al.)
  - Risk of fire (Berredo et al.)
  - Wildfire per municipality

- Hotspot buffer (375 m x 375 m)
- Hotspots Vs. outage data per span
- Heatmap of Fire Archive (hotspots) from SV-C2-250344 VIIRS C2 BR
- Wildfire per month
- Line length per biome
- Line length per municipality
- Aggregated hotspot analysis (Enhanced Berredo et al.)
- Aggregated risk of fire (Berredo et al.)
- Hotspot buffer union (Enhanced Berredo et al.)

Every information obtained from GIS data in this research belongs to spatial analysis. The use of spatial layers enables the overlay analysis of, for example, hotspots contained in the OHTL footprint buffer, or how hotspot buffers intersect between themselves.

3.3 Remote Sensing and Surveys applied to Vegetation Classification

One of the operational challenges of modeling fire ignition and spreading is the requirement of heavy satellite image processing. The identification and classification of patterns such as vegetation coverage can be performed by working mathematically with different wavelengths of the electromagnetic spectrum. Thereby, satellite images can be manipulated in such a manner to result in products such as polygon shapes of different land coverages (e.g., forests, human footprint, urban spread, land occupation, encroachment, etc.)

When the identification of small objects is required (e.g., individual species of vegetation), the image source should provide a compatible resolution per pixel. Thus, the application may be limited by image resolution, and it should be considered in the result analysis. The highest resolution satellite imagery products commercially and freely available are currently offered in 25 cm and 10 m/pixel of spatial resolution, respectively. Therefore, currently available free imagery collections will result in minimum pattern identification of 10 m x 10 m objects or larger.

Images obtained by means of aircraft or drones may result in better resolution. However, the carrier must be equipped with multi-spectral cameras if remote sensing for pattern classification is required.

3.4 Chapter Summary

This chapter presents an overview of the current GIS technology available, what technologies were used in this research, what sources of GIS data were applied, and what GIS outputs were generated. This chapter also discussed the challenges and limitations of applying remote sensing in surveys applied to vegetation classification.

CHAPTER 4: PROPOSED NEW METHODOLOGY

4.1 Chapter Introduction

This chapter includes the tasks and deliverables and the explanation of the calculation steps of the new methods for assessing the risks of wildfire and fire-induced flashover as they relate to the overall contributions of the thesis.

As previously mentioned, this research explores methods for estimating the risk of line outage by wildfire-induced flashovers. The methods include estimating the risks of wildfire and the vulnerability of the line spans to flashover in terms of minimum clearance distance to vegetation. In addition, a new complete methodology is presented. It proposes estimating the risk of wildfire by doing the spatial analysis of the historical GIS dataset of hotspots using the Getis-Ord Gi* statistics. In order to estimate the vulnerability to wildfire-induced flashovers, it proposes enhancing the existing method proposed in Berredo et al. for estimating minimum clearance distances to vegetation and uses historical data of outages caused by wildfire-induced flashovers from a case study to adjust and validate the method. The case study was carried out on a 500 kV transmission line installed in northern Brazil, notably impacted by wildfires.

4.2 Research Plan for Proposed New Methods

4.2.1 Tasks and Deliverables

This subsection provides information on the proposed project tasks. This research was structured into six tasks and the thesis defense, each resulting in one or multiple deliverables to provide three research outcomes, including a novel approach to establish the criticality of outage for transmission lines exposed to wildfires.

As mentioned previously, this work's main goal consists of evaluating and comparing different methods of determining the risk of wildfire and the vulnerability to wildfire-induced flashovers by estimating safe clearance distances. This work may help engineers to design transmission lines resilient to wildfire-related risks, and to provide guidance on how to effectively address vegetation management to prevent wildfire-related outages.

4.2.1.1 Task 1 - Literature Review

A literature review was done to justify why further research on the relationship between wildfires and the performance of overhead power lines is needed. The topics below were gathered:

- Statistics of outages in the North American and Brazilian bulk power grids.
- Influence of the environment in the performance of OHTLs installed in the Brazilian territory.
- US and Brazilian standards and guidelines on overhead transmission line design and reliability aspects related to wildfire.
- Wildfire characteristics and prediction models for ignition and propagation
- Remote sensing and geoprocessing applied to wildfires
- Physics related to electrical breakdown strength of air

The milestone of this task was the overview report presenting the above-related topics.

4.2.1.2 Task 2 - Data Collection

This task seeks to identify and collect all data regarding GIS, line design, and operational performance required to establish the risks of wildfire and outage due to flashover using equations for minimum clearance distance to vegetation in accordance with NBR 5422, FAC-003-4, West & McMullan (1979), J.R. Fonseca et al. (1990), Lanoie & Mercure (1997) and Berredo A. et al. (2019). The data (not limited to) is listed below:

1. Classification of Risk of Wildfire.
    (a) Topographic Aspects (relief, bodies of water)
    (b) Biomes (Vegetation)
    (c) Remote Sensing of Wildfire (hotspots)
2. Line Vulnerability to Flashover.
    (a) GIS Data
        i. Topographic Aspects (relief, bodies of water)
        ii. Vegetation (average height, calorific power)
        iii. Remote Sensing of Wildfire (hotspots)
        iv. Line Outage (location)
        v. Line Structures and Conductors
    (b) Transmission Line
        i. Clearance Distances (to the ground and between conductors)
        ii. Conductors
        iii. Structures
        iv. Climate
        v. Line Outage (reports)

The milestone of this task was the overview report presenting the above-related topics.

4.2.1.3 Task 3 - Data Processing

This task aims to generate and normalize the GIS data and the transmission line information (design and operational performance) for use in the prediction models and in further calculations.

The milestone of this task comprises the delivery of the following datasets:

- Spatial Datasets: Risk of Wildfire
- Spatial Dataset: Line Vulnerability (Risk of Outage)
- Design and performance datasets and calculations of the overhead line object of this research

4.2.1.4 Task 4 - Application of Models

This task seeks to generate the risks of fire and flashover using the proposed models (where applicable) as listed below:

1. Risk of Wildfire (Ignition and Propagation)
   (a) CQFS-QGIS (Berredo et al.) [17]
2. Historical Data of Remote Sensing of Wildfire (10 years)
   (a) Generation of Land Polygonization
   (b) Hotspot Analysis using Getis-Ord Gi*
3. Line Vulnerability - Clearance Distance Calculations
   (a) NBR 5422 [21]
   (b) FAC-003-4 [20]
   (c) Berredo et al. [17]
   (d) Fonseca et al. [2]

   (e) Lanoie & Mercure [19]

   (f) FAC-003-4 corrected by West & McMullan [20, 18]

The milestone of this task comprises the delivery of the following datasets:

- GIS shapefiles and spatial datasets (where applicable) of classification of risk of wildfire –Berredo et al.
- GIS shapefile and spatial dataset (where applicable) of hotspots analysis of occurred wildfire using Getis-Ord Gi* Correlation method
- Calculation results of clearance distance per the proposed methodologies

4.2.1.5 Task 5 - Model Evaluation and Results

This task aims to analyze and compare results of the risk of wildfire from Berredo et al. and Hotspot Analysis and the line vulnerability to flashover using approaches stated in NBR 5422, FAC-003-4, Berredo, et al., Fonseca et al., Lanoie & Mercure and West & McMullan), with existing line information and performance.

1. Evaluation and comparison of results from the risk of wildfire

   (a) Berredo et al.

   (b) Hotspot Analysis based on Getis-Ord Gi*

2. Evaluation and comparison of results from line vulnerability to flashover

   (a) NBR 5422 [21]

   (b) FAC-003-4 [20]

   (c) Berredo et al.[17]

   (d) Fonseca et al. [2]

   (e) Lanoie & Mercure [19]

(f) FAC-003-4 corrected by West & McMullan [20, 18]

The milestone of this task comprises the delivery of the following :

- Correlation analysis of wildfire events between Berredo et al. and hotspot analysis
- Calculation results and comparison of clearance distance from the proposed methodologies.
- Correlation analysis of line vulnerability between proposed models and historical failure data of the Transmission Line 500 kV Colinas—Ribeiro Gonçalves—São João do Piauí—Sobradinho.

4.2.1.6 Task 6 - Documentation and Report

This task intends to produce a compendium of detailed information, including consulted literature, reference data, normalized datasets, maps, illustrations, calculations, and finally, a structured thesis connecting all research steps, findings, results, and conclusion.

The milestone of this task comprises a written report in the format of a thesis. Figure 4.1 shows what data and models are collected, processed, applied, and evaluated for each task of this research.

4.2.2 Project Outcomes

Table 4.1 shows the project outcomes planned.

4.3 Model of Risk of Wildfire - Enhanced Berredo et al.

This research seeks to propose an alternative model to classify the risk of wildfire. Instead of a two-step approach proposed by Berredo et al. [17], and FlamMap [42][44] and Chuvieco[23] where the user is required to identify both risks of ignition and propagation of fire to obtain the risk of fire, this proposed new method looks exclusively into statistically significant hotspots generated from a large dataset of active

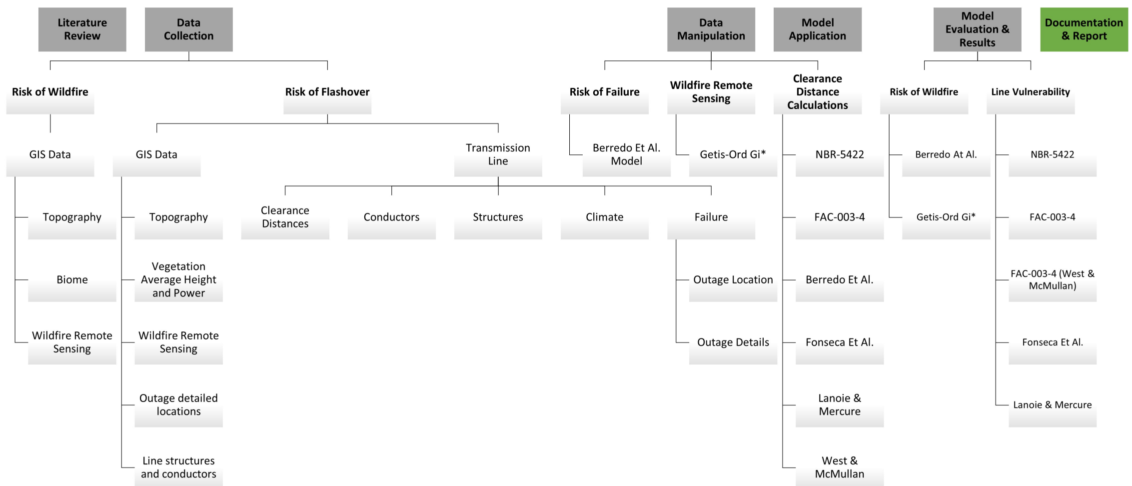

Figure 4.1: Detailed application of data and models.

Table 4.1: Project outcomes.

Outcome	Outcome Name	Outcome Description	Metric
1	Correlation of Risk of Fire	Results of correlation between Berredo et al. vs. Hotspot Analysis (Getis-Ord GI*).	Threshold: 90%
2	Correlation of Vulnerability to Flashover	Results of correlation between Berredo et al. and: NBR 5422, FAC-003-4, Fonseca et al., Lanoie & Mercure, and West & McMullan.	Threshold: 90%
3	Enhanced Methodology Proposed	Results of applying both best confidence levels for wildfire and vulnerability to flashover.	Threshold: 90%

fire obtained by satellite imagery. This research used ten years of data (2012 to 2022) from the Visible Infrared Imaging Radiometer Suite (VIIRS) Suomi NPP/NOAA-20 satellite. The data is available on the Fire Information for Research Management System (FIRMS)[33] website managed by NASA.

This step results in the classification of the risk of wildfire for each line span of the analyzed section of the transmission line. The risk of fire is classified into three qualitative risk levels, Low, medium, and high risk, which represent confidence levels of 10% and under, 10 to 50%, and above 50% of occurrence of fire, respectively.

Considering uncertainties such as the spatial accuracy of the remote sensing, and factors that influence fire spread, this model accounts for the significant hotspots in a buffer of 2 km wide around the line route. As previously mentioned, a buffer of 10 km is adopted in Berredo et al. 2.3.1. Therefore, in order to provide normalized means of comparison with the proposed model, only the results contained inside a 2 km wide buffer were considered. Figure 4.2 shows the dimensions of the buffer (2,000 m), right of way (70 m), and outer phases spacing (10 m), of the case study.

4.3.1 Spatial Resolution of the VIIRS Satellite Sensor

The proposed model of risk of wildfire uses data exclusively from the satellite VIIRS Suomi NPP/NOAA-20. That sensor was effectively available on January 20$^{\text{th}}$, 2012. Thus, the VIIRS Suomi NPP/NOAA-20 completed 10 years of fire data in January 2022.

The method uses higher-resolution fire data in comparison to the Berredo et al. method. While the Berredo et al. method adopted post-processed fire data with 1 km spatial resolution from the satellite MODIS, the proposed new method uses 375 m spatial resolution hotspot data obtained from the Polar-orbiting Active Fire Detection of the satellite VIIRS Suomi NPP/NOAA-20. This is of high importance since the pixel size represents the size of the hotspot.

Each hotspot is located in the center of a pixel containing one or more fires or

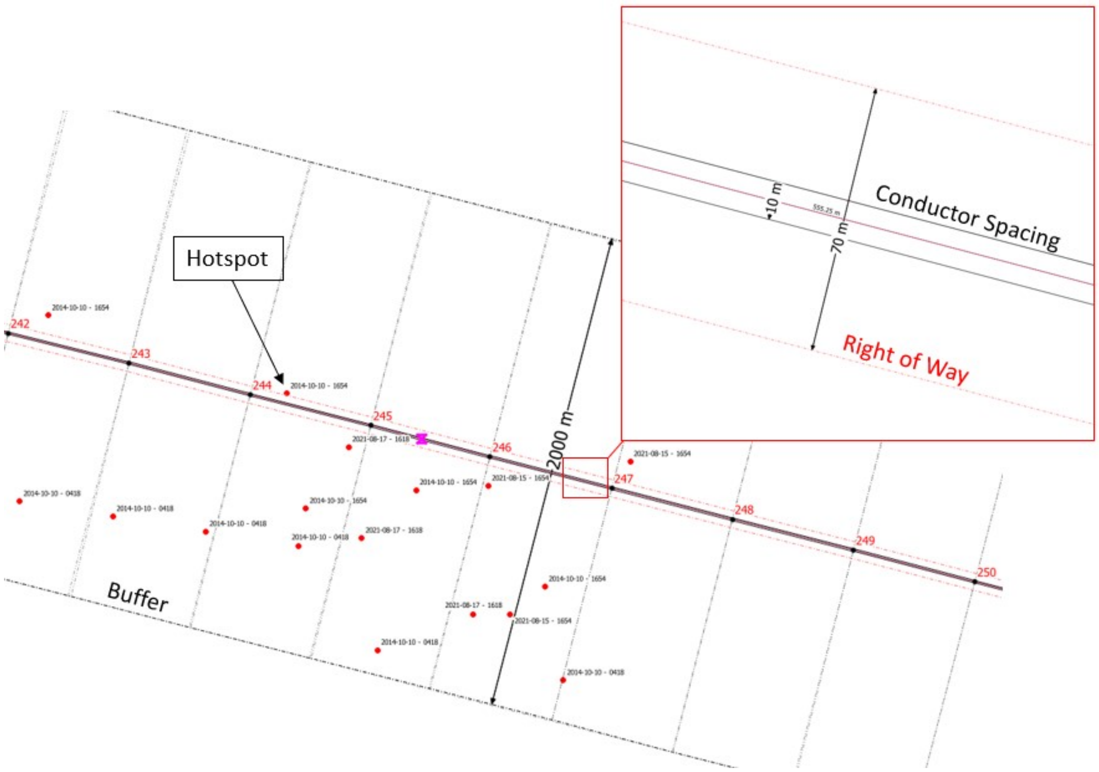

Figure 4.2: Physical Boundaries for the classification of risk of wildfire.

other thermal sources such as thermal power plants or volcanoes. A hotspot detected by the MODIS sensor will measure 1 km x 1 km, while VIIRS will measure 375 m x 375 m [58]. A large wildfire will be sensed as a sequence of aligned hotspots where each one is located in the center of each pixel.

Figure 4.3 shows the spatial resolution of the sensors MODIS and VIIRS. Three scenarios are shown for a total area of four pixels. For MODIS, each quadrant (or pixel) measures 1 km x 1 km, while VIIRS measures 375 m x 375 m. In the event of the detection of fire anywhere inside the area corresponding to one pixel, it will be represented by a point with the coordinates of the center of the quadrant (i.e. pixel). When two or more fire events are detected in the same quadrant, it will be translated into a single point with the coordinates of the center of the quadrant. When a major fire is detected in an area superior to a single quadrant, each quadrant with detection of fire will be populated with a point in the center [58].

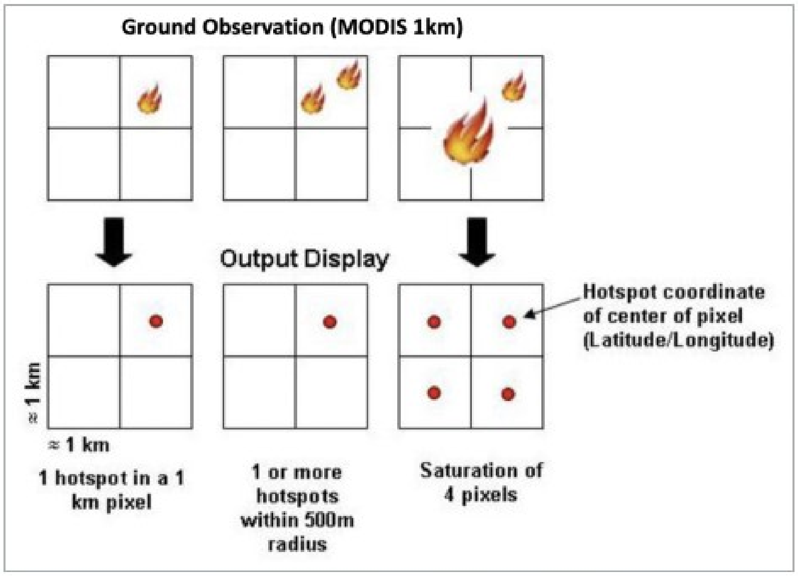

(a) Modis Spatial Resolution

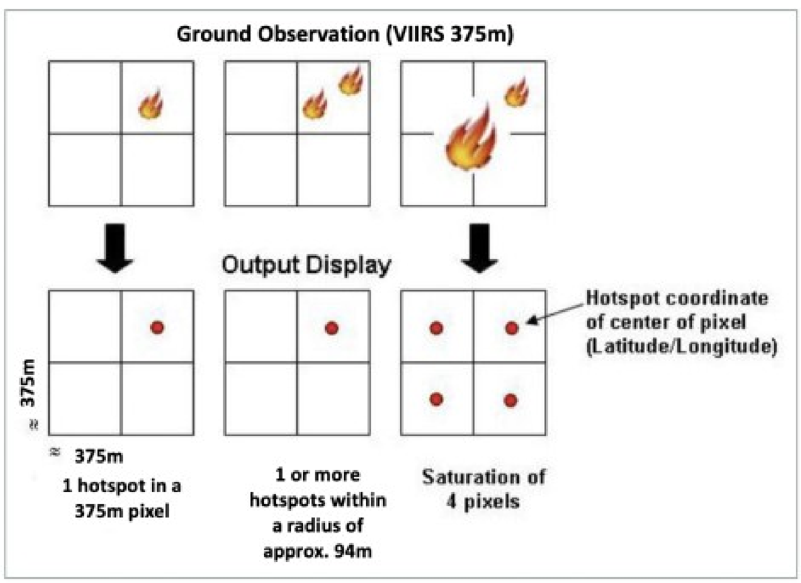

(b) VIIRS Spatial Resolution

Figure 4.3: Comparison between MODIS and VIIRS sensor Resolutions [58].

Figure 4.4 shows the comparison of spatial resolution between the 1 km Terra/MODIS sensor (left), the 375 m VIIRS sensor (center), and the 1 km Aqua/MODIS (right) sensor. The higher spatial resolution of VIIRS enables more accurate wildfire detection than MODIS Terra/Aqua satellites.

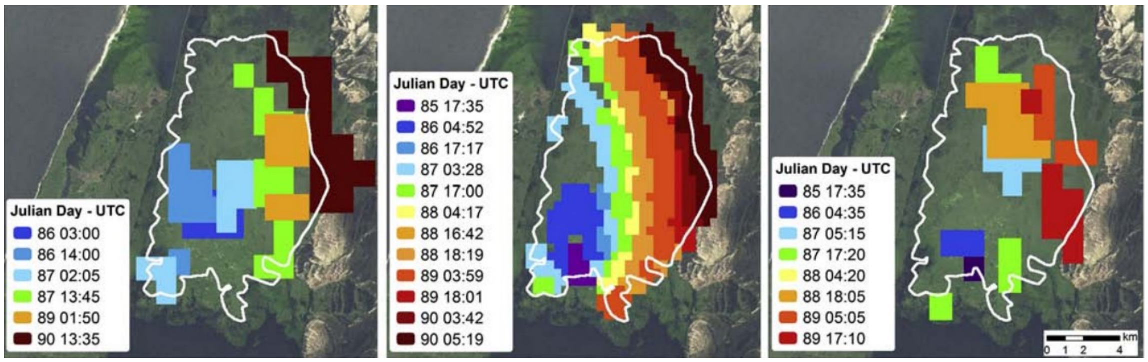

Figure 4.4: Daily fire spread detected by the sensors Terra/MODIS (left), VIIRS (center), and Aqua/MODIS (right) at the Taim Ecological Reserve in southern Brazil (-32.7°lat, -52.55°lon)[8]

Figure 4.5 shows the detection and post-processing of several wildfire events in a line section of the ATE 2 OHTL. Note the spatial resolution of 375 m x 375 m (green squares) and the related hotspot coordinates in the center of the quadrants (red points).

The new method assumes the number of hotspots in a span as the maximum value of overlapping green squares in the slice of buffer corresponding to the line span. The number of overlapping squares is populated in the attribute table of each span buffer and used as an input parameter for the spatial statistic tool to perform the hotspot analysis.

4.3.2 Getis-Ord GI* Hotspot Analysis

The Gi Statistics was proposed by Artur Getis and J.K. Ord to “provide researchers with a straightforward way to assess the degree of spatial association at various levels of spatial refinement in an entire sample or in relation to a single observation.”[59] The tool identifies areas where high or low values cluster in space.

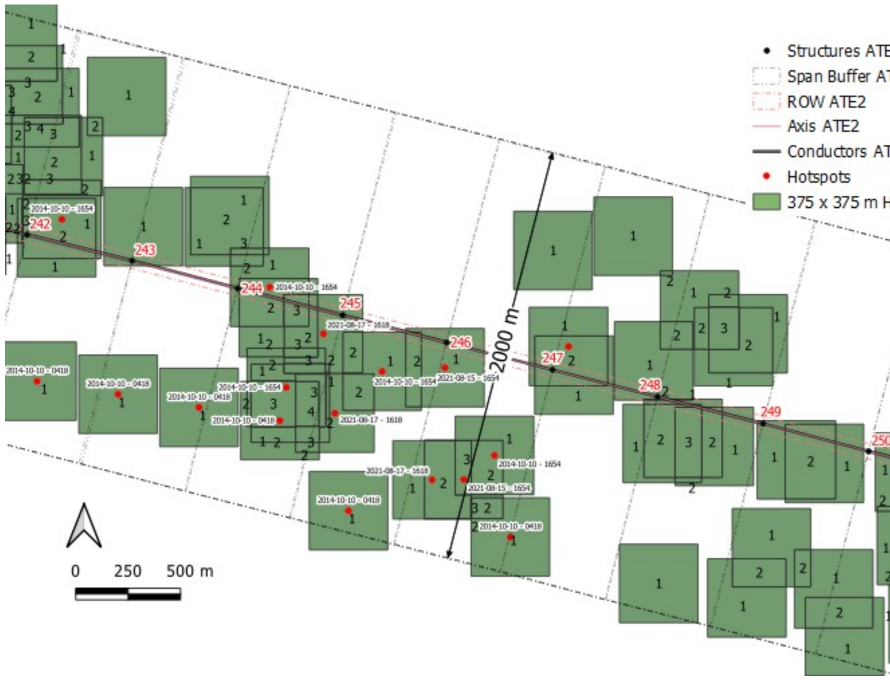

Figure 4.5: Hotspot detection size (375 m x 735 m).

This method of spatial analysis has been largely used to identify spatial correlation in many different investigations. For the application proposed in this thesis - modeling of risk of wildfire - the tool measures the relationship between the concentration of weighted hotspots in a given line span and all other weighted line spans included within a radius of distance d from the original weighted span. The standard score (Z-Score) for Getis-Ord Gi* is given by (4.1)

$$Z(Gi^{*}) = \frac{\sum_{j=1}^{N} \cdot w_i j \cdot x_j - \bar{z} \sum_{j=1}^{N} \cdot w_i^2 j \cdot x_j}{\sqrt[s]{\frac{N \sum_{j=1}^{N} \cdot w_i^2 j - \sum_{j=1}^{N} \cdot w_i j}{N-1}}} \tag{4.1}$$

where $w_i j$ is the spatial weight between observations i and j. $w_i j$ is a binary (one-or-zero) with $w_i j = 1$ if observations j is within a threshold distance d of observation i and 0 otherwise. N is the total number of line spans in the area of analysis (line section). x is a weight associated with each region.

The proposed model of risk of wildfire exploits the spatial statistic tool to identify patterns of wildfire by resolving z-scores and p-values of statistically significant wildfires within neighboring events. A cluster of wildfire spots should have a high value and be surrounded by other events with high values to be statistically significant.

The Z-score measures how many standard deviations (σ) from the mean value (μ) of the entire hotspot dataset a particular line span is, and the P-Value measures the probability that a given hypothesis (Z-score) occurs.

Since the density of hotspots alone cannot tell if the cluster is statistically significant, to address this issue, Getis-Ord Gi* proportionally compares the local sum of a cluster of hotspots and its neighbors to the sum of all wildfire events. When the local sum is very different from the expected result, and when that difference is too significant to be the result of random chance, a statistically significant z-score results [40].

The interpretation of the results requires both Z-Score and P-Value. The combination of very high or very low Z-Scores, associated with very small p-values, are found in the tails of the normal distribution. When you perform a feature pattern analysis and it results in small p-values and either a very high or a very low (negative) Z score, this indicates it is very unlikely that the event analyzed represents a null hypothesis.

For the classification of risk of wildfire, statistically significant line spans will have a positive standard deviation (Z-Score), which means that the more intense the clustering of wildfires in a line span, the higher the Z-Score will be. Line spans with lower occurrences of wildfires are less statistically significant. Therefore, it will result in negative values of Z-Score.

Figure 4.6 shows a Gaussian distribution chart where the mean value of risk of wildfire is represented by mu in the vertical axis at the center of the chart. The additional vertical lines to either side of the chart represent intervals of standard deviation (σ). As shown, the closer to the center line, the more likely a wildfire will occur.

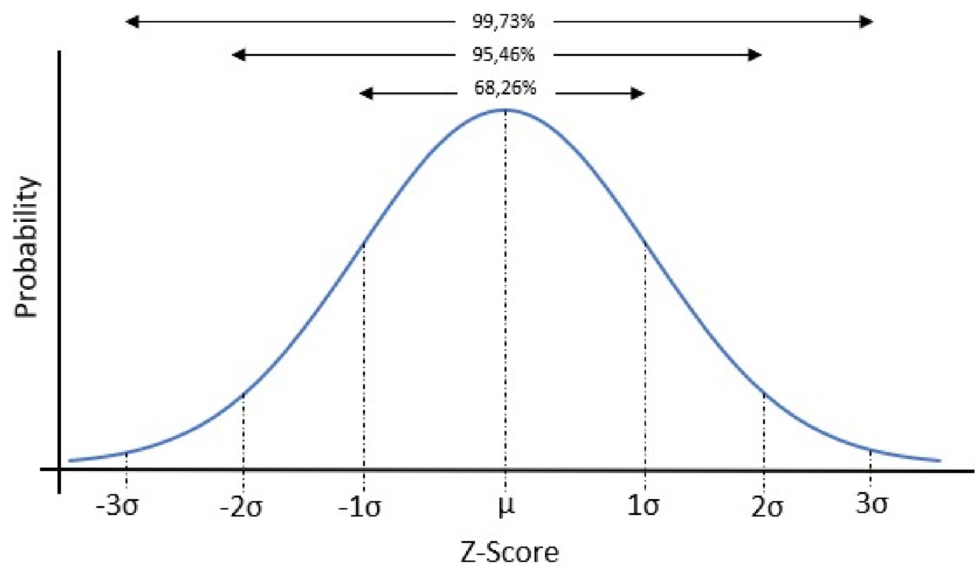

Figure 4.6: Gaussian Distribution chart

4.3.3 Risk of Wildfire - QGIS Classification Process

This subsection explains how the proposed modeling of risk of wildfire is processed using the QGIS software. QGIS 3.16.14 and the plugin Hotspot Analysis were used in this research.

The research adopted the Projected coordinate system for Brazil, between 48Â°W and 42Â°W, and the DATUM SIRGAS 2000 (EPSG 31983) in order to standardize and facilitate the calculations of distance. Spatial features (GIS layers) using different coordinate systems (e.g., geographic coordinate system) and *datum* were transformed into the adopted system (EPSG 31983). The following sequence describes the step-by-step procedure to apply the model of risk of wildfire using Getis-Ord GI*.

1. **Load map layers**

   The spatial features required for the analysis (structures, line spans, ROW, and hotspots) are loaded into the software.

2. **Filter relevant hotspots**

   The hotspot layer contains 15 attributes, including the class of pixel (hotspot) detected. According to [3], the VIIRS active fire detection algorithm can classify a hotspot into 10 different fire masks as listed in Table 4.3. This research adopted only 8-and-9 hotspot classes (nominal and high-confidence fire pixels) in bold.

Table 4.3: Hotspot fire mask classification.

Pixel Class	**Definition**
0	Not processed
1	Bow-tie deletion
2	Sun glint
3	Water
4	Cloud
5	Land
6	Unclassified
7	Low confidence fire pixel
8	**Nominal confidence fire pixel**
9	**High confidence fire pixel**

3. **Create area of analysis**

   A 2 km buffer around the line axis is created using the "buffer" tool.

4. **Selection of hotspots in the buffer of analysis**

   For the sake of computational performance, the hotspots of interest are filtered using the "selection" tool. Only the hotspots included in the 2 km buffer are considered. The hotspots located outside the buffer are discarded from the analysis.

5. **Generate 375 m wildfire area (pixel buffer)**

   Using the "buffer" tool, a squared buffer of 375 m x 375 m is created around each point of hotspot detection to represent the wildfire resolution. This is important because the hotspot data is the centroid of a square of approximately 375 m. Note that the spatial data should be previously converted to metric units in order to facilitate the generation of the buffer size.

6. **Indexing of hotspot data**

   The hotspot buffer (square) layer is spatially indexed in order to speed up the computational processing time.

7. **Create a Unique identity number (UID) of hotspot buffers**

   Using the "field calculator" tool, a new numerical attribute data of unique identity number (UID) is created in order to identify each hotspot buffer. The function "@rownumber" is used in the field calculator tool to populate the UID attribute.

8. **Count hotspot buffer overlaps**

   The tool "Vector overlay" is used to count the number of overlaps of square buffers. The field calculator is used for this step with the function below:

   $count(``UID'', group\_by := geom\_to\_wkt(\$geometry))$

   Overlapping hotspots represent areas with a higher frequency of fire events (see Figure 4.7).

9. **Perform Getis-Ord Gi* hotspot analysis**

   The "hotspot analysis" tool is used to resolve the z-scores and p-values of statistically significant wildfires

10. **Merge hotspot buffer with line span buffer**

    The "Union" tool is used to merge the hotspot buffers (layer "buffer_span_ATE2") with the line span buffer (layer "hotspot_squared_buffer"). This step verifies the overlaps hotspot and creates new geometries from overlapped and non-overlapped geometries. Figure 4.7 shows an example of a geometry created from two overlapped fire buffers.

11. **Populating the z-score into the span buffer**

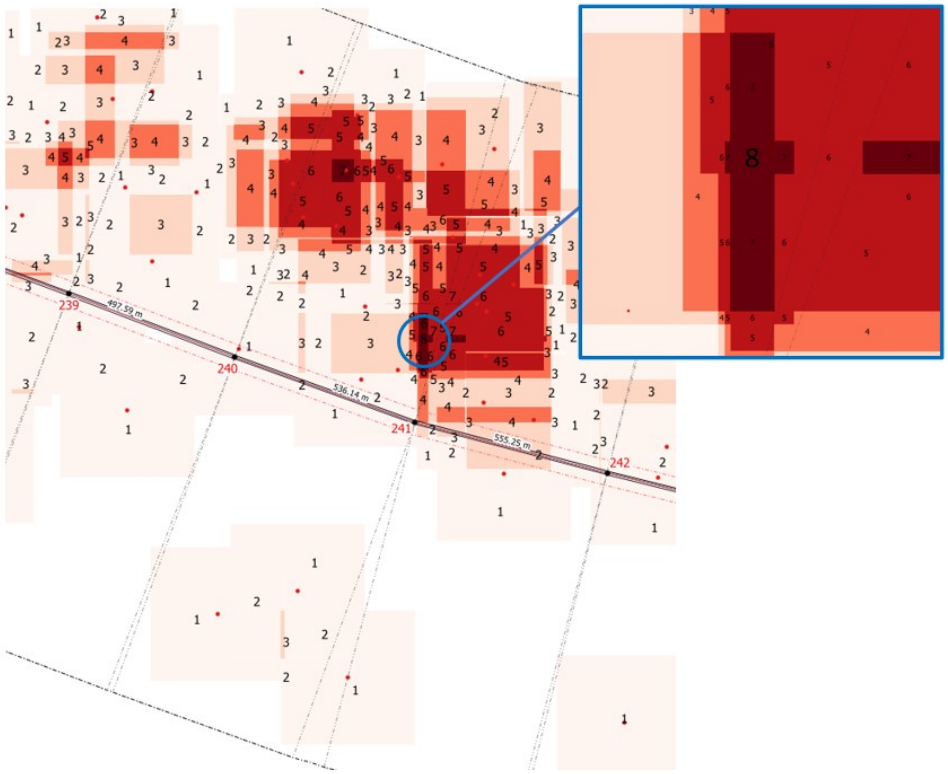

Figure 4.7: Identification of overlaps at span.

Using the tool "Aggregate," the information of the maximum z-score of a hotspot buffer is populated in the span buffer. The transferred attribute of the z-score is the confidence of the risk of wildfire in a particular area. The "Aggregate" GIS tool groups the value by "UID" and uses the maximum value of Z-Score to populate the area.

12. **Merge attributes by location**

    Attribute data from layer "hotspot buffer" including Z-score and P-value, are copied to layer "span buffer" where layers intersect.

    Figure 4.8 shows the final result of risk of wildfire for a line section of the OHTL. Note that the risk of wildfire is classified into four confidence levels.

13. **Classification of risk of wildfire**

    As mentioned previously, this thesis proposes a classification for the risk of wild-

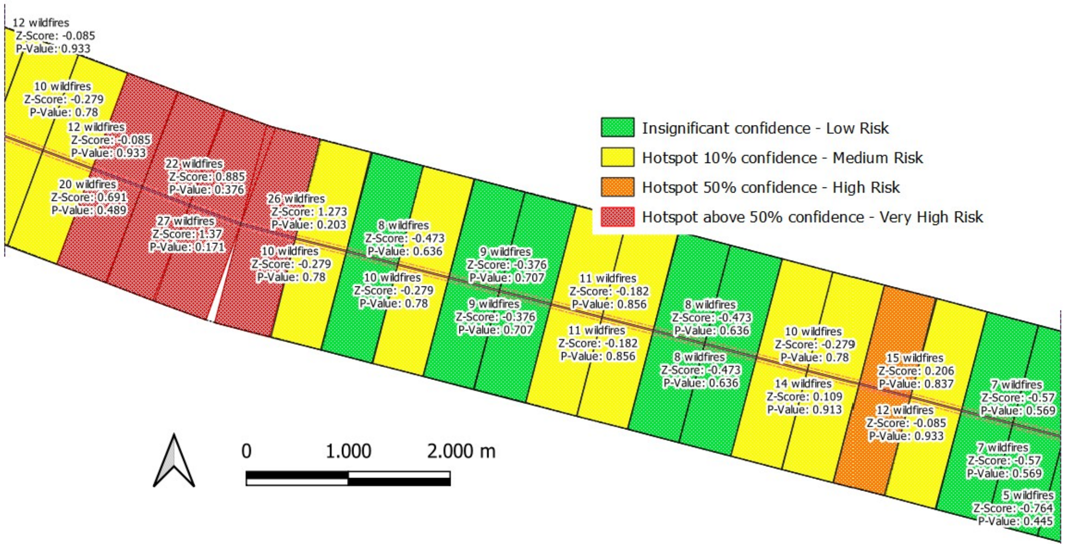

Figure 4.8: Classification of risk of wildfire.

fire based on the statistical confidence level. The process listed above populates each line span with the standard deviation (Z-Score) and probability (P-Value) of wildfire. The quantitative results represented by ranges of Z-scores and P-values were translated into risk classes in order to enable the comparison of results with the methodology proposed by Berredo et al., as listed below:

- **Low risk of wildfire** - Insignificant risk of wildfire represented by a Z-score over -0.28.
- **Medium risk of wildfire** - up to 10% confidence level represented by Z-scores ranging from -0.28 to 0.124.
- **High risk of wildfire** - up to 50% confidence level represented by Z-scores ranging from 0.125 to 0.673.
- **Very high risk of wildfire** - confidence level above 50% represented by Z-scores above 0.674.

When the absolute value of the z-score is large, and the probability is small, the observed spatial pattern is probably too unusual to be considered significant, and the p-value will be small to reflect this. Although not relevant to the desired risk analysis, it is important to mention that unusual scenarios could represent interesting situations. For example, a region identified with a high risk of wildfire over the past years that suddenly stops to present hotspots could be explained by a change in land use, such as native bushland converted into agricultural land.

4.4 Model of Risk of Wildfire-Induced Flashover (Vulnerability)

This thesis proposes enhancing Berredo et al. [17] vulnerability model by including additional flame and vegetation height parameters into the MVCD calculation in order to address the unmanaged portions on the sides of the ROW. The new model adjusts the equation of MVCD (See 5.8) to suit the safe clearance distance identified in the data-driven analysis performed in the 108 line outages caused by wildfire-induced flashovers in the ATE II OHTL.

During wildfires, a proper clearance distance to vegetation may prevent OHTLs from flashing between conductors or the conductor and ground. Studies have proposed equations to determine the minimum vegetation clearance distance (MVCD) to OHTL. However, no current standards have addressed the calculation of MVCD to prevent fire-induced flashovers. Moreover, from the references studied in this thesis, only Fonseca et al.[2] used line outage analysis to validate the fire-induced flashover model. Other studies explored in this thesis, West & McMullan [18], Lanoie & Mercure [19], and Sukhnandan [16], used laboratory testing to investigate the parameters that may influence the occurrence of flashovers and to determine minimum approach distances to prevent fire-induced flashovers.

Berredo et al.[17] investigates the vegetation management practiced on a specific OHTL (ATE II) installed across 923 km in northern Brazil. Its proposed vulnerability model assumes that the vegetation under the conductors is managed, allowing for a 10 cm high vegetation cover to prevent soil erosion. Thus, since nearly no vegetation is left under the conductors, flames are not considered relevant in the MVCD equation.

It is important to mention that since the ATE II line is in operation, the clearance distances cannot be increased by means other than vegetation management. Assuming the occurrence of wildfire, the only means of preventing outages related to wildfire-induced flashovers is by removing the available fuel, which increases the vertical clearance distance to the conductors by shortening the vegetation under the conductors.

For obvious reasons, the maximum vertical clearance achievable is limited to the distance between conductors and bare ground. Furthermore, the environmental permit of that particular installation constraints the vegetation management to a 28 m strip (14 m to each side from the axis of the right of way). Figure 4.9 illustrates the typical support structure used in ATE II with dimensions of minimum clearance distance. Because of the environmental permit constraints, vegetation management results in about 11.50 m of clearance distance from the unmanaged vegetation to the outer conductors.

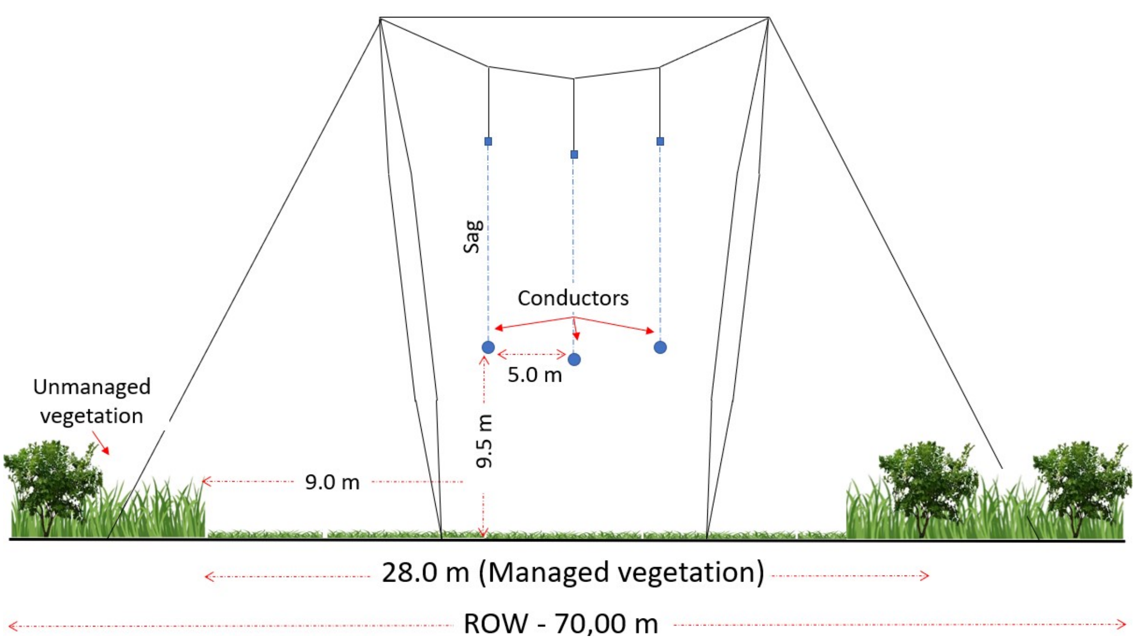

Figure 4.9: Illustration of the vegetation management setup adopted in ATE II

In worse scenarios, environmental permits of other overhead lines forbid vegetation management, resting no solution to mitigate wildfire-induced flashovers other than elevating the conductors. Engineers can improve the reliability and resilience of new transmission lines by adopting safe clearance distances in the design stage. This approach can also be implemented in those ROWs with forbidden or constrained vegetation management.

The original equation shown in 2 proposed in Berredo et al. [17] calculates the breakdown strength of air associated with a minimum clearance distance at elevated temperatures to prevent flashover incidents. The equation is derived from a method of calculating the breakdown voltage of air between sphere electrodes. However, it varies the air density factor in order to reflect the estimated gradient of temperature from wildfires in the Cerrado biome for the existing conductor height above the vegetation in midspan (see algorithm 3). Note that the equation presented in 4.4 differs from 2.8 as it adopts the result of peak voltage instead of the rms voltage.

Algorithm 3 Berredo et al. [17] - Calculation Steps

1: Calculate the Air Density for phase-to-ground via (4.2).

$$\delta(pg) = \frac{\rho T_0}{\rho_0 \cdot \left(273 + \frac{\left(\sum_{n=1}^{h}\right) \cdot T_s \cdot (h^{-0.992})}{h}\right)} \tag{4.2}$$

2: Calculate the Air Density for phase-to-phase via (4.3).

$$\delta(pp) = \frac{\rho T_0}{\rho_0 \cdot (273 + T_s \cdot (h^{-0.992})} \tag{4.3}$$

3: Calculate the Breakdown Strength of Air (4.4).

$$V_{r(peak)} = \frac{22.7 \cdot \delta \cdot 12.5 \cdot \left(1 + \frac{0.54}{\sqrt{\delta \cdot 12.5}}\right) \cdot \frac{h}{12.5}}{0.25 \cdot \left(\frac{h}{12.5} + 1 + \sqrt{\left(\frac{h}{12.5} + 1\right)^2 + 8}\right)} \tag{4.4}$$

In (2.7): δ is the air density correction factor (pg and pp corresponding to phase-to-ground and phase-to-phase respectively), ρ is the atmospheric pressure on place (mm/HG), ρ_0 is the reference atmosphere pressure (760mm/HG), T_0 is the reference temperature (293 K), T_s is the air temperature, and h is the clearance between the conductor and the top of the vegetation or flame.

The proposed new methodology in this thesis considered the maximum clearance distance found in the analyzed dataset of outages to back-calculate the additional fire parameters, which were not considered in the original equation proposed in Berredo et al.[17] The new equation also considers the height of the unmanaged vegetation present beyond the 28-m managed corridor. The flames resulting from the burning of the unmanaged vegetation can fill the air gap between the unmanaged vegetation and the outer conductor.

The new model assumed that for the ATE II designed minimum clearance distance, on average, wildfires would result in a temperature of around 212°C in the air gap between conductors and ground for a free air gap (with no flames spanning) of 8 m, resulting in the air density correction factor of 0.56. This air gap distance considers 3 m of vegetation height and 2 m of flame height. It also assumed that under the estimated fire conditions, the air gap between phases would be exposed to a temperature of around 80° C.

In (4.3): $V_{r(peak)}$ is the peak voltage associated with the breakdown strength of air, ρ_0 is the reference atmosphere pressure (760mm/HG), T_0 is the reference temperature (293 K), and h is the vertical clearance between the conductor and the top of the vegetation.

Subsection 4.4.1 shows that most outage events involved the outer phases, which justifies the concern with the unmanaged side vegetation.

4.4.1 Line Outages Dataset

The failure mode investigation relied on a 9-year outage dataset obtained exclusively from the line of the case study, comprising 108 fire-induced-related outage events. The dataset includes information on existing clearance distances, vegetation management statuses, phase conductors involved, predominant vegetation type, and span location in order to identify patterns that are likely to influence the failure mode. Figures 4.10 and 4.11 show the footprint of outage events by transmission line distributed over the years and their frequency per month. Several important pieces of information were obtained from these charts, as listed below:

1. No outage events are associated with the third section of the transmission line (TL 500 kV São João do Piauí - Sobradinho)

2. Outage events are predominant in the TL 500 kV Colinas - Ribeiro Gonçalves until 2017, when the TL 500 kV Ribeiro Gonçalves - São João do Piauí started to lead the number of outages.

3. Number of wildfires in the line sections between Colinas and São João do Piauí are 10 times higher each compared to the line section between São João do Piauí and Sobradinho.

4. The distribution of fire-induced outage events is concentrated between August and October, corresponding to the dry season in northern Brazil.

5. Outage events are more frequent in the TL 500 kV Ribeiro Gonçalves - São João do Piauí. However, there is a slight predominance of outages in the TL 500 kV Colinas - Ribeiro in September.

6. Outages involving side conductors are predominant. Side conductors are more exposed to heating and higher flames due to the proximity with the unmanaged vegetation, resulting in more flashovers involving those phases and flashovers between the outer and middle phases.

Figures 4.12 and 4.13 show that most events involved two phases

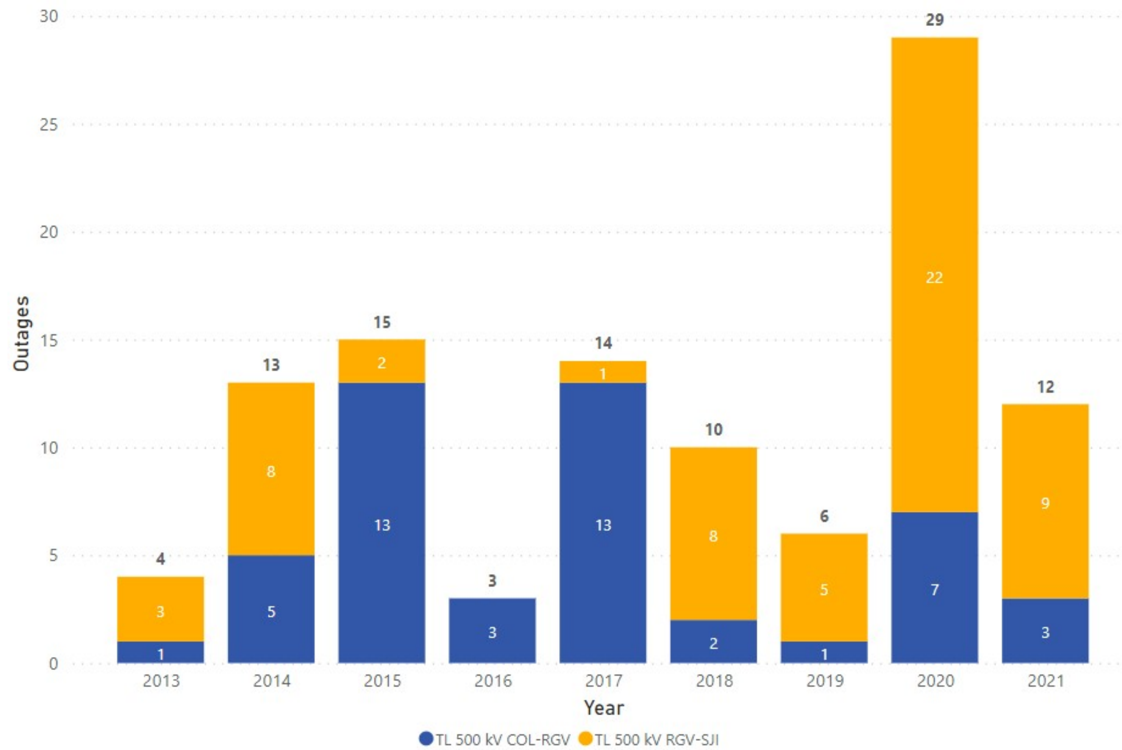

Figure 4.10: Number of outages per year

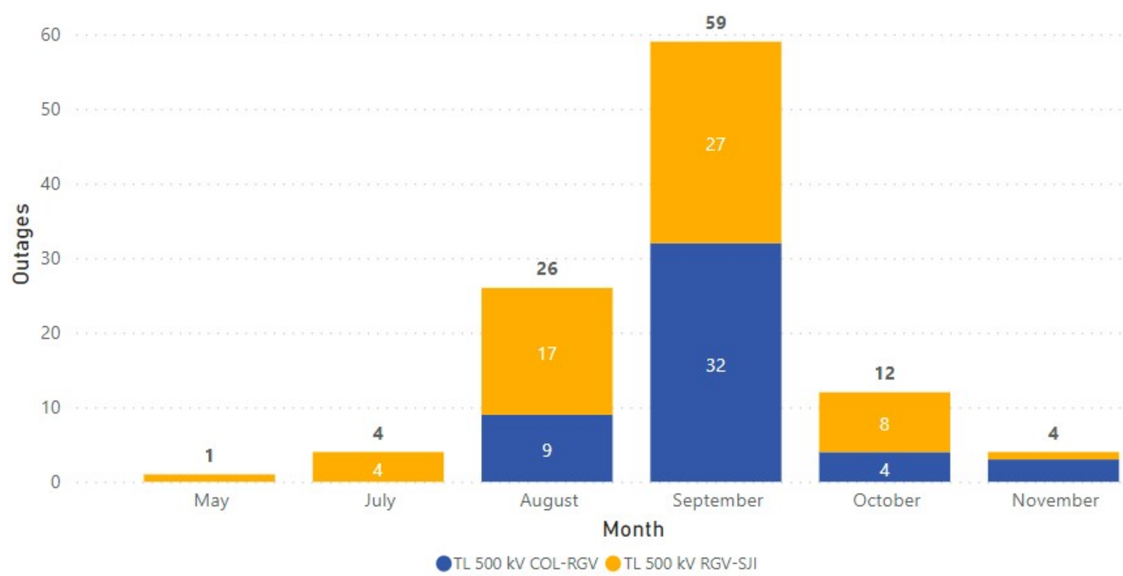

Figure 4.11: Distribution of outage events per month

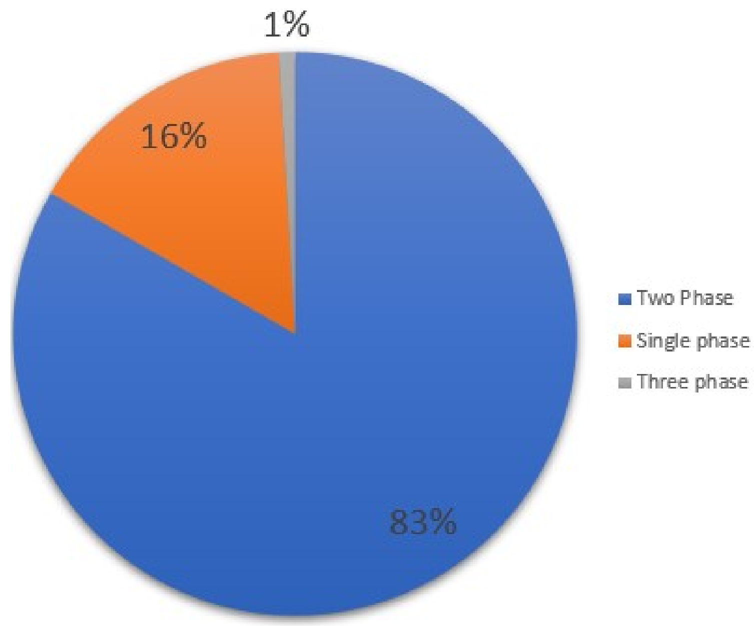

Figure 4.12: Number of phases involved on outage

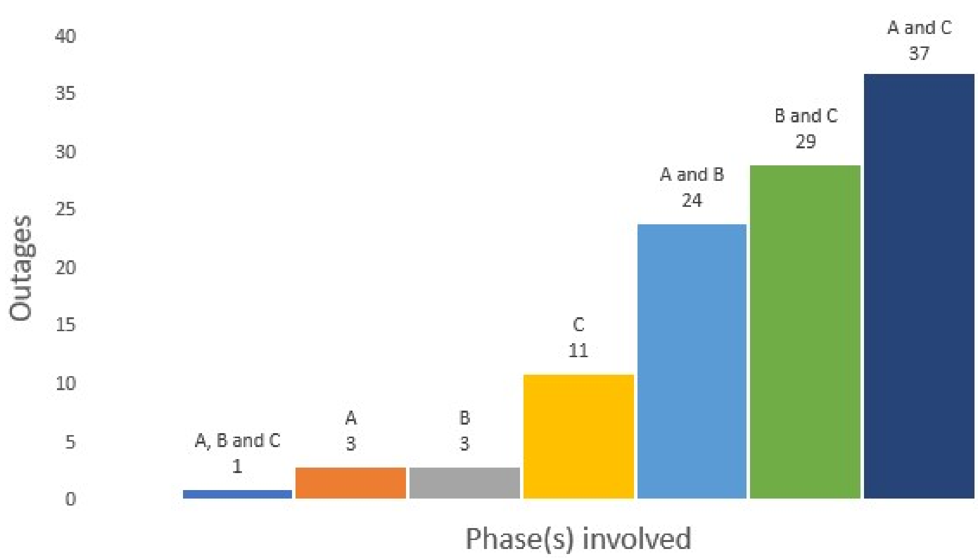

Figure 4.13: Phases involved on outage

According to the utility, the change in performance between the two transmission lines from 2018 is due to changes in the selection of critical line sections for vegetation management and in seasonal wildfire social-environmental campaigns.

Each of the line spans identified was assessed in combination with the design reports of ATE II. Figure 4.14 shows the design profile of the line span between the support structures 616 and 617. The green line represents the conductor's catenary, and the red line represents the offset of the minimum clearance distance to the ground. The dimension in blue color in the mid-span identifies the critical clearance distance (sag) of 9.42 m between conductors and bare ground. The hatched area shows the original vegetation profile violating the MVCD when routing the overhead line.

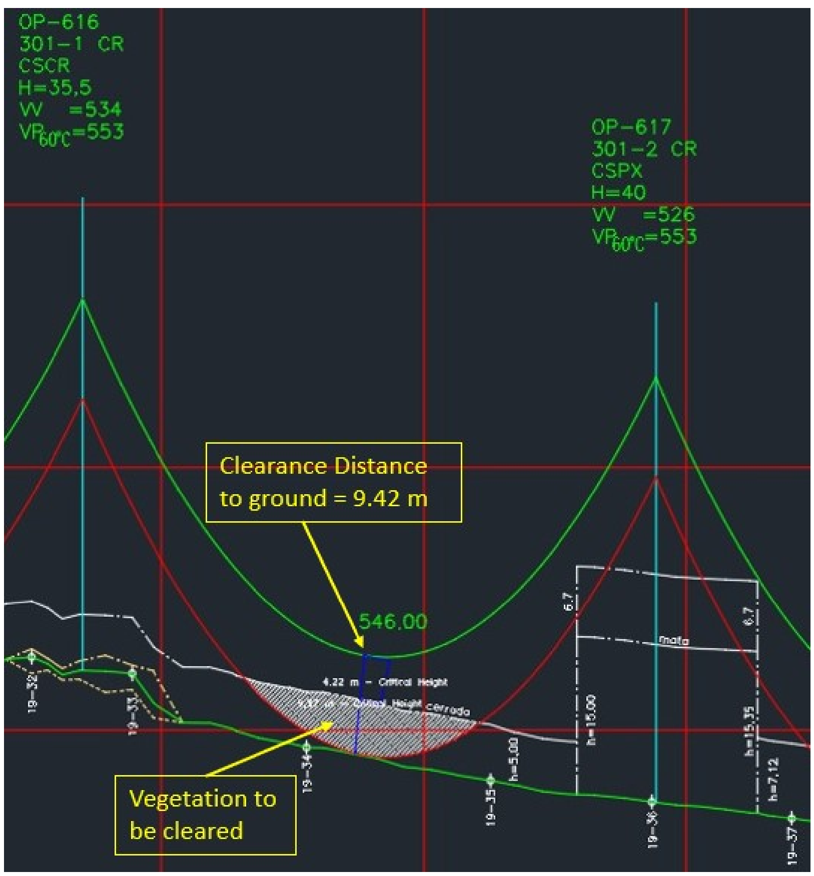

Figure 4.14: Example of profile drawing assessed in the outage investigation to obtain the critical clearance distance to vegetation.

The investigation also verified the correlation between hotspots and outages as part of the data validation. The complete dataset of outages can be found in Appendix A. The descriptive statistics listed in Table 4.4 were obtained from Appendix A. The analysis of outages includes the maximum clearance distances of all line spans after vegetation management and those which involved flashover of multiple phases.

Table 4.4: Outage data - Descriptive Statistics.

Span Data	**Result**
Total Number of events	108
Number of events (One Phase Managed)	14
Number of events (Multiple Phases Managed)	74
Average Height	9.84 m
Average Height (Single Phase Managed)	10.18 m
Average Height (Multiple Phases Managed)	9.78 m
Std. Error	0.058 m
Std. Error (Single Phase Managed)	0.24 m
Std. Error (Multiple Phases Managed)	0.088 m
Variance	0.30 m
Variance (Single Phase Managed)	0.82 m
Variance (Multiple Phases Managed)	0.70 m
Std. Dev.	0.54 m
Std. Dev. (Single Phase Managed)	0.90 m
Std. Dev. (Multiple Phases Managed)	0.84 m
Minimum	9.10 m
Minimum (Single Phase Managed)	9.38 m
Minimum (Multiple Phases Managed)	9.10 m
Maximum	16.80 m
Maximum (Single Phase Managed)	12.80 m
Maximum (Multiple Phases Managed)	10.83 m

Only one flashover was considered an outlier. The particular line span, with a clearance distance of 16.8 m, was not managed at the time of the wildfire event. The data analysis showed that only line spans with clearance distances below 12.48 m resulted in flashovers where vegetation management was performed. In addition, outages involving flashover of simultaneous phases occurred in managed line spans with clearance distances below 10.83 m. Figures 4.15 and 4.16 show the histograms of outage events by clearance distance of managed single and multiple-phase.

Note that single-phase and multiple-phase outages present different clearance distances. Outages involving two or three phases required lower clearance distances to flashover. From 14 single-phase outages, 10 events flashed at 10.52 meters of clearance distance, and 24 of the 74 outages involving multiple phases required 9.53 m to cause a flashover.

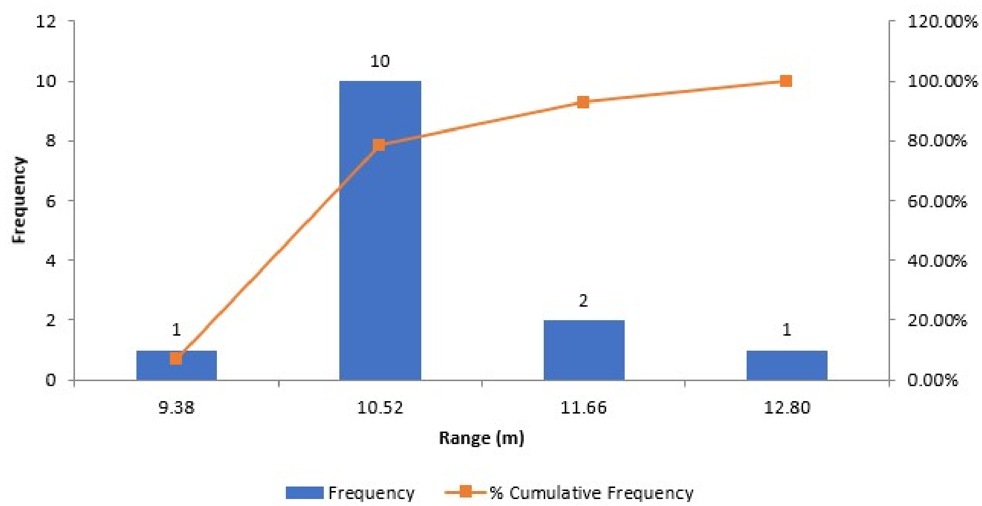

Figure 4.15: Histogram - single phase outages - clearance distances of managed line spans.

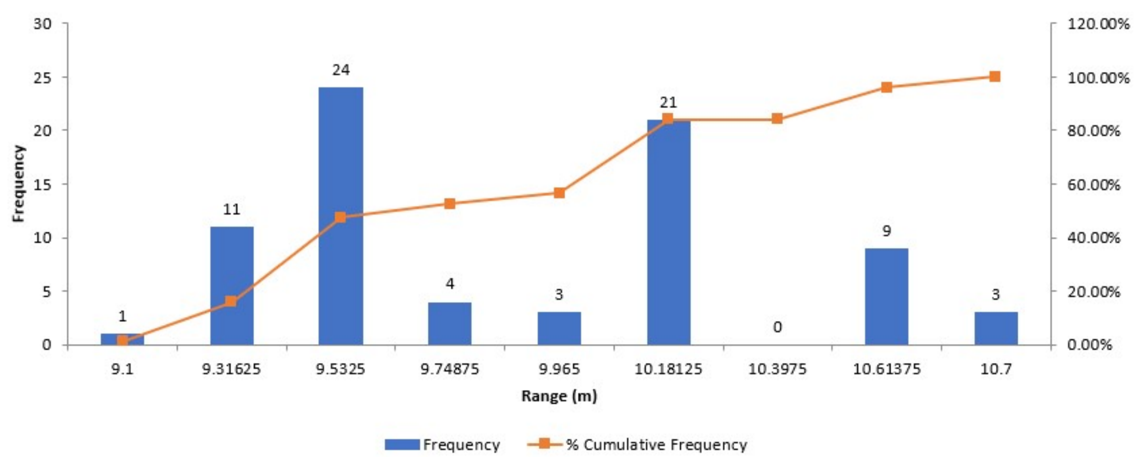

Figure 4.16: Histogram - Multiple-phases outages - clearance distances of managed line spans.

Figure 4.17 shows the graphical comparison of statistics results of vertical clearance distance for managed line spans subjected to single-phase and two-phase outages and clearance distance to vegetation on the sides of the service easement. This chart includes only outages involving line spans subjected to vegetation management. The average and maximum vertical clearance involving one-phase outages is larger than line spans involving two-phase outages. In addition, The maximum vertical clearance involving one-phase outages is larger than the direct clearance distance to side vegetation, resulting in flashover between two phases. The chart shows that line spans subjected to flashover between two phases have lower values in comparison with line spans subjected to phase-to-ground flashovers.

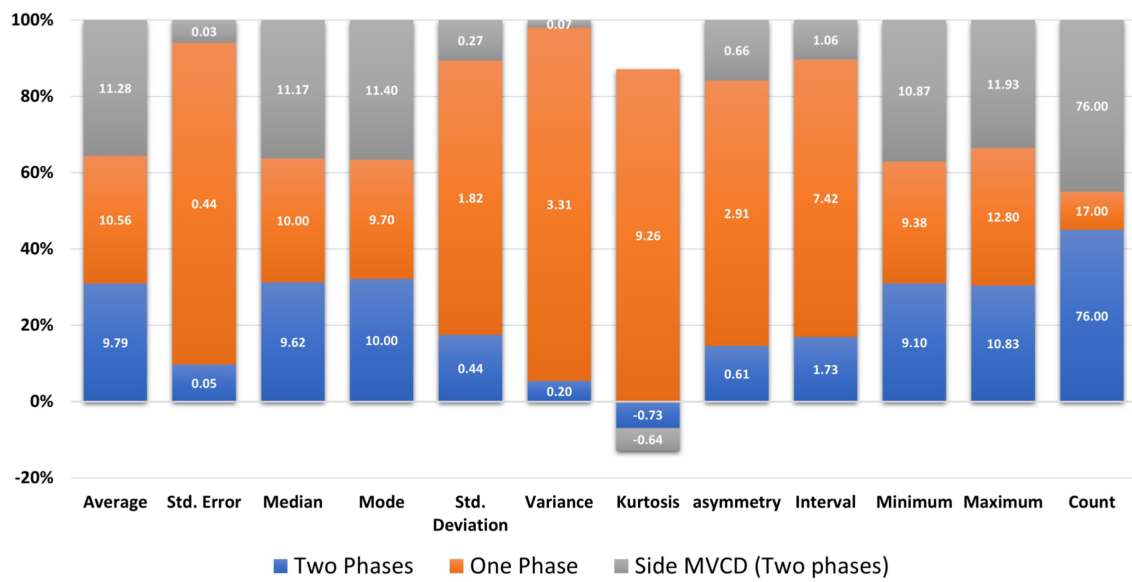

Figure 4.17: Comparison of statistics results between cleared spans with one-phase (vertical), two-phase (vertical), and side vegetation involving two phases

4.4.2 Classification of Vulnerability

The classification of vulnerability to flashover was determined based on the probability of outage obtained from the values of clearance distance of each line span involved in flashover events. Table 4.5 shows the ranges of clearance distance, the associated frequency, and the probability of flashover occurrence. The frequency of outages by the clearance distance range determined the risk level. The high vulnerability spans, comprising clearance distances up to 11.68 m, accounted for 87.6% of the analyzed outages. Medium vulnerability spans, comprising 11.95 to 12.49 m, accounted for 11.2% of the outages. Low vulnerability spans comprise distances above 12.49 m. Only one outage occurred at a clearance distance above 12.49.

Table 4.5: Classification of Vulnerability - Outage Probability

Clearance Distance	**Frequency**	**Cumulative %**	**% Total**	**P(x)**	**Risk**
10.87	1	1.12%	1.12%	0.52	High
11.14	39	44.94%	43.82	1.02	High
11.41	27	75.28%	30.34	1.10	High
11.68	11	87.64%	12.36	0.65	High
11.95	9	97.75%	10.11	0.21	Medium
12.22	0	97.75%	0.00	0.04	Medium
12.49	1	98.88%	1.12	3.50×10^{-3}	Medium
12.76	0	98.88%	0.00	1.83×10^{-4}	Low
13.04	0	98.88%	0.00	5.21×10^{-6}	Low
13.30	1	100%	1.12	8.90×10^{-8}	Low

The assumed clearance distance ranges listed below were used to classify the line spans for vulnerability to wildfire-induced flashovers.

- **Low vulnerability** - line spans with clearance distance above 12.49 m.
- **Medium vulnerability** - line spans with clearance distance between 11.69 and 12.49 m.
- **High vulnerability** - line spans with clearance distance up to 11.68 m.

4.4.3 Vegetation and Fire Characteristics

This study investigates two tropical savanna biomes (i.e., Cerrado and Caatinga) as the OHTL object of study crosses both biomes. It is important to highlight that most events occurred in the Cerrado biome. Only 30 of the 108 outages (27.7%) occurred under line spans crossing the Caatinga biome but still close to the boundaries with the

Cerrado biome. None of the outage events occurred in the section between substations São João do Piauí (SJI) and Sobradinho (SOB) with 212,452 km of length. This line section responds to 23% of the total OHTL length.

The proposed method to estimate the minimum clearance distance to prevent wildfire-induced flashovers considers the height of the remaining vegetation on the sides of the ROW, and the height of the flame, to compose a realistic clearance distance available in a wildfire event. The unmanaged vegetation is inside the boundaries of the ROW but not under the phase conductors.

This information is relevant since that in the case study, a fraction of unmanaged vegetation occupies 48 of the 70m of the width of the ROW. Thus, the unmanaged fraction may provide fuel to sustain higher temperatures in the air gap for longer periods of time. In addition, since the unmanaged vegetation is intact, it may produce higher flames with the potential to shorten the air gap between the conductors and the ground.

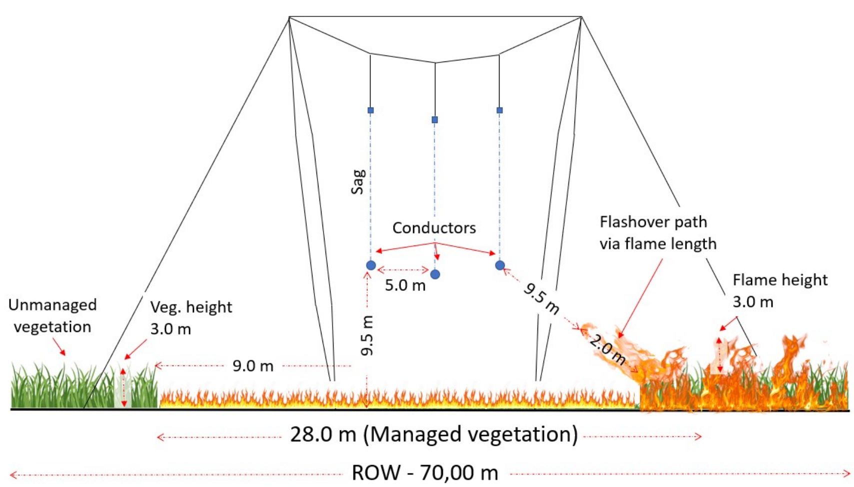

Figure 4.18: General dimensions of ATE 2's ROW subjected to wildfire

Figures 4.19, 4.20 and 4.21 show the relation of outages involving the middle and side phases. Note that outages involving side and middle phases represent 76% of the total outages, suggesting that flames and heating from side vegetation could be the main contributor to line outages. The balanced distribution of outages involving the left and middle phases, and the right and middle phases confirms that the exposure to fire and high temperature are very similar, as are the vegetation characteristics such as height and calorific power of species.

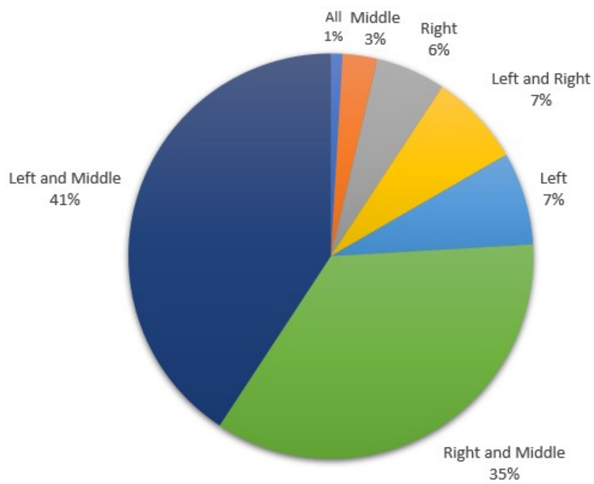

Figure 4.19: Classification of outages by phase positioning - Analysis of all line sections

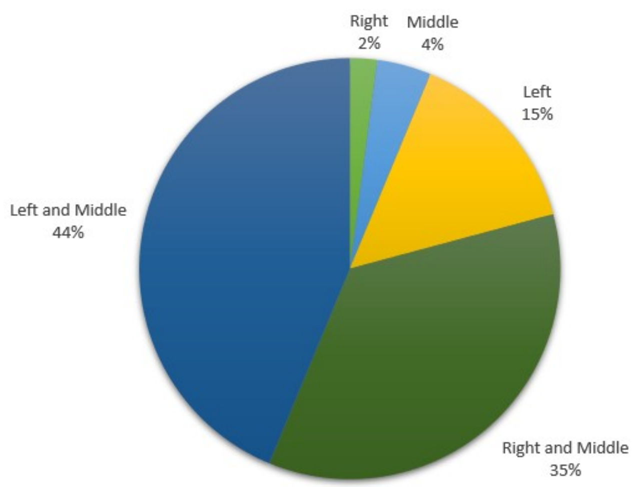

Figure 4.20: Classification of outages by phase positioning - Analysis of the TL Colinas - Ribeiro Gonçalves

4.4.4 Additional Research

In this research, 108 outages associated with line spans were analyzed in order to understand the causes that contributed to fire-induced flashovers. Three causes are cited in the listed literature: a) degradation of the air density by temperature, b)

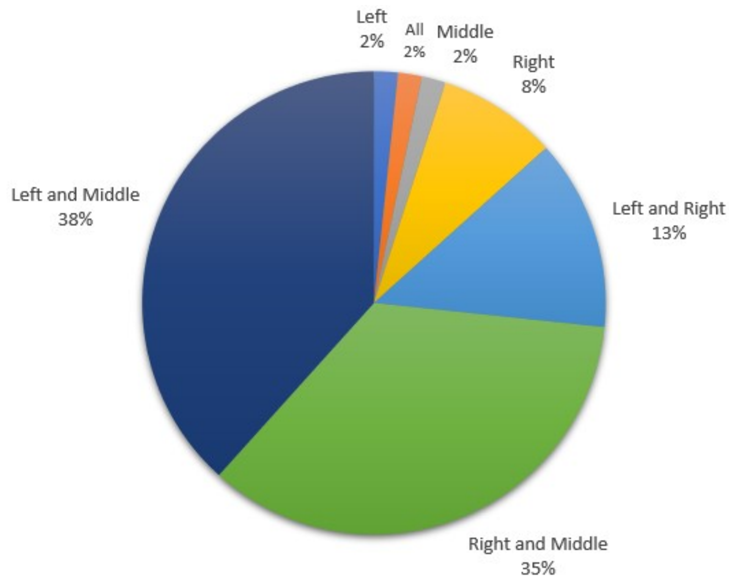

Figure 4.21: Classification of outages by phase positioning - Analysis of the TL Ribeiro Gonçalves - São João do Piauí

airborne particles in the smoke, and c) flames filling the air gap. Additional spans without records of outages, but subject to an elevated number of wildfire events, were also analyzed. Curiously, these spans presented an average vertical distance to the ground of 9.46 m. For example, spans 168 to 183 presented a very high risk of wildfire (confidence level above 50% that a wildfire would occur), ranging from 22 to 51 wildfire events per span in the last 20 years, and they still have not presented any outage.

Outages also occurred in spans with a low number of wildfire events. It can be easily explained if the conditions for the wildfire-induced flashover are satisfied. If a line span has an insufficient distance to the ground and the vegetation is not managed, it would be a matter of having the weather conditions and vegetation characteristics with a wildfire event (risk of wildfire) to increase the probability of outage by fire-induced flashover. Figure 4.22 presents an updated satellite image showing the line section between structures 166 and 184 of the OHTL 500 kV Ribeiro Gonçalves - São João do Piauí, the wildfire events in the last 20 years (red dots), and a detailed image of the span 171. That line section, despite showing a very high occurrence of wildfires in the last 20 years and no activity vegetation management at all, presents no records of outages related to wildfires.

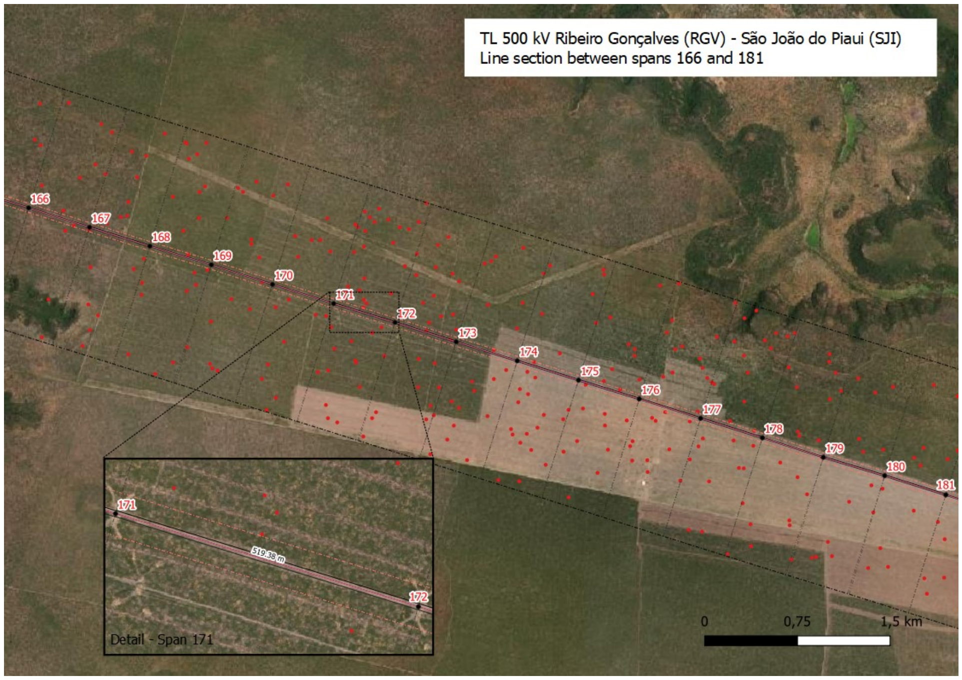

Figure 4.22: Map detailing the line section between structures 166 and 184 of the TL 500 kV Ribeiro Gonçalves - São João do Piauí

4.5 Chapter Summary

This chapter describes the novel approach proposed for estimating the risk of outage due to wildfire for OHTLs installed in the Brazilian Savanna. The approach includes estimating the risk of wildfire using spatial data and geoprocessing techniques and, subsequently, estimating the risk of wildfire-induced flashover (vulnerability to flashover) based on the investigation of 108 outage events obtained from the studied OHTL.

The case study was developed based on design, construction, and operating data from compact transmission line operating at 500 kV, located in the north of Brazil, notably impacted by wildfires. As a matter of fact, two line sections of this case study (TL Colinas - Ribeiro Gonçalves and TL Ribeiro Gonçalves - São João do Piauí) are in the second and third places in the number of outages caused by wildfire in Brazil from 2014 to 2016 [14].

Since every wildfire-induced flashover exhibits singular and dynamic interactions between environmental, climatic, social, and line design variables, laboratory testing may not be feasible to replicate realistic scenarios, including all conditions that make a flashover possible. Therefore, the compilation, investigation, and analysis of the available data were essential to suggest the root cause, and failure modes, and to estimate safe clearance distances to vegetation in order to prevent future outages.

This chapter showed that the investigated transmission line configuration is prone to outages involving multiple phases, particularly the side and middle phases. The compact clearance distance between phase conductors associated with the maintenance of existing clearance distances to the ground exposes the line to higher voltage stress. The design of conventional overhead lines operating at 500 kV typically adopts 10 meters of clearance distance between phase conductors, while the case study of this thesis uses 5 meters, 50% lower than the conventional design.

The main hypothesis is that the increased temperature of the air in the gap surrounding the phase conductors, in addition to the shortened distance between conductors and ground caused by flames, created the conditions for the breakdown of the insulating strength of air.

CHAPTER 5: TEST CASES, RESULTS, AND DISCUSSION

5.1 Chapter Introduction

This chapter presents and compares the results of the risk of wildfire and the vulnerability of outages due to wildfire-induced flashovers.

For the risk of wildfire, Berredo et al. [17] is used as a reference (i.e., baseline) to compare and discuss the results of the proposed methodology using Hotspot Analysis. However, in practice, Berredo et al. was never implemented by utilities. Thus, there is no information regarding its practical effectiveness. Result deviations between Berredo et al. and the methodology proposed in this thesis, here identified as Enhanced Berredo et al., should not be assumed as wrong. The new methodology uses data from 20 years of wildfires to identify the locations with a higher probability of occurrence of wildfires.

For the vulnerability to outages due to wildfire-induced flashover, results from six calculation methods, NBR 5422 [21], FAC-003-4 [20], Berredo, et al. [17], Fonseca et al. [2], Lanoie & Mercure [19] and West & McMullan [18], are presented, and compared with the results from the analysis of clearance distance of 58 line spans subjected to 108 outage events caused by fire-induced flashovers.

1. Evaluation and comparison of results from the risk of wildfire
    (a) Berredo et al. [17]
    (b) Hotspot Analysis based on Getis-Ord Gi*
2. Evaluation and comparison of results from line vulnerability to flashover
    (a) NBR 5422 (Agricultural Machinery) [21]

(b) NBR 5422 (Vegetation) [21]

(c) FAC-003-4 [20]

(d) Berredo et al. [17]

(e) Fonseca et al. [2]

(f) Lanoie & Mercure [19]

(g) West & McMullan [18]

This chapter includes the results of and comparison between the risks of wildfire and line vulnerability to wildfire-induced flashovers and highlights the key contributions of the chapter as they relate to the overall contributions of the thesis. This section also compares the results and provides a discussion regarding the effectiveness of the approached methods in relation to the clearance distances identified in the 108 analyzed outages.

5.2 Risk of Wildfire

This section addresses the calculation steps and results of risk of wildfire proposed in Berredo et al. [17] including the three steps (i.e., risk of ignition, risk of propagation, and risk of wildfire), and in the new methodology based on Getis-Ord Gi*. It also provides comparative results of both methods.

5.2.1 Test Scenario A - Berredo et al.

This section presents the results for the risk of wildfire proposed in Berredo et al. for the line section between structures 80 to 434 of the TL 500 kV Ribeiro Gonçalves - São João do Piauí. The results were compared with the proposed new methodology, here called “Enhanced Berredo et al” using Hotspot Analysis based on Getis-Ord Gi*.

Berredo et al. requires two models (i.e., risk of ignition of fire and risk of propagation of fire) to determine the classification of risk of wildfire. Berredo et al. classifies the risk of wildfire into five classes as shown in Table 5.1. Subsection 2.3.1 explains the models related to the risk of wildfire in detail.

Table 5.1: Risk of Wildfire - Berredo et al. - Risk classes.

Risk Class	**Value**
Very Low	Risk <=0.2
Low	0.2 < Risk <= 0.4
Medium	0.4 < Risk <= 0.6
High	0.6 < Risk <= 0.8
Very High	0.8 < Risk <= 1

Figure 5.1 shows the results of the classification of risk of wildfire. From top to bottom, the first step shows the risk of ignition. The second step shows the risk of propagation. The third step shows the risk of wildfire that is the result of merging the risks of ignition and propagation. The risk of wildfire is classified in a grid of 500 m x 500 m cells. Thus, since a line span can intercept several cells, the final classification of risk of wildfire used the cell with the highest score intersecting the line span.

Table 5.2: Risk of Wildfire - Berredo et al. - Descriptive Statistics.

Information	**Result**
Number of Hotspots	2351
Number of cells	354
Average	0.779
Std. Error	0.010
Median	0.865
Mode	0.330
Std. Deviation	0.201
Variance	0.040
Minimum	0.327
Maximum	0.980
Count of Low Risk Line Spans	30
Count of Medium Risk Line Spans	37
Count of High Risk Line Spans	86
Count of Very High Risk Line Spans	201

5.2.2 Test Scenario B - Enhanced Berredo et al.

This section presents the results of the proposed new model to classify the risk of wildfire by Hotspot Analysis based on Getis-Ord Gi* using a ten-year data collection. Instead of a two-step approach proposed in Berredo et al. [17] and FlamMap [42],

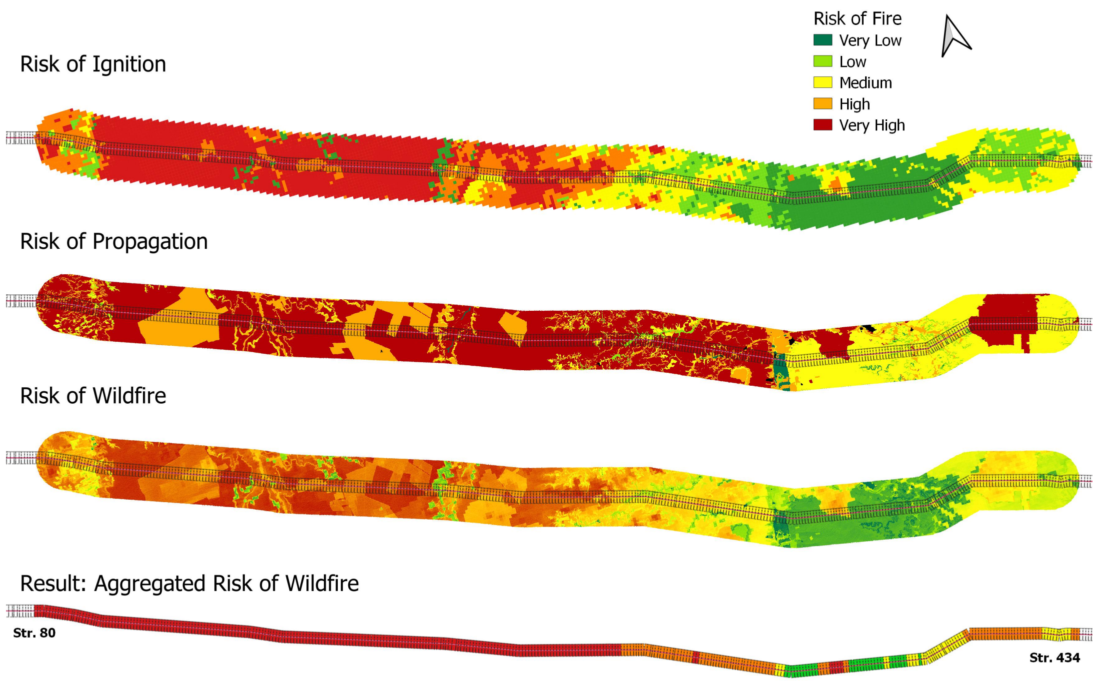

Figure 5.1: Classification of Risk of Wildfire according to Berredo et al. - Structures 80 to 434

this method classifies the hotspot dataset by Z-Score.

In this test, the Z-score measures the statistical significance - the distance from a particular line span to the entire hotspot dataset's mean value (μ), in standard deviations (σ). The model also provides the probability that a given hypothesis (Z-score) occurs (P-Value) for each of the line spans analyzed.

The statistically significant line spans with a very high risk of wildfire will have a positive standard deviation (Z-Score), which means that the more intense the clustering of wildfires in a line span, the higher the Z-Score will be. Line spans with lower occurrences of wildfires are less statistically significant. Therefore, it will result in values of Z-Scores below zero. Figure 5.2 shows the Gaussian distribution for the proposed model.

Interpretation of results requires both Z-Score and P-Value. The combination of very high or very low Z-Scores, associated with very small P-Values, are found in the tails of the normal distribution. When a feature pattern analysis yields small p-values and either a very high or a very low (negative) Z-Score, this indicates it is very unlikely that the wildfire represents a null hypothesis.

As previously mentioned in 4.3.3, the proposed model classifies the risk of wildfire based on the statistical confidence level that a fire event will occur. Every line span is populated with the standard deviation (Z-Score) and probability (P-Value) that a fire event will occur. In order to enable the comparison of results with the methodology proposed by Berredo et al., the quantitative results represented by ranges of Z-scores and P-values were translated into risk classes as listed below:

- **Low risk of wildfire** - Insignificant risk of wildfire represented by a Z-score over -0.28

- **Medium risk of wildfire** - up to 10% confidence level represented by Z-scores ranging from -0.28 to 0.124.

- **High risk of wildfire** - up to 50% confidence level represented by Z-scores ranging from 0.125 to 0.673.

- **Very high risk of wildfire** - confidence level above 50% represented by Z-scores above 0.674.

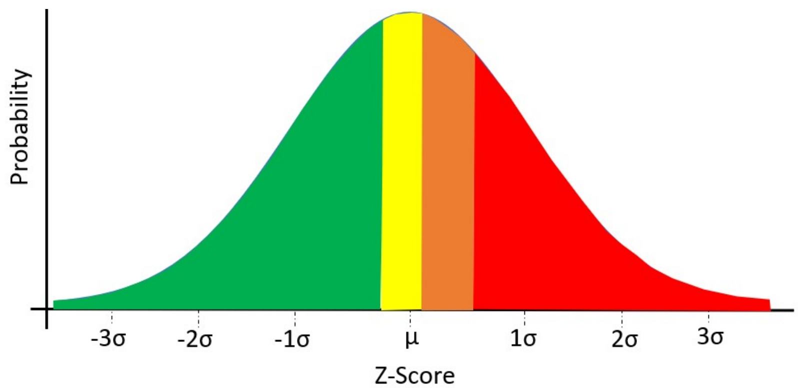

Figure 5.2: Gaussian curve for Enhanced Berredo et al.

Spans with a large absolute value of Z-Score and a small value of P-Value are probably too insignificant. Unusual scenarios could represent interesting situations, though, as land use may change over the years. For instance, a forest could change into agricultural land.

Figure 5.3 shows the results of the classification of the risk of wildfire between structures 80 and 434 using the new method. The classification adopts the maximum value of cells overlapping each other in a line span. The cell size is 375 m x 375 m, corresponding to the spatial resolution of the remote sensing source.

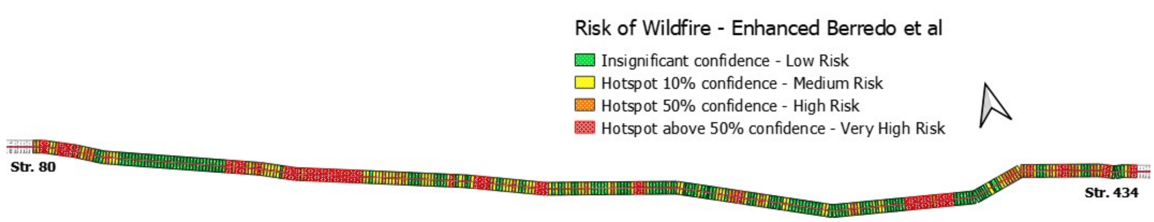

Figure 5.3: Classification of Risk of Wildfire according to Enhanced Berredo et al. - Structures 80 to 434

Table 5.3: Risk of Wildfire - Enhanced Berredo et al. - Descriptive Statistics.

Information	**Result**
Number of Hotspots	2351
Number of cells	2372
Average	-2.54^{-12}
Std Error	0.053
Median	-0.181
Mode	-1.248
Std. Deviation	1.001
Variance	1.002
Minimum	-1.248
Maximum	3.989
Count of Low Risk Line Spans	148
Count of Medium Risk Line Spans	81
Count of High Risk Line Spans	50
Count of Very High Risk Line Spans	75

5.2.3 Comparative Results - Berredo et al. vs. Enhanced Berredo et al.

The two methodologies of classification of risk of wildfire were compared and analyzed by means of correlation and confusion matrix. The comparison approach consisted in identifying spans matching risk levels. In order to make the confusion matrix possible, the results of the proposed methodology were translated from Z-Scores to risk levels (see 5.2.2). In practice, utilities can establish risk levels based on Z-Score ranges in accordance with their risk management policies. Figure 5.4 shows the results of the classification of risk of wildfire for both analyzed methods. Note that whereas results from Berredo et al. concentrates most of the line spans in a very high risk of wildfire, the proposed new method concentrates most of the spans in a low risk of wildfire. For the new method, a very high risk of wildfire means that there is a minimum 50% confidence level that a wildfire will occur, based on the analysis of 20 years of hotspot events.

Figure 5.5 shows the correlation of results between Berredo et al. (Predicted Label) and Enhanced Berredo et al. (True Label). Only 83 out of 354 line spans (23%)

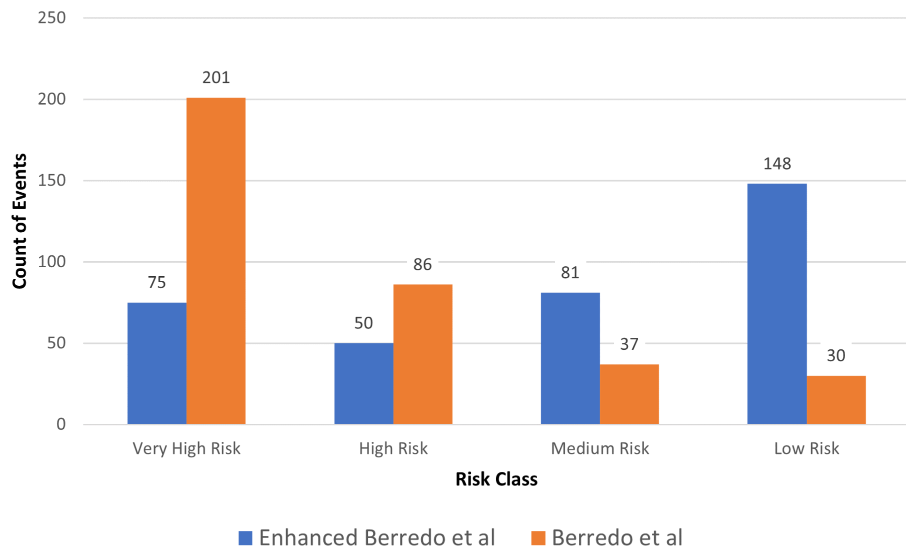

Figure 5.4: Results of the Classification of Risk of Wildfire

presented identical results. In this study, the correlated risks categories are distributed as follows:

- 51 out of the total spans are positively correlated with very high risk level of wildfire.
- 15 out of the total spans are positively correlated with high risk level of wildfire.
- 6 out of the total spans are positively correlated with medium risk level of wildfire.
- 11 out of the total spans are positively correlated with low risk level of wildfire.

Figure 5.6 shows the correlation of results between the risk levels classified in Berredo et al. and the results of Z-Score from Enhanced Berredo et al. Results matching are those inside the colored boxes. Results outside the colored boxes are those failing to match the risk.

Figure 5.7 shows the comparison of results between Berredo et al., the proposed new method (Enhanced Berredo et al.), and a heatmap analysis using kernel density estimation based on the 20-year hotspot data. The Kernel Density estimation is

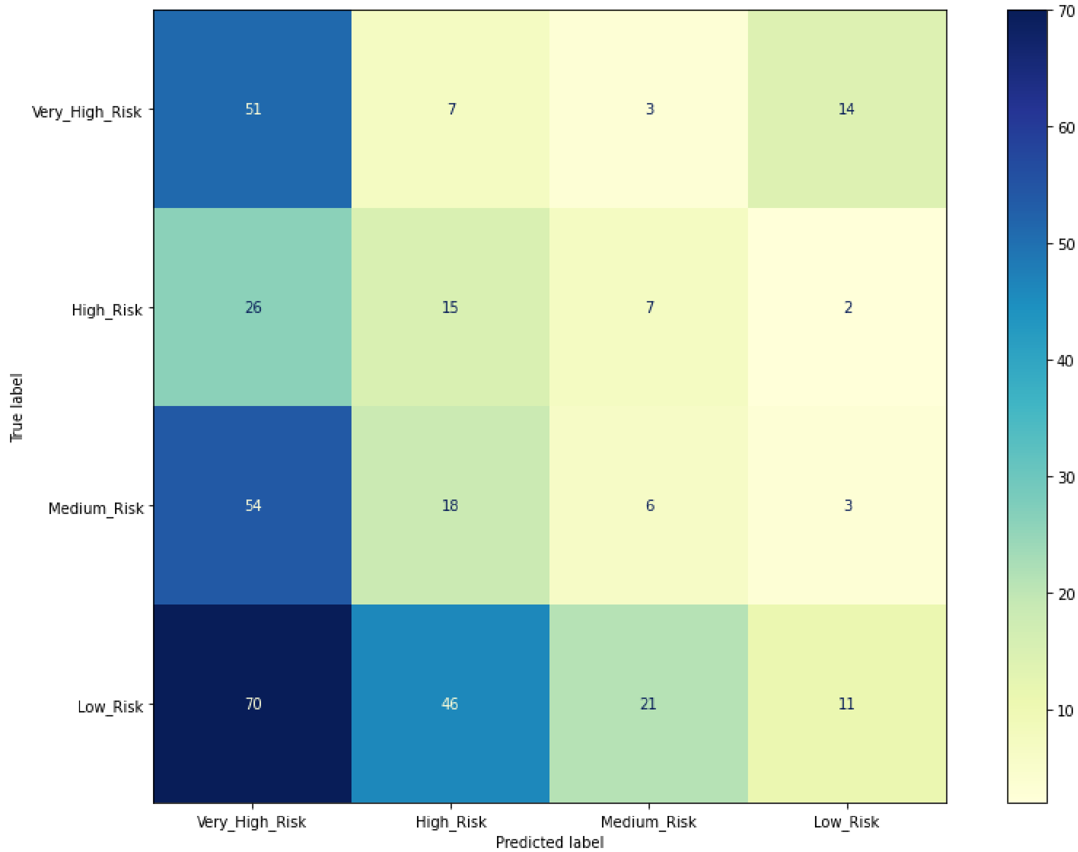

Figure 5.5: Confusion matrix between results of Berredo et al. and Enhanced Berredo et al.

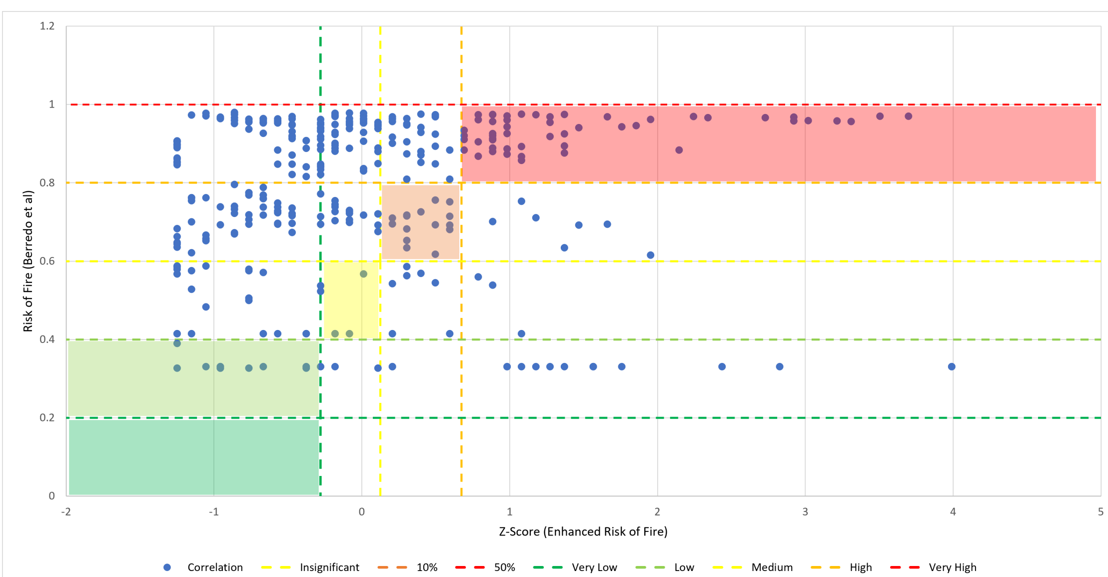

Figure 5.6: Correlation chart between results of Berredo et al. (Risk levels) and Enhanced Berredo et al. (Z-Scores)

a non-parametric method to estimate the probability density function of a random variable. In GIS, Kernel Density estimation calculates the density of a given point feature.

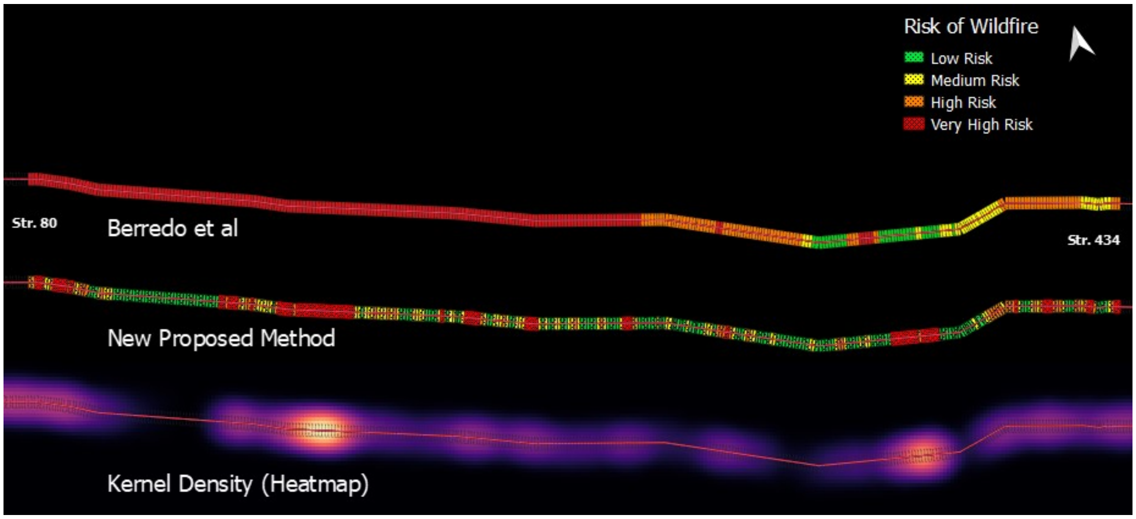

Figure 5.7: Comparison between Berredo et al., Enhanced Berredo et al. and Kernel Density Estimation (Heatmap)

The proposed method presents a strong visual correlation with the Kernel Density map shown in Figure 5.7. Whereas denser sections of the heatmap (white sections) match spans classified with a very high risk of wildfire (red spans) in the proposed new method, regions with dispersed hotspots (dark blue to dark sections) match low-risk spans (green sections). This comparison evidences the effectiveness of the proposed new methodology for classifying the risk of wildfire. In addition, Figure 5.7 evidence that Berredo et al. may not be sufficient to predict the risk of wildfire effectively. Detailed results are available in Appendix B.

5.3 Risk of Wildfire-Induced Flashover

This section presents the results of the six different approaches/test scenarios (i.e., NBR 5422 [21], FAC-003-4 [20], Berredo et al. [17], Fonseca et al. [2], FAC-003-4 corrected by West & McMullan [18] and Lanoie & Mercure [19]) in the included subsections to determine the MVCD for the 500 kV case study. It also addresses the results of vulnerability based on the comparison with the statistics of outages and the comparative results of vulnerability between Berredo et al. and the proposed new methodology.

5.3.1 Test Scenario A - NBR 5422:1985

MVCD calculations using NBR 5422 for 500 kV lines subject to vegetation resulted in 6.67m of clearance distance. However, ATE II adopts a 9.5m of clearance distance due to the presence of agricultural lands in some parts of the corridor. Agricultural lands imply the risk of contact with agricultural machinery, often in the region.

As Section 2.4.1 explains, NBR 5422 uses a two-part equation to calculate the minimum clearance distance (D). Assuming that the obstacle is vegetation, the parameters a and Du are 4m and 550kV, respectively (see (5.1)).

$$\begin{aligned} D &= a + 0.01 \cdot \left(\frac{Du}{\sqrt{3}} - 50 \right) \\ &= 4 + 0.01 \cdot \left(\frac{550}{\sqrt{3}} - 50 \right) \\ &= 6.67m \end{aligned} \tag{5.1}$$

Table 5.4 shows the results of electric field strength (kV/m) (phase-to-ground) for all typical voltage levels of OHTL present in the Brazilian bulk grid. The electric field strength across 6.67m in a 500 kV line is 61.5% above the electric field strength across 4.96 m in a 230 kV line. It could mean that as the voltage level of the transmission line increases, the more vulnerable the OHTL will be to wildfire-induced flashovers.

The MVCD and electric field strength of a typical 230 kV line is highlighted in Table 5.4 for comparison with a typical 500 kV line.

Although higher than the minimum clearance required by the Brazilian standard, adopting 9.5m will still result in electric field strength (phase-to-ground) 13.5% above that for 230 kV lines. Table 5.4 shows the MVCD based on NBR 5422, and Table 5.5

Table 5.4: Minimum Vegetation Clearance Distances (MVCD) per Voltage Level - ABNT NBR 5422

Voltage Level (kV)	**MVCD (m)**	**E (kV rms/m) Ph-Gnd**
138	4.37	18.20
230	**4.96**	**26.76**
345	5.69	34.99
440	6.29	40.35
500	**6.67**	**43.24**
750	8.26	52.40

shows the results of electric field strength for the clearance distance of 9.5m adopted in the line design of ATE II.

Table 5.5 also highlights the electric field strength between phases. The OHTL object of this study uses compact geometry with 5m between phases, resulting in an electric field strength of 100 kV/m. The strong electrical stress between phases could justify the high frequency of outages involving multiple phases compared to a typical 500 kV configuration that typically adopts 10m between phases.

Table 5.5: Clearance Distance for ATE II - ABNT NBR 5422

Voltage Level	**MVCD**	**Electric Field Strength**	
(kV)	**(m)**	**Ph-Ph (kV/m)**	**Ph-Gnd (kV/m)**
500	9.5	**100**	30.38

Additional analysis of Table 5.4 and Fig. 5.8 shows a non-linear increase of electric field strength as the voltage level increases. A 500 kV line with 6.67m of MVCD (i.e., larger red point in Fig. 5.8) will be subject to 43.24 kV/m (phase-to-ground), 61.5% above a typical 230 kV line (26.76 kV/m), which is historically not associated with poor insulation performance to wildfire.

In practice, the non-linear increase of electric field strength will result in lower insulation performance as the voltage level increases. In Brazil, wildfire-related outages are more frequent in overhead lines operating at 500 kV in Northern Brazil and Minas

Gerais State [14]. Lines operating at 230 kV, 345, and 440 kV are more frequently associated with sugarcane-related flashovers in Northeast and Southeast Brazil [14].

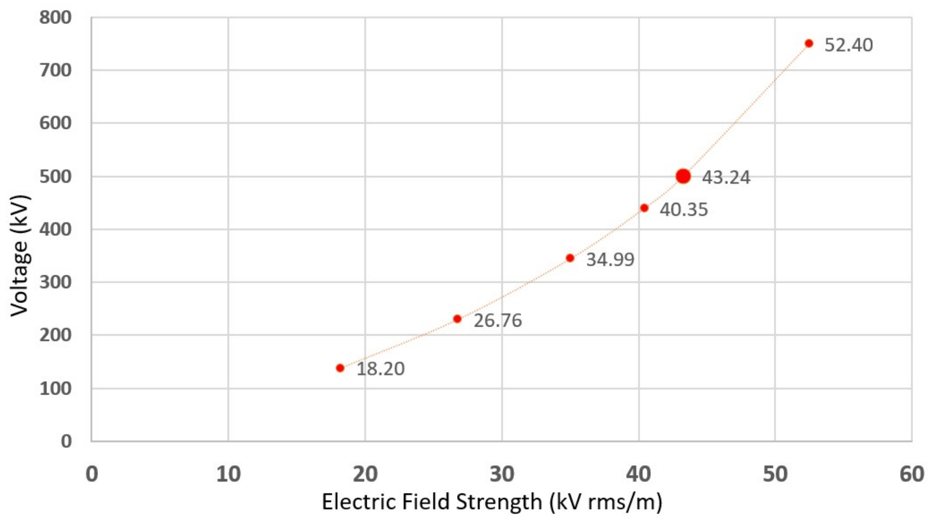

Figure 5.8: Line Voltage (kV) vs. Electric Field Strength (kV/m) - NBR 5422.

While the calculated MVCD for vegetation using NBR 5422 is 46.55% lower compared to the baseline MVCD established in 4.4.1 (i.e., 12.48m) if assuming agricultural lands, the MVCD results in a distance of 23.87% lower compared to the baseline MVCD.

5.3.2 Test Scenario B - FAC-003-4 (Gallet Equation)

The calculation proposed in NERC FAC-003-4 [20] resulted in a minimum clearance distance of 3.93m, assuming a transient overvoltage of 2.2 pu (V_m) (see Table 5.6). The clearance distance is much lower than the established MVCD of 9.5m practiced in the ATE II transmission line. However, as mentioned previously, the MVCD in FAC-003-4 is not intended to prevent fire-induced flashover but to prevent outages due to vegetation approximation. Of interest, the latest revision of FAC-003 (i.e., FAC 003-4) presents a table summarizing minimum approach distances to vegetation for the typical line voltages. That table assumes an anticipated transient overvoltage of 1.4 p.u. According to ATE II design documents, a transient overvoltage of 2.2 p.u. is expected to lead to a much higher result of MVCD using the Gallet equations.

In West & McMullan (see Section 5.3.6), the result from FAC-003-4 is corrected to reflect the increased temperature due to wildfire. As mentioned in Section 2.4.2, FAC-003-4 [20] adopts the Gallet equation, which calculates the insulation coordination in OHTL design. The approach calculates the voltage crest of a given line, estimates the initial minimum clearance distance, then calculates the critical flashover voltage, corrects the results to a specific atmospheric pressure, and calculates the withstand voltage at the same atmospheric pressure. The calculation is shown in the Algorithm 4 as follows:

Table 5.6: Minimum Vegetation Clearance Distances (MVCD) - FAC-003-4

Voltage Level (kV)	**MVCD (m)**	**E (kV rms/m) Ph-Gnd**
500	3.93	73.45

5.3.3 Test Scenario C - Enhanced Berredo et al.

Berredo et al. method proposes that 12.5 m would be sufficient to prevent most of the flashover events in the 500 kV compact line. The original method was developed based on the equation of breakdown strength of air between sphere electrodes varying the air density to reflect the elevated air temperature in the gap between conductor and ground and between conductors.

The enhanced method assumed an air density correction factor of 0.56 resulting from an average temperature of 212 °C, estimated based on the gradient of temperatures in the convective air in a 12.5 m gap between the ground and conductors.

In this thesis, the author included relevant factors from the outage analysis. The utility validated the average vegetation height on the sides of the cleared corridor (3 m). The adopted flame length/height (2.8 m) and the temperature profile, published in Frost, P.H.G.; Robertson [31], were also considered in determining these factors.

The proposed new model adopts the tip of the flames under the conductors as a

Algorithm 4 NERC FAC-003-4 500 kV Case Study

1: Calculate the voltage crest V_m via (5.2), where TOV is the transient overvoltage factor in pu and V is the nominal voltage (kV).

$$V_m = TOV \cdot V \cdot \sqrt{\frac{2}{3}} = 2.2 \cdot 550 \cdot \sqrt{\frac{2}{3}} = 987.96kV \tag{5.2}$$

2: Compute the initial clearance distance D_i per (5.3), where K_w is the wet/dry conditions factor and K_g is the gap factor.

$$D_i = \frac{8}{\frac{3400 \cdot K_w \times K_g}{\left(\frac{1,162.31}{0.85}\right)} - 1} = \frac{8}{\frac{3400 \cdot 1.037 \times 1}{\left(\frac{550}{0.85}\right)} - 1} = 3.93m \tag{5.3}$$

3: Calculate the Critical Flashover Voltage (CFO) for D_i at standard atmospheric conditions CFO_s via (5.4), where D is the air gap distance.

$$\begin{aligned} CFO_s &= K_w \cdot K_g \cdot \frac{3400}{1 + \frac{8}{D}} \\ &= 1.037 \cdot 1 \cdot \frac{3400}{1 + \frac{8}{3.93}} = 1,162.31kV \end{aligned} \tag{5.4}$$

4: Calculate the CFO at a specific height above sea level CFO_A by applying the atmospheric correction factor via (5.5), where A is the altitude (km).

$$\begin{aligned} G_0 &= \frac{CFO_s}{V \cdot D} \\ &= \frac{1,162.31}{550 \cdot 3.42} = 0.1 \\ m &= 0.125 \cdot G_0 \cdot (G_0 - 0.2) \\ &= 0.125 \cdot 0.1 \cdot (0.1 - 0.2) = -0.012 \\ CFO_A &= CFO_s \cdot \exp\left(-m \cdot \frac{A}{8.6}\right) \\ &= 1,162.31 \cdot \exp\left(-(-0.012) \cdot \frac{0.9}{8.6}\right) = 1,163.83kV \end{aligned} \tag{5.5}$$

5: Calculate the withstand voltage of the gap at a given height above sea level via (5.6), where σ = standard deviation.

$$\begin{aligned} V_{m(3\sigma)} &= CFO_A \cdot \left(1 - 3 \cdot \frac{\sigma}{CFO_A}\right) \\ &= 1,163.83 \cdot (1 - 3 \cdot 0.05) = 988.83kV \end{aligned} \tag{5.6}$$

ground reference. For example, a conductor positioned 10 meters above vegetation being engulfed by flames at 5 meters height would mean that the conductor is, in fact, 5 meters away from the ground.

The outage analysis showed that the burning of unmanaged vegetation on the sides of the corridor (i.e., side fires) is the main factor contributing to most of the flashover incidents when fuel and flames play a role. One of the possibilities to mitigate the number of flashovers is the widening of the clearing.

The algorithm below shows the application of Enhanced Berredo et al. for the case study.

Algorithm 5 Enhanced Berredo et al. [17] - Phase-to-Ground Calculation Steps for the Case Study

1: Calculation of the the Air Density via (5.7).

$$\begin{aligned}\delta &= \frac{\rho T_0}{\rho_0 \cdot \left(273 + \frac{\left(\sum_{n=1}^{h}\right)\cdot T_s \cdot (h^{-0.992})}{h}\right)} \\ \delta &= \frac{705.01 \cdot 293}{101.31 \cdot \left(273 + \frac{\left(\sum_{n=1}^{8}\right)\cdot 212 \cdot (8^{-0.992})}{8}\right)} \\ \delta &= \frac{705.01 \cdot 293}{101.31 \cdot (273 + 212.02)} \\ \delta &= 0.56\end{aligned} \tag{5.7}$$

2: Calculation of the Breakdown Strength of Air (5.8).

$$\begin{aligned}V_{r(peak)} &= \frac{22.7 \cdot \delta \cdot 0.125 \cdot \left(1 + \frac{0.54}{\sqrt{\delta \cdot 0.125}}\right) \cdot \frac{h}{0.125}}{0.25 \cdot \left(\frac{h}{0.125} + 1 + \sqrt{\left(\frac{h}{0.125} + 1\right)^2 + 8}\right)} \\ V_{500(peak)} &= \frac{22.7 \cdot 0.56 \cdot 0.125 \cdot \left(1 + \frac{0.54}{\sqrt{0.56 \cdot 0.125}}\right) \cdot \frac{8}{0.125}}{0.25 \cdot \left(\frac{8}{0.125} + 1 + \sqrt{\left(\frac{8}{0.125} + 1\right)^2 + 8}\right)} \\ V_{500(peak)} &= 451.71\ kV\end{aligned} \tag{5.8}$$

As shown in Algorithm 5 in (5.7): δ is the air density correction factor, ρ is the atmospheric pressure on place (705.01 mm/HG or 94.09 kPA), ρ_0 is the reference atmosphere pressure (760mm/HG), T_0 is the reference temperature (293 K), T_s is the average temperature of the air gap (212 °C), and h is the clearance between the conductor and the top of the vegetation or flame.

In (5.8): $V_{r(peak)}$ is the peak voltage associated with the breakdown strength of air, ρ_0 is the reference atmosphere pressure (760mm/HG), T_0 is the reference temperature (293 K), and h is the vertical clearance between the conductor and the top of the vegetation.

Using the same calculation process, 80° C in the air gap between the conductors (equivalent to an air density factor of 0.77) should be sufficient to prevent the line from flashing between the conductors as long as the flames do not bridge the air gap. Additional height should be provided to compensate for the flame length.

5.3.3.1 Vulnerability to Flashover

As mentioned in subsection 4.4.2, this research adopted the ranges of clearance distance listed below to classify the line spans for vulnerability to wildfire-induced flashovers based on the probability of outage obtained from the ATE II outage dataset (see appendix A).

The

- **Low vulnerability** - line spans with clearance distance above 12.49 m.
- **Medium vulnerability** - line spans with clearance distance between 11.69 and 12.49 m.
- **High vulnerability** - line spans with clearance distance up to 11.68 m.

5.3.4 Test Scenario D - Fonseca et al.

As mentioned in 2.4.4, this method was developed for OHTLs subject to the burning of sugarcane that can result in a flashover event. According to Fonseca et al.,[2], the

MVCD calculation for overhead lines operating at 500 kV should use the equation shown in (5.9), for lines operating above 245 kV.

$$D = D_{basic} + D_{el_{<245kV}} + D_{sag} \tag{5.9}$$

The calculation steps listed in (5.10) and (5.11) resulted in an MVCD of 13.58 m, including the additional sag due to the increase of the conductor temperature by the heat absorption from the burning of sugarcanes. The author estimates a temperature increase of the conductor of about 30 °C.

$$\begin{aligned} D_{el500kV} &= 7 + \frac{317.54 - 245}{150} kV/m \\ D_{el500kV} &= 7.48 kV/m \end{aligned} \tag{5.10}$$

Therefore:

$$\begin{aligned} D &= 5 + 7.48 + 1.1 \\ D &= 13.58 m \end{aligned} \tag{5.11}$$

Fonseca et al. considered two electric distances (i.e., $D_{el_{<245kV}}$ and $D_{el_{>245kV}}$) to distinct the influence of the flame that partially or completely fills the air gap. Table 5.7 shows the results of the dielectric strength of air for different percentages of air gap flame bridging.

Table 5.7: Fonseca et al. % of gap bridging vs dielectric strength

% of gap bridging	**Dielectric Strength (kV rms/m)**
100	35.0
90	46.5
80	58.0
70	69.5
60	81.0
50	92.5

Table 5.8 shows the results of MVCD calculations for OHTL operating at different voltage levels.

Table 5.8: Fonseca et al. MVCD by voltage level

Nominal Voltage (kV)	**Span Length (m)**	**Conductor (kcmil)**	D_{el} **(m)**	D_{sag} **(m)**	**MVCD (m)**
138	300	336.4	2.4	1.0	8.4
230	350	795.0	4.0	1.0	10.0
440	400	954.0	7.2	1.1	13.3
500	400	954.0	7.4	1.1	13.5
750	450	1113.0	8.4	1.1	14.5

5.3.5 Test Scenario E - Lanoie & Mercure

Experiments performed by Lanoie & Mercure [19] demonstrated that conductors engulfed in flames of spruce trees result in electric field strength of 12kV/m. Adopting this parameter, OHTLs exposed to the burning of spruce trees would require 24.1m of MVCD in order to prevent flashover. Results based on Lanoie & Mercure are significantly higher than the other methods presented in this thesis and are particularly applied to spruce trees.

It is important to highlight that the electric field strength of 12 kV/m was estimated based on the burning of spruce trees. Thus, new trials are needed to estimate the stress corresponding to the vegetation present in the Brazilian savanna biomes.

5.3.6 Test Scenario F - West & McMullan

This test scenario used the equation proposed in West & McMullan [18] to include the effects of the reduction of the air density in the breakdown strength of air due to the heated air in the gap between conductors and ground.

West & McMullan [18] is not a calculation method to determine MVCD but to estimate the reduction of the breakdown strength of air at high temperatures. Therefore, this test adopted the MVCD proposed in FAC-003-4 based on the Gallet equations to apply West & McMullan's equation.

The initial CFO_A, as calculated in 5.3.2, decreases from 1,169.38 to 655.70 kV if subjected to 250°C, decreasing the withstand voltage (3σ) from 988.83 to 557.34 kV, insufficient for 3.97 m of MVCD.

Based on (5.12) through (5.17), where CFO_A is the critical flashover voltage under actual conditions, CFO_s is critical flashover voltage under standard conditions, p is barometric pressure (kPa), T is the temperature (C), and Vm is the withstand voltage, if the air gap is exposed to 250°C, the dielectric strength across the nominal voltage 550 kV would be reduced in 44%. The withstand voltage (peak phase-to-ground) would be reduced from 987.96 kV to 553.25 kV.

As shown in (5.12) through (5.17), in order to compensate for the high temperature across the air gap, an air gap of 11.45m would be required to withstand the voltage for a transient overvoltage of 2.2 p.u. The CFO_a will be to 1,162.90 kV at 250 °C, resulting in a withstand voltage (3 σ) of 988.46 kV, slightly above the estimated phase-to-ground voltage peak (987.96 kV).

$$CFO_{s\ (3.97m)} = 1.037 \cdot 1 \cdot \frac{3400}{1 + \frac{8}{3.93}} = \mathbf{1{,}169.38\ kV} \tag{5.12}$$

$$\begin{gathered} CFO_{A\ (3.97m)} = CFO_{s(3.97m)} \cdot \exp\left(-m \cdot \frac{A}{8.6}\right) \\ CFO_{A\ (3.97m)} = 1,169.38 \cdot \exp\left(-(-0.012) \cdot \frac{0.9}{8.6}\right) = \mathbf{1{,}170.09\ kV} \end{gathered} \tag{5.13}$$

$$\begin{gathered} CFO_{A_{250C}\ (3.97m)} = CFO_{A\ (3.97m)} \cdot \frac{2.892 \cdot p}{T + 273.15} \\ CFO_{A_{250C}\ (3.97m)} = 1,170.09 \cdot \frac{2.892 \cdot 101.3}{250 + 273.15} = \mathbf{655.70\ kV} \end{gathered} \tag{5.14}$$

$$\begin{gathered} CFO_{A\ (11.45m)} = CFO_{s(11.45m)} \cdot \exp\left(-m \cdot \frac{A}{8.6}\right) \\ CFO_{A\ (11.45m)} = 2,075.60 \cdot \exp\left(-(-0.012) \cdot \frac{0.9}{8.6}\right) = \mathbf{2{,}076.63\ kV} \end{gathered} \tag{5.15}$$

$$CFO_{A_{250C}\ (11.45m)} = CFO_{A\ (11.45m)} \cdot \frac{2.892 \cdot p}{T + 273.15}$$
$$CFO_{A_{250C}\ (11.45m)} = 2,076.63 \cdot \frac{2.892 \cdot 101.3}{250 + 273.15} = \mathbf{1,162.90\ kV} \tag{5.16}$$

$$V_{m(3\sigma)} = CFO_{A_{250C}\ (11.45m)} \cdot \left(1 - 3 \cdot \frac{\sigma}{CFO_A}\right)$$
$$V_{m(3\sigma)} = 1,162.90 \cdot (1 - 3 \cdot 0.05) = \mathbf{988.46\ kV} \tag{5.17}$$

5.3.7 Comparative Results of Vulnerability Berredo et al. vs. Enhanced Berredo et al.

The two methodologies of classification of vulnerability to wildfire-induced flashover were compared and analyzed by means of correlation and confusion matrix for the analyzed line section. Figure 5.9 shows the confusion matrix results. Note that 277 spans matched the high vulnerability, resulting in an 81.3% correlation. 299 of the 354 spans analyzed matched results. The vulnerability results for each line span analyzed can be found in Appendix C.

5.4 Chapter Summary

Table 5.9 and Fig. 5.10 provide comparative results of the MVCD based on NBR 5422 for two scenarios (i.e., lines with traffic of agricultural vehicles and vegetation), FAC-003-4, FAC-003-4 corrected by West & McMullan (W&M), Berredo et al., Fonseca et al., and Lanoie & Mercure using the maximum height found between the conductor and the ground, under conductors and without vegetation (i.e., after vegetation clearing) as the baseline.

Regarding the risk of wildfire, Berredo et al. was compared with a new methodology based on Getis Ord GI*. The results showed a low-risk correlation with only 83 out of 354 line spans (23%) presenting identical results. However, the proposed new method presented a strong visual correlation with a Kernel Density map. Whereas denser sections of the heatmap were equivalent to spans classified with a very high risk of wildfire in the proposed new method, regions with dispersed hotspots presented

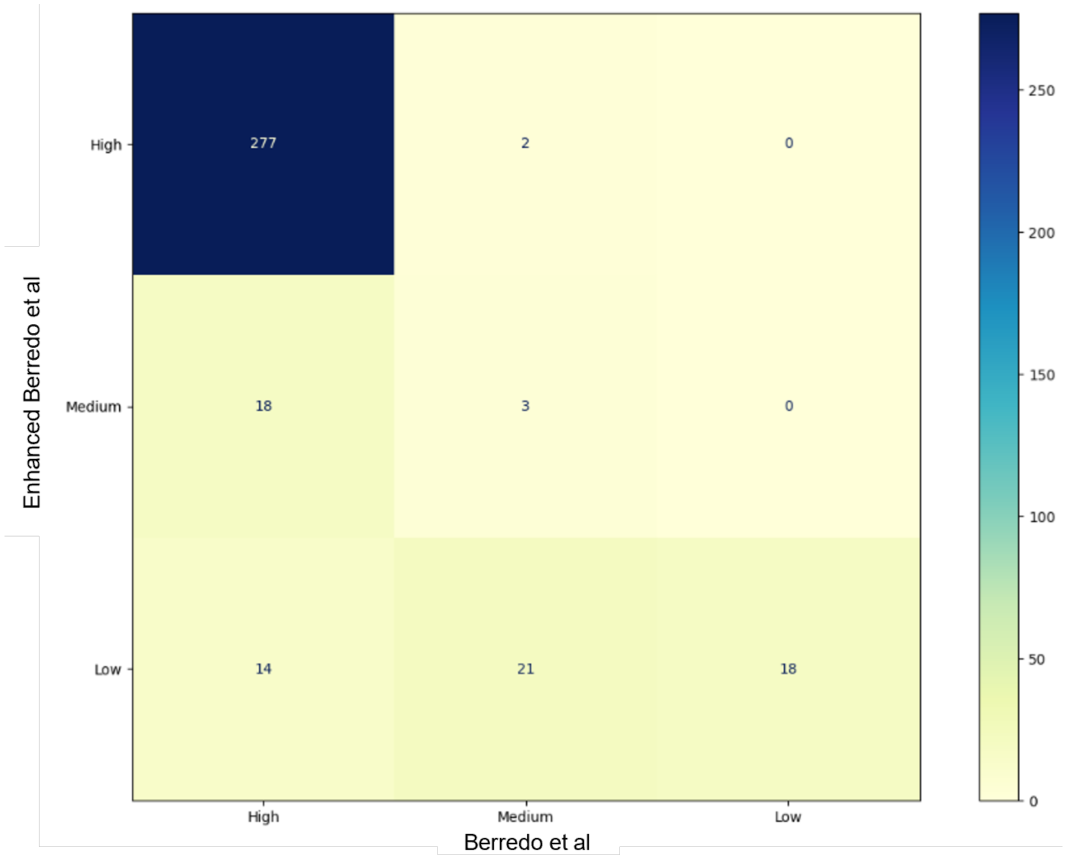

Figure 5.9: Results of vulnerability to flashover - Confusion Matrix between Enhanced Berredo et al. and Berredo et al.

Table 5.9: Comparison of Results of MVCD Calculation Approaches

Method	**MVCD (m)**	**Stress (kV/m) Ph-Gnd**	**% Baseline**
Baseline	**12.8**	**22.55**	-
FAC-003-4	3.42	84.40	26.71
NBR 5422 (Vegetation)	6.67	43.24	52.10
NBR 5422 (Agriculture)	9.5	30.42	74.21
FAC-003-4 (W&M)	11.45	25.21	89.45
Berredo et al.	12.50*	23.09	97.65
Fonseca et al.	13.58	21.25	106.09
Lanoie & Mercure	24.1	11.97	188.28

Notes: No flame height included

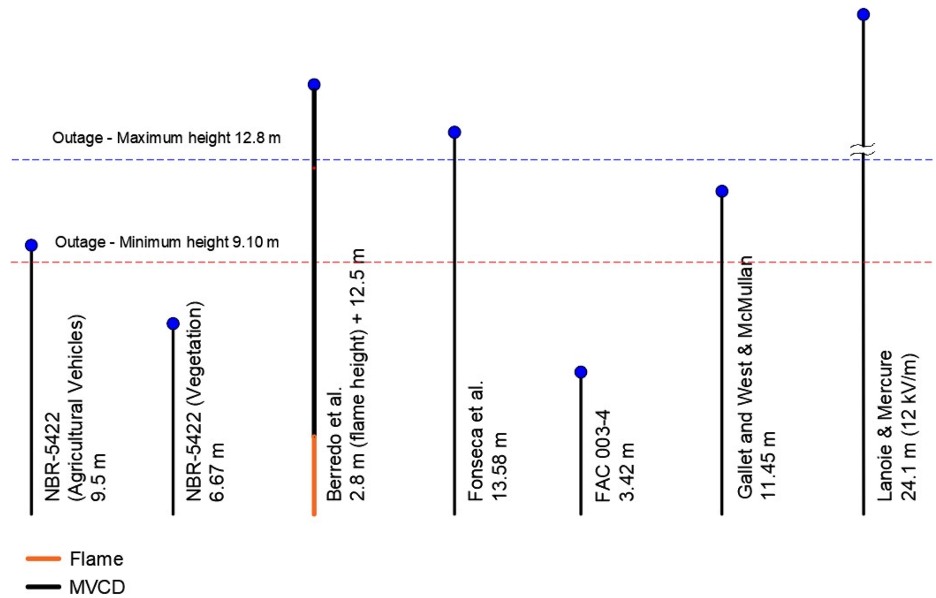

Figure 5.10: Method vs MVCD (m).

similar results of low-risk spans. These results evidenced that the existing model may be overly conservative since many spans classified with very high risk had not been exposed to wildfires in the past 20 years.

In terms of risk of wildfire-induced flashover, six models were investigated and compared with clearance distances from line spans responding to 108 outages in the past 9 years. The Berredo et al. and Fonseca et al. models presented the best results, with 97.65% and 106.09% of the baseline clearance distance obtained from the outage and line datasets.

5.5 Criticality of Outage

The criticality of outage weighs the risk of an outage based on the risk of wildfire and the vulnerability to wildfire-induced flashovers for a given line span. As previously mentioned, a line span exposed to a very high risk of wildfire may not be sufficient to cause an outage if the clearance distance is sufficiently large to maintain the dielectric strength of the air gaps higher than the exposed electric field strength. The criticality combines risks of wildfire and vulnerability to wildfire-induced flashovers to provide the risk of outage.

Berredo et al. adopts the criteria shown in Table 5.10 while the proposed new method (i.e., Enhanced Berredo et al.) adopts the criteria shown in table 5.11.

Table 5.10: Criticality of Outage - Berredo et al.

		Risk of Wildfire				
		Very Low	**Low**	**Med.**	**High**	**Very High**
Vul.	**Low**	Low	Low	Med.	Med.	Med.
	Med.	Low	Med.	Med.	High	High
	High	Med.	Med.	High	High	High

Notes: Vul. = Vulnerability, Med. = Medium.

Table 5.11: Criticality of Outage - Enhanced Berredo et al.

		Risk of Wildfire			
		Low	**Medium**	**High**	**Very High**
Vulnerability	**Low**	Low	Low	Low	Medium
	Medium	Low	Medium	Medium	High
	High	Medium	High	High	High

5.5.1 Comparative Results of Criticality for Berredo et al. vs. Enhanced Berredo et al.

The two methodologies of classification of criticality to outage were compared and analyzed by means of correlation and confusion matrix for the analyzed line section. Figure 5.11 shows the confusion matrix results. Note that 144 spans matched the high vulnerability, resulting in a correlation of 47.1%. From the 354 spans analyzed, 167 matched the results. Appendix D shows the criticality results for each line span analyzed.

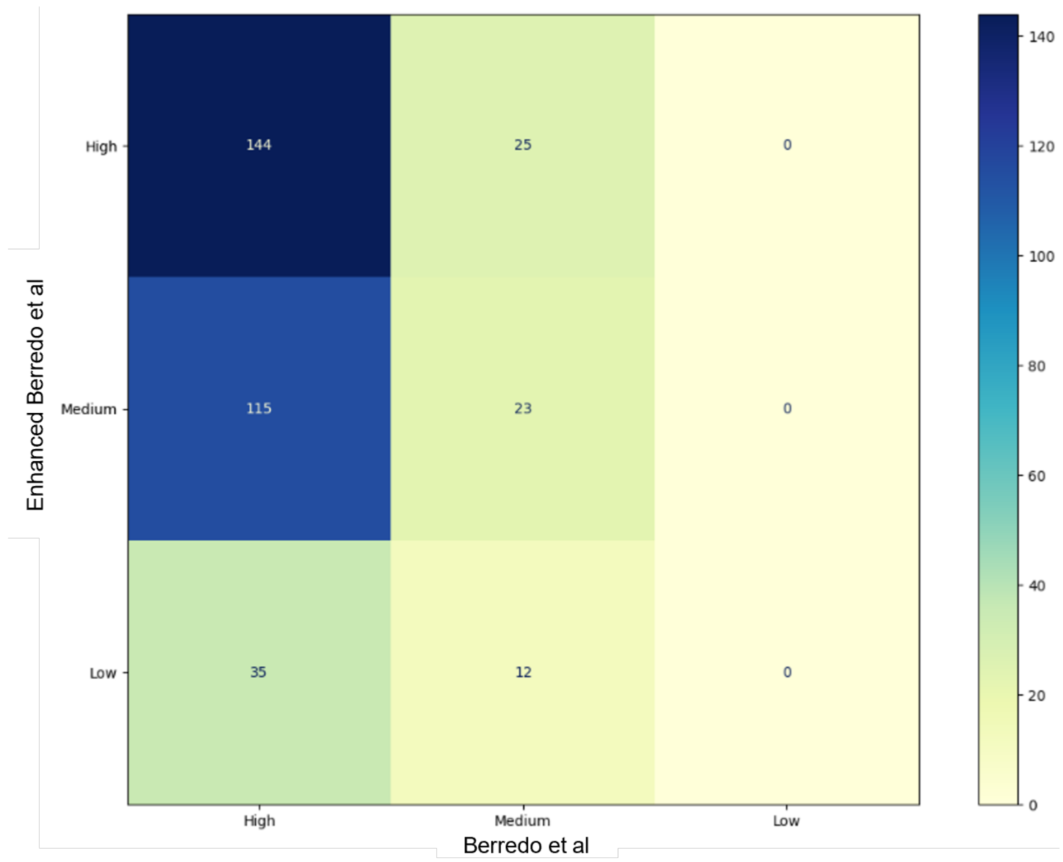

Figure 5.11: Results of criticality to outage - Confusion Matrix between Enhanced Berredo et al. and Berredo et al.

CHAPTER 6: CONCLUSIONS AND FUTURE WORK

6.1 Summary of Contributions

This thesis presents a new method to estimate the risk of outages by wildfire-induced flashovers. The new method, organized into two models, risk of wildfire and risk of outage due to wildfire-induced flashover (vulnerability), are developed and showcased based on a case study of a 500 kV compact line. Results are compared with other methods present in the literature and discussed. New contributions provided in this thesis include:

- A spatial analysis based on historical data of wildfires can be used to design wildfire-resilient OHTL or line sections by identifying the locations with a high risk of wildfires.

- For existing OHTLs, the same spatial analysis can be used to identify critical line spans and prioritize actions of vegetation management.

- The outage analysis highlighted the importance of establishing a safe clearance distance to vegetation present on the sides of the conductors, especially for compact transmission lines. Specific vegetation management protocols should be developed in agreement with environmental policies.

- The study highlights the fragility of the current Brazilian standard in determining safe clearance distances to prevent wildfire-induced flashovers in overhead lines.

- The substantial number of outages associated with compact lines due to phase-to-phase flashovers highlights the need to adopt higher phase-to-ground clearance distances to compensate for the elevated temperatures in the air gap between phases.

- Analysis of existing MVCD calculation methods applied to 108 outages is presented, which shows that these methods are insufficient to prevent wildfire-induced flashovers.

- The existing clearance distances adopted in ATE II show that results from different MVCD calculation approaches are insufficient to prevent wildfire-induced flashovers.

The proposed new method for calculating the risk of wildfire presented a low correlation with the original method proposed in Berredo et al. [17], with 23% of identical results. Conversely, results presented a strong visual correlation with the Kernel Density map (see figures 5.7 and 5.7). Denser sections of the heatmap (white sections) matched spans classified with a very high risk of wildfire (red spans) in the proposed new method. Regions with dispersed hotspots in the heatmap (dark blue to dark sections) matched low-risk spans (green sections). These results evidence the effectiveness of the proposed new methodology in classifying the risk of wildfire. In addition, results suggest that the reference method (i.e., Berredo et al.) may not accurately predict the risk of wildfire with the inputted data, as the comparison with the 20 years of hotspot data resulted in many false positives.

The proposed new model for estimating the risk of wildfire-induced flashover was adapted from Berredo et al. [17] to include aspects such as flame length and vegetation height. The study used data from 108 outage events to identify a clearance distance with a low probability of outage to refine the inputs of vegetation height and flame length. The result of clearance distance was compared with six methods listed in the literature. The comparison of results highlights that the new method (i.e., Enhanced Berredo et al.) provides the MVCD with the closest distance to the safe clearance identified in the outage analysis.

The methodology proposed in Berredo et al. offers the basis for developing an enhanced approach considering relevant aspects missing in the original model. The new method may improve the resiliency of existing and new OHTL subjected to fire-induced flashovers in the Brazilian savanna. The details are presented, and the implementation is explained with validation via assessment of several outage cases between 2013 and 2021, demonstrating the best performance for the Cerrado biome. The test results, summarized in Table 5.9 and Fig. 5.10, provide the performance evaluation.

6.2 Future Research

Future work will focus on improving the proposed risk analysis of fire-induced flashover by assessing characteristics of the Cerrado and Caatinga vegetation during wildfire events (e.g., flame conductivity and chemical properties of suspended particles in the smoke). In addition, future work will consider the reduction of clearance distance due to the conductor swing and span sag due to heating, in the MVCD equation. Winds can impact the clearance distance to the side vegetation in events of wind. Line design standards and guidelines address the effects of wind in the insulator strings at the structures by assuming that a probabilistic wind speed will occur at a specific return period (e.g., every 5 years).

Although the MVCD for the ATE II OHTL is expected to be not less than 9.5 m, the entire transmission line will be assessed to obtain a larger population for the statistical analysis in order to extend the correlation analysis between MVCD and wildfires. Future wildfire and outage events data will be included in the database to update and refine the results of the risk of wildfire and clearance distance to vegetation.

This thesis defends the hypothesis that, in addition to the increased air temperature in the gap, intense flames filling the air gap between the unmanaged vegetation and the side conductors have significantly contributed to the degradation of the dielectric strength of air. Since the proposed equation to determine the minimum approach distance to vegetation relies on suggested flame length and fire temperature, flame and burning characteristics of the Cerrado biome, as well as the current practices of vegetation management, will be investigated in depth.

This thesis addresses the risk of outages due to wildfire-induced flashovers in a "single-transmission line" scale. Wildfires can impact corridors of multiple transmission lines and affect the load flow of an entire system. Future work is intended to understand the threats of wildfires, their consequences to the bulk system, and what operation protocols can be done to ensure grid resiliency.

REFERENCES

[1] NERC, "Transmission Availability Data System (TADS)." Online, jan 2022. data retrieved from TADS Dashboard Supporting Data, `https://www.nerc.com/pa/RAPA/tads/SiteAssets/TADS_Dashboard_Supporting_Data.xlsx"`.

[2] J. Fonseca *et al.*, "Effects of agricultural fires on the performance of overhead transmission lines," in *IEEE Transactions on Power Delivery*, vol. 5, 1990.

[3] W. Schroede and L. Giglio, "NASA VIIRS land science investigator processing system (sips), visible infrared imaging radiometer suite (VIIRS), 375 m & 750 m active fire products: Product user's guide version 1.4," product guide, National Aeronautics and Space Administration (NASA), Ogden, UT: U.S., July 2018.

[4] ONS - Operador Nacional do Sistema Elétrico, "Sobre o SIN: O Sistema em Números." Accessed on 08.31.2022, `http://www.ons.org.br/paginas/sobre-o-sin/o-sistema-em-numeros`.

[5] ONS, "SINtegre - Outages caused by wildfires in the Interconnected System between 2017 and 2021." Online, Nov 2022. data obtained from ONS (SINtegre) via Call Center ticket n.#202210-012197.

[6] D. D. (Director). Ali Kamel, "Globo Reporter - "Fogo do bem" revigora e aduba a terra na Chapada das Mesas - 22/04/2016." `https://globoplay.globo.com/v/4976162/`, 2016.

[7] ATE II Transmissora de Energia SA, "Projeto Executivo," Executive Line Design, ATE II Transmissora de Energia SA, Rio de Janeiro, RJ, 2006.

[8] W. Schroeder, P. Oliva, L. Giglio, and I. A. Csiszar, "The New VIIRS 375 m active fire detection data product: Algorithm description and initial assessment," *Remote Sensing of Environment*, vol. 143, pp. 85–96, 03 2014.

[9] B. Mehmood, M. Akbar, and R. Ullah, "Accelerated aging effect on high temperature vulcanized silicone rubber composites under DC voltage with controlled environmental conditions," *Engineering Failure Analysis*, vol. 118, p. 104870, Dec. 2020.

[10] M. G. Shaik and V. Karuppaiyan, "Investigation of Surface Degradation of Aged High Temperature Vulcanized (HTV) Silicone Rubber Insulators," *Energies*, vol. 12, p. 3769, Jan. 2019.

[11] T. R. V. d. Costa, "Transmission line safety zones and their performance model regarding forest fires," in *Ph.D. Dissertation*, Universidade de Brasília, Brasília, Brazil, 2021.

[12] Eskom Transmission, "Transmission vegetation management guidelines," report, Eskom Transmission, Johannesburg, RSA, 2009.

[13] F. A. Albini, "Estimating wildfire behavior and effects," tech. rep., U.S. Department of Agriculture, Forest Service, Intermountain Forest and Range Experiment Station, 1976.

[14] ANEEL, "Nota Técnica 31/2018-SFE/ANEEL," tech. rep., Agência Nacional de Energia Elétrica - ANEEL, Brasilia Brazil, Apr. 2018.

[15] g1.globo.com Economia, "Apagão foi causado por queimada no Piauí, diz ministro." Accessed on 09.01.2022, `https://g1.globo.com/economia/noticia/2013/08/apagao-foi-causado-por-queimada-no-piaui-diz-lobao.html`.

[16] A. Sukhnandan, "A theoretical and experimental investigation into fire induced flashover of high voltage transmission lines," in *Master's thesis*, University of KwaZulu Natal, South Africa, 2005.

[17] Berredo *et al.*, "Innovative methodology for modelling the criticality of shutdowns by fires in transmission line spans and optimum area design for the suppression of vegetation," in *CIGRE-IEC 2019 Conference on EHV and UHV (AC & DC)*, 2019.

[18] D. M. M. West, H.J., "Fire induced Flashovers of EHV Transmission Lines," in *IEEE PES Winter meeting New York*, 1979.

[19] R. Lanoie and H. P. Mercure, "Influence of forest fires on power line insulation," in *Proceedings of the Sixth International Symposium on High Voltage Engineering*, 1989.

[20] North American Electric Reliability Corporation (NERC), *FAC-003-4 Transmission Vegetation Management*. NERC, 4 ed.

[21] ASSOCIAÇÃO BRASILEIRA DE NORMAS TÉCNICAS, "NBR 5422: Projeto de linhas aéreas de transmissão de energia elétrica: Procedimento," tech. rep., ABNT, Rio de Janeiro, 1985.

[22] NERC, "Transmission Availability Data System Reporting Training 101." Online, jan 2022. data retrieved from NERC TADS website, `https://www.nerc.com/pa/RAPA/tads/Training/TADS_101_Training_October_2020.pdf"`.

[23] E. Chuvieco, I. Aguado, S. Jurdao, M. L. Pettinari, M. Yebra, J. Salas, S. Hantson, J. de la Riva, P. Ibarra, M. Rodrigues, M. Echeverría, D. Azqueta, M. V. Román, A. Bastarrika, S. Martínez, C. Recondo, E. Zapico, and F. J. Martínez-Vega, "Integrating geospatial information into fire risk assessment," *International Journal of Wildland Fire*, vol. 23, no. 5, p. 606, 2014.

[24] Amazon Aid, "The Amazon Biome." Accessed on 03.30.2023, `https://https://amazonaid.org/resources/about-the-amazon/the-amazon-biome/`.

[25] One Earth, "Cerrado." Accessed on 03.30.2023, `https://www.oneearth.org/ecoregions/cerrado/`.

[26] Center for Environmental Peacebuilding, “The Caatinga Biome.” Accessed on 03.30.2023, https://cepb.ngo/the-caatinga-biome/.

[27] UNESCO, “Caatinga Biosphere Reserve, Brazil.” Accessed on 03.30.2023, https://en.unesco.org/biosphere/lac/caatinga.

[28] UNESCO, “Mata Atlântica Biosphere Reserve, Brazil.” Accessed on 03.30.2023, https://en.unesco.org/biosphere/lac/mata-atlantica.

[29] UNESCO, “Pantanal Biosphere Reserve, Brazil.” Accessed on 03.30.2023, https://en.unesco.org/biosphere/lac/pantanal.

[30] Luiz Fernando Wurdig Roesch, Frederico Costa Beber Vieira, Vilmar Alves Pereira, Adriano Luis Schünemann, Italo Filippi Teixeira, Ana Julia Teixeira Senna and Valdir Marcos Stefenon, “The Brazilian Pampa: A Fragile Biome,” *diversity*, vol. 1, pp. 182–198, 12 2009.

[31] P. FROST and F. ROBERTSON, “The ecological effects of fire in savannas,” *Determinants of Tropical Savannas*, 1987.

[32] J. M. C. da Silva and T. E. Lacher, “Cerrado - South America,” in *Encyclopedia of the World’s Biomes* (M. I. Goldstein and D. A. DellaSala, eds.), pp. 546–553, Oxford: Elsevier, 2020.

[33] NASA, “Fire Information for Resource Management System (FIRMS).” Online, Jan. 2022. data retrieved from FIRMS, https://firms.modaps.eosdis.nasa.gov/download/.

[34] J. M. C. da Silva and T. E. Lacher, “Caatinga - South America,” in *Encyclopedia of the World’s Biomes* (M. I. Goldstein and D. A. DellaSala, eds.), pp. 554–561, Oxford: Elsevier, 2020.

[35] International Trade Administration, “Brazil - Country Commercial: Guide.” Accessed on 08.31.2022, https://www.trade.gov/country-commercial-guides/brazil-energy.

[36] “Enabling spatial autocorrelation mapping in QGIS: The hotspot analysis Plugin.” Accessed on 2022-09-28, http://hdl.handle.net/11311/1040664.

[37] D. Paül i Agustí, “The clustering of city images on Instagram: A comparison between projected and perceived images.,” *Journal of Destination Marketing & Management*, vol. 20, p. 100608, June 2021.

[38] S. C. Pal, A. Saha, I. Chowdhuri, D. Ruidas, R. Chakrabortty, P. Roy, and M. Shit, “Earthquake hotspot and coldspot: Where, why and how?,” *Geosystems and Geoenvironment*, vol. 2, p. 100130, Feb. 2023.

[39] I. U. Khan, K. Vachal, S. Ebrahimi, and S. S. Wadhwa, “Hotspot analysis of single-vehicle lane departure crashes in North Dakota,” *IATSS Research*, Dec. 2022.

[40] ESRI, “How Hot Spot Analysis (Getis-Ord Gi*) works.” Accessed on 12.18.2022, https://pro.arcgis.com/en/pro-app/latest/tool-reference/spatial-statistics/h-how-hot-spot-analysis-getis-ord-gi-spatial-stati.htm.

[41] QGIS, “QGIS Python Plugin Repository.” Accessed on 12.10.2022, https://plugins.qgis.org/plugins/.

[42] U.S. Department of Agriculture, Forest Service, Rocky Mountain Research Station, “FlamMap.” Accessed on 15.10.2022, https://www.firelab.org/project/flammap.

[43] “C2-2017 - 2017 National Electrical Safety Code(R) (NESC(R)).” https://ieeexplore.ieee.org/servlet/opac?punumber=7526277.

[44] R. C. Rothermel, “A mathematical model for predicting fire spread in wildland fuels.,” Research Paper INT-115, U.S. Department of Agriculture, Intermountain Forest and Range Experiment Station., Ogden, UT: U.S., jan 1972.

[45] QGIS, “Discover QGIS.” Accessed on 12.10.2022, https://qgis.org/en/site/about/index.html.

[46] R. E. Scott, Joe H.; Burgan, “Standard fire behavior fuel models: a comprehensive set for use with rothermel’s surface fire spread model,” Gen Tech. Report RMRS-GTR-153, U.S. Department of Agriculture, Forest Service, Rocky Mountain Research Station, Fort Collins, CO, 2005.

[47] “4-2013 - IEEE standard for high-voltage testing techniques.” https://ieeexplore.ieee.org/document/6515981.

[48] J. Pandey and D. Pathak., *Geographic Information System*. New Delhi: TERI, 2014.

[49] ESRI, “ArcGIS Pro: Overview.” Accessed on 12.10.2022, https://www.esri.com/en-us/arcgis/products/arcgis-pro/overview.

[50] Hexagon, “Hexagon Geomedia.” Accessed on 12.10.2022, https://hexagon.com/products/geomedia.

[51] Precisely, “MapInfo Pro.” Accessed on 12.10.2022, https://www.precisely.com/product/precisely-mapinfo/mapinfo-pro.

[52] B. M. Geographics, “Global Mapper Pro.” Accessed on 12.10.2022, https://www.bluemarblegeo.com/global-mapper-pro/.

[53] G. GIS, “Grass GIS: Overview.” Accessed on 12.10.2022, https://grass.osgeo.org/learn/overview/.

[54] GE, “SmallWorld GIS.” Accessed on 12.10.2022, https://www.ge.com/digital/applications/smallworld-gis-geospatial-asset-managemen.

[55] Saga, "Saga Overview." Accessed on 12.10.2022, https://saga-gis.sourceforge.io/en/index.html.

[56] Bentley, "Bentley OpenCities Map." Accessed on 12.10.2022, https://www.bentley.com/software/opencities-map/.

[57] OSGeo, "The Open Source Geospatial Foundation." Accessed on 12.10.2022, https://www.osgeo.org/.

[58] NASA, "FIRMS Frequently Asked Questions." Online, Jan. 2022. Accessed on 12.22.2022, https://www.earthdata.nasa.gov/faq/firms-faq#ed-viirs-375m-product.

[59] A. Getis and J. K. Ord, "The analysis of spatial association by use of distance statistics," *Geographical Analysis*, vol. 24, no. 3, pp. 189–206, 1992.

APPENDIX A: OUTAGE DATA

This appendix provides the ATE II outage data details in Table A.1.

Table A.1: ATE II outage dataset.

Date	Time	Line	Fault Type	Phases	Location	Reclosing	TWS Span	P&P Page	MVCD Height	MVCD Status	Specimen	City
Begin of Table A.1												
29/07/2013	17:37:21	RGV-SJI	Two Phase	A and C	Span between towers 409 and 413	YES	411	59	10.53	Cleared	Mamona	Canto do Buriti
28/08/2013	15:08:00	RGV-SJI	Single phase	B	Line sections between towers 411 and 416	NO	413	59	9.38	Cleared	Mamona	Canto do Buriti
20/09/2013	17:26:00	RGV-SJI	Single phase	C	Tower 098	YES	98	14	12.80	Cleared	Cerrado	Urucui
14/10/2013	15:26:00	COL-RGV	Single phase	A	Line sections between towers 570 and 574	YES	573	81A	10.60	Cleared	Cerrado	Riachao
06/07/2014	16:16:00	RGV-SJI	Two phase	A and C	Line sections between towers 200 and 201	YES	200	29	10.10	Cleared	Cerrado	Urucui
03/08/2014	10:52:25	RGV-SJI	Two phase	B and C	Line sections between towers 061 and 067	YES	62	9	9.46	Cleared	Cerrado	Urucui
03/08/2014	10:51:36	RGV-SJI	Two phase	B and C	Line sections between towers 061 and 067	YES	62	9	9.46	Cleared	Cerrado	Urucui
03/08/2014	11:01:09	RGV-SJI	Two phase	B and C	Line sections between towers 061 and 067	YES	62	9	9.46	Cleared	Cerrado	Urucui
03/08/2014	10:51:58	RGV-SJI	Two phase	B and C	Line sections between towers 061 and 067	YES	62	9	9.46	Cleared	Cerrado	Urucui
03/08/2014	10:52:31	RGV-SJI	Two phase	B and C	Line sections between towers 061 and 067	YES	62	9	9.46	Cleared	Cerrado	Urucui
04/08/2014	14:50:00	COL-RGV	Two phase	A and B	Line sections between towers 615 and 617	YES	165	87	9.30	Cleared	Cerrado	Sambaiba
04/08/2014	14:56:00	COL-RGV	Two phase	A and B	Line sections between towers 615 and 617	YES	165	87	9.30	Cleared	Cerrado	Sambaiba
09/08/2014	13:56:00	COL-RGV	Single phase	C	Line sections between towers 506 and 509 and 512 and 517	YES	512	73A	9.84	Cleared	Pasto	Balsas
19/08/2014	13:51:00	RGV-SJI	Two phase	B and C	Line sections between towers 90, 91 and 93	YES	96	13	9.53	Cleared	Cerrado	Urucui
20/08/2014	12:41:00	RGV-SJI	Two phase	B and C	Line sections between towers 88, 91 and 93	YES	90	13	9.40	Cleared	Cerrado	Urucui

Continuation of Table A.1

Date	Time	Line	Fault Type	Phases	Location	Reclosing	TWS Span	P&P Page	MVCD Height	MVCD Status	Specimen	City
17/09/2014	12:06:00	RGV-SJI	Two phase	A and B	Line sections between towers 186 a 195	YES	191	28	9.38	Cleared	Cerrado	Urucui
19/09/2014	11:39:00	COL-RGV	Two phase	B and C	Line sections between towers 640, 641 and 643	NO	640	90	9.40	Not Cleare	Cerrado Babacu	Sambaiba
10/10/2014	15:31:00	COL-RGV	Two phase	A and B	Line sections between towers 652 and 655	YES	655	92	13.70	Not Cleare	Cerrado	Loreto
01/11/2014	17:35:00	RGV-SJI	Two phase	B and C	Tower 479	YES	477	68	14.22	Not Cleare	Capoeira	Canto do Buriti
26/07/2015	15:14:00	RGV-SJI	Two phase	A and B	Line sections between towers 165, 166 e 167	YES	199	29	10.60	Cleared	Cerrado	Urucui
05/08/2015	12:58:00	RGV-SJI	Two phase	A and B	Line sections between towers 255 a 263	YES	261	37	9.34	Cleared	Cerrado and Caatinga	Bertolinia
16/09/2015	10:08:00	COL-RGV	Two phase	A and B	Tower 072	NO	72	10	9.27	Not Cleare	Cerrado	Palmeirante
16/09/2015	11:49:00	COL-RGV	Two phase	A and B	Tower 072	NO	72	10	9.27	Not Cleare	Cerrado	Palmeirante
16/09/2015	10:08:00	COL-RGV	Two phase	A and B	Tower 072	NO	72	10	9.27	Not Cleare	Cerrado	Palmeirante
20/09/2015	17:15:00	COL-RGV	Single phase	B	Tower 283	YES	283	40	10.67	Not Cleare	Cerrado	Carolina
21/09/2015	10:58:00	COL-RGV	Two phase	A and C	Line sections between towers 404 a 409	YES	404	57	9.70	Cleared	Cerrado	Riachao
21/09/2015	17:32:00	COL-RGV	Single phase	C	Line sections between towers 404 a 409	YES	404	57	9.70	Cleared	Cerrado	Riachao
21/09/2015	17:33:00	COL-RGV	Single phase	C	Line sections between towers 404 a 409	YES	404	57	9.70	Cleared	Cerrado	Riachao
23/09/2015	13:01:00	COL-RGV	Two phase	A and C	Line sections between towers 355 e 359	YES	358	50A	9.40	Not Cleare	Cerrado	Carolina
23/09/2015	13:01:00	COL-RGV	Two phase	B and C	Line sections between towers 355 e 359	YES	358	50A	9.40	Not Cleare	Cerrado	Carolina
23/09/2015	13:51:00	COL-RGV	Two phase	B and C	Line sections between towers 355 e 359	YES	358	50A	9.40	Not Cleare	Cerrado	Carolina

Continuation of Table A.1

Date	Time	Line	Fault Type	Phases	Location	Reclosing	TWS Span	P&P Page	MVCD Height	MVCD Status	Specimen	City
23/09/2015	13:51:00	COL-RGV	Single phase	C	Line sections between towers 355 e 359	YES	358	50A	9.40	Not Cleare	Cerrado	Carolina
27/09/2015	14:31:00	COL-RGV	Two phase	A and C	Line sections between towers 517 a 521	YES	520	73A	9.10	Cleared	Pasture	Balsas
21/10/2015	16:32:00	COL-RGV	Single phase	C	Line sections between towers 485 e 486	YES	495	70	11.33	Cleared	Cerrado	Balsas
05/11/2016	13:08:00	COL-RGV	Two phase	B and C	Line sections between towers 673 and 674	YES	673	95	9.50	Cleared	Cerrado	São João do Piauí
05/11/2016	13:05:00	COL-RGV	Two phase	B and C	Line sections between towers 673 and 674	YES	673	95	9.50	Cleared	Cerrado	São João do Piauí
05/11/2016	12:56:00	COL-RGV	Two phase	A and B	Line section between towers 673 and 674	YES	673	95	9.50	Cleared	Cerrado	São João do Piauí
13/08/2017	15:40:00	COL-RGV	Two phase	A and B	Tower 503	YES	503	71	9.60	Not Cleare	Cerrado	Balsas
13/08/2017	16:02:00	COL-RGV	Two phase	A and C	Tower 503	YES	503	71	9.60	Not Cleare	Cerrado	Balsas
31/08/2017	14:47:00	COL-RGV	Two phase	B and C	Line sections between towers 711, 713 and 714	YES		100	10.70		Cerrado	Loreto
03/09/2017	13:08:00	COL-RGV	Two phase	B and C	Line sections between towers 373 and 375	NO	372	52	10.40	Cleared	Cerrado	Riachao
19/09/2017	15:49:00	COL-RGV	Two phase	A and C	Line sections between towers 338 and 346	NO	338	48A	9.30	Cleared	Cerrado	Carolina
19/09/2017	13:27:00	COL-RGV	Two phase	A and C	Line sections between towers 338 and 346	NO	338	48A	9.30	Cleared	Cerrado	Carolina
19/09/2017	13:51:00	COL-RGV	Two phase	B and C	Line sections between towers 338 and 346	NO	338	48A	9.30	Cleared	Cerrado	Carolina
19/09/2017	13:50:00	COL-RGV	Two phase	B and C	Line sections between towers 338 and 346	NO	338	48A	9.30	Cleared	Cerrado	Carolina
19/09/2017	15:50:00	COL-RGV	Two phase	A and C	Line sections between towers 338 and 346	NO	338	48A	9.30	Cleared	Cerrado	Carolina
19/09/2017	13:49:00	COL-RGV	Two phase	A and C	Line sections between towers 338 and 346	NO	338	48A	9.30	Cleared	Cerrado	Carolina

Continuation of Table A.1												
Date	**Time**	**Line**	**Fault Type**	**Phases**	**Location**	**Reclosing**	**TWS Span**	**P&P Page**	**MVCD Height**	**MVCD Status**	**Specimen**	**City**
19/09/2017	13:27:00	COL-RGV	Two phase	A and C	Line sections between towers 338 and 346	NO	338	48A	9.30	Cleared	Cerrado	Carolina
26/09/2017	11:43:00	COL-RGV	Two phase	A and B	Line sections between towers 053 and 059	NO	62	9	9.87	Not Cleare	Cerrado	Palmeirante
26/09/2017	13:29:00	COL-RGV	Two phase	A and B	Line sections between towers 053 and 059	NO	62	9	9.87	Not Cleare	Cerrado	Palmeirante
15/10/2017	16:38:00	RGV-SJI	Two phase	A and C	Line sections between towers 191 and 196	YES	194	28	9.40	Cleared	Cerrado	Urucui
04/08/2018	13:24:00	RGV-SJI	Single phase	B	Tower 450	YES	450	64	16.80	Not Cleare	Capoeira	Canto do Buriti
07/08/2018	14:51:00	RGV-SJI	Two phase	A and C	Line sections between towers 446 and 449	YES	447	64	9.80	Cleared	Capoeira	Canto do Buriti
11/08/2018	11:43:00	RGV-SJI	Two phase	A and C	Line sections between towers 430, 431 and 433 a 436	YES	432	62	9.50	Cleared	Capoeira	Canto do Buriti
19/08/2018	14:31:00	RGV-SJI	Single phase	C	Line sections between towers 403 and 411	YES	408	58	10.00	Cleared	Mamona	Canto do Buriti
04/09/2018	12:22:00	RGV-SJI	Two phase	A and C	Line section between towers 344 and 348	YES	347	50	9.52	Cleared	Capoeira	Eliseu Martins
22/09/2018	14:41:00	RGV-SJI	Two phase	B and C	Line sections between towers 515 and 519	YES	513	74	9.50	Cleared	Cerrado	Canto do Buriti
24/09/2018	12:32:00	COL-RGV	Single phase	C	Line sections between towers 405 and 412	YES	408	58	10.20	Cleared	Cerrado	Riachao
24/09/2018	12:36:00	COL-RGV	Single phase	C	Line sections between towers 405 and 412	YES	408	58	10.20	Cleared	Cerrado	Riachao
10/10/2018	13:40:00	RGV-SJI	Two phase	A and B	Line sections between towers 642 and 643	YES	643	92	9.42	Cleared	Cerrado	São João do Piauí
14/10/2018	15:21:00	RGV-SJI	Single phase	C	Line sections between towers 660 and 663	NO	662	95	9.80	Cleared	Cerrado	São João do Piauí
18/08/2019	16:54:00	RGV-SJI	Two phase	A and C	Tower 256	YES	256	37	9.46	Cleared	Cerrado	Sebastiao Leal
18/08/2019	16:55:00	RGV-SJI	Two phase	A and C	Tower 256	NO	256	37	9.46	Cleared	Cerrado	Sebastiao Leal

Continuation of Table A.1

Date	Time	Line	Fault Type	Phases	Location	Reclosing	TWS Span	P&P Page	MVCD Height	MVCD Status	Specimen	City
07/09/2019	13:23:00	COL-RGV	Two phase	B and C	Tower 731	NO	731	103	12.45	Not Cleare	Capoeira	Ribeiro Gonçalves
16/09/2019	13:07:00	RGV-SJI	Two phase	B and C	Tower 439	YES	439	63	10.50	Cleared	Capoeira	Canto do Buriti
16/09/2019	13:15:00	RGV-SJI	Two phase	A and C	Tower 438	YES	438	63	10.70	Cleared	Capoeira	Canto do Buriti
25/09/2019	13:35:00	RGV-SJI	Two phase	A and B	Tower 113	NO	112	16	9.55	Cleared	Cerrado	Urucui
10/08/2020	16:22:00	COL-RGV	Two phase	A and B	Line sections between towers 673 and 677	YES	673	95	9.30	Cleared	Cerrado	Loreto
01/09/2020	16:32:00	COL-RGV	Two phase	A and B	Tower 646 (628 in real)	YES	646	88	10.10	Cleared	Cerrado	Sambaiba
08/09/2020	15:11:00	COL-RGV	Two phase	A and B	Line sections between towers 547 and 548	YES	547	77A	9.98	Cleared	Cerrado	Balsas
08/09/2020	15:14:00	COL-RGV	Two phase	A and B	Line sections between towers 547 and 548	YES	547	77A	9.98	Cleared	Cerrado	Balsas
11/09/2020	13:32:00	RGV-SJI	Two phase	B and C	Line sections between towers 405 and 406	YES	405	58	10.53	Cleared	Mamona	Canto do Buriti
23/09/2020	13:31:00	RGV-SJI	Two phase	A and B	Tower 116	YES	114	17	10.14	Cleared	Cerrado	Urucui
23/09/2020	13:01:00	RGV-SJI	Two phase	B and C	Tower 116	YES	114	17	10.14	Cleared	Cerrado	Urucui
23/09/2020	13:52:00	RGV-SJI	Two phase	B and C	Tower 116	YES	114	17	10.14	Cleared	Cerrado	Urucui
23/09/2020	13:51:00	RGV-SJI	Two phase	B and C	Tower 116	YES	114	17	10.14	Cleared	Cerrado	Urucui
28/09/2020	11:19:00	COL-RGV	Two phase	A and C	Tower 401	YES	401	57	10.00	Cleared	Cerrado	Riachao
28/09/2020	11:19:00	COL-RGV	Two phase	A and C	Tower 401	YES	401	57	10.00	Cleared	Cerrado	Riachao
29/09/2020	17:19:00	RGV-SJI	Two phase	A and C	Line sections between towers 448 and 450	NO	448	64	10.43	Cleared	Capoeira	Canto do Buriti
29/09/2020	16:41:00	RGV-SJI	Two phase	A and C	Line sections between towers 448 and 450	NO	448	64	10.43	Cleared	Capoeira	Canto do Buriti
30/09/2020	12:56:00	RGV-SJI	Two phase	A and B	Line sections between towers 441 and 450	YES	445	64	10.00	Cleared	Capoeira	Canto do Buriti
30/09/2020	12:28:00	RGV-SJI	Two phase	A and C	Line sections between towers 441 and 450	YES	445	64	10.00	Cleared	Capoeira	Canto do Buriti
30/09/2020	12:51:00	RGV-SJI	Two phase	A and C	Line sections between towers 441 and 450	YES	445	64	10.00	Cleared	Capoeira	Canto do Buriti
30/09/2020	12:52:00	RGV-SJI	Two phase	A and C	Line sections between towers 441 and 450	YES	445	64	10.00	Cleared	Capoeira	Canto do Buriti

Continuation of Table A.1

Date	Time	Line	Fault Type	Phases	Location	Reclosing	TWS Span	P&P Page	MVCD Height	MVCD Status	Specimen	City
30/09/2020	12:53:00	RGV-SJI	Two phase	A and C	Line sections between towers 441 and 450	YES	445	64	10.00	Cleared	Capoeira	Canto do Buriti
30/09/2020	12:54:00	RGV-SJI	Two phase	A and C	Line sections between towers 441 and 450	YES	445	64	10.00	Cleared	Capoeira	Canto do Buriti
30/09/2020	13:16:00	RGV-SJI	Two phase	A and C	Line sections between towers 441 and 450	YES	445	64	10.00	Cleared	Capoeira	Canto do Buriti
30/09/2020	13:17:00	RGV-SJI	Two phase	A and C	Line sections between towers 441 and 450	YES	445	64	10.00	Cleared	Capoeira	Canto do Buriti
30/09/2020	13:19:00	RGV-SJI	Two phase	A and C	Line sections between towers 441 and 450	YES	445	64	10.00	Cleared	Capoeira	Canto do Buriti
30/09/2020	14:20:00	RGV-SJI	Three phase	A, B and C	Line sections between towers 441 and 450	YES	445	64	10.00	Cleared	Capoeira	Canto do Buriti
30/09/2020	14:38:00	RGV-SJI	Single phase	A	Line sections between towers 441 and 450	YES	445	64	10.00	Cleared	Capoeira	Canto do Buriti
30/09/2020	17:08:00	RGV-SJI	Two phase	A and C	Line sections between towers 441 and 450	YES	445	64	10.00	Cleared	Capoeira	Canto do Buriti
01/10/2020	11:16:00	COL-RGV	Two phase	A and C	Tower 568	YES	568	80A	9.30	Cleared	Cerrado	Balsas
01/10/2020	11:49:00	RGV-SJI	Single phase	A	Line Section 162	YES	162	24	9.52	Cleared	Cerrado	Urucui
07/10/2020	14:04:00	RGV-SJI	Two phase	A and C	Tower 423	NO	423	61	10.55	Cleared	Capoeira	Canto do Buriti
07/10/2020	13:54:00	RGV-SJI	Two phase	A and C	Tower 423	NO	423	61	10.55	Cleared	Capoeira	Canto do Buriti
08/05/2021	15:39:00	RGV-SJI	Two phase	B and C	Torre 624	NO	622	89	12.37	Not Cleare	Dense Vegetation	São João do Piauí
22/07/2021	15:05:00	RGV-SJI	Two phase	A e B	Line sections between towers 67, 68 e 69	YES	70	10	9.64	Cleared	Cerrado	Urucui
13/08/2021	14:39:00	RGV-SJI	Two phase	B and C	Line sections between towers 437, 438 e 439	YES	438	63	10.83	Cleared	Capoeira	Canto do Buriti
15/08/2021	12:50:00	RGV-SJI	Two phase	A and C	Line sections between towers 245 e 246	YES	247	36	9.60	Cleared	Cerrado	Sebastiao Leal
17/08/2021	14:52:00	RGV-SJI	Two phase	A and C	Line sections between towers 241 a 244	YES	243	35	9.48	Cleared	Cerrado	Sebastiao Leal

Continuation of Table A.1

Date	Time	Line	Fault Type	Phases	Location	Reclosing	TWS Span	P&P Page	MVCD Height	MVCD Status	Specimen	City
17/08/2021	12:05:00	COL-RGV	Two phase	A and C	Line sections between towers 478, 479 e 480	YES	478	68	9.87	Cleared	Corn Straw	Balsas
17/08/2021	12:20:00	COL-RGV	Two phase	A and B	Line sections between towers 478, 479 e 480	YES	478	68	9.87	Cleared	Corn Straw	Balsas
22/08/2021	11:35:00	RGV-SJI	Two phase	B and C	Line sections between towers 89, 90, 91 e 92	YES	92	13	9.50	Cleared	Cerrado	Urucui
05/09/2021	11:57:00	COL-RGV	Single phase	C	Line sections between towers 630 a 632	YES	643	89	9.50	Cleared	Cerrado	Sambaiba
12/09/2021	16:03:00	RGV-SJI	Two phase	A and B	Line sections between towers 63, 64, 65 e 66	NO	66	10	9.42	Cleared	Cerrado	Urucui
11/10/2021	10:09:00	RGV-SJI	Two phase	B and C	Line sections between towers 617 and 618	NO	617	88	9.42	Cleared	Capoeira	São João do Piauí
11/10/2021	10:08:00	RGV-SJI	Two phase	B and C	Line sections between towers 617 and 618	YES	617	88	9.42	Cleared	Capoeira	São João do Piauí

End of Table

APPENDIX B: RESULTS OF RISK OF WILDFIRE

This appendix section provides the results of the correlation of risk of wildfire between Berredo et al. and Getis Ord* GI. Details in Table B.1.

Table B.1: Results of Correlation of Risk of Wildfire

Begin of Table B.1							
UID	Getis Ord* GI Analysis			Berredo et al. Analysis		Correlation	Count of Hotspots
	P-Value	Z-Score	Risk Class	Risk Value	Risk Class		
15	0.836515029	0.206353195	High Risk	0.968773127	Very High Risk	FALSE	15
18	0.618917446	0.497385191	High Risk	0.968773127	Very High Risk	FALSE	18
21	0.430452721	0.788417188	Very High Risk	0.960833907	Very High Risk	TRUE	21
18	0.618917446	0.497385191	High Risk	0.92435801	Very High Risk	FALSE	18
10	0.780474961	-0.278700132	Medium Risk	0.932803094	Very High Risk	FALSE	10
10	0.780474961	-0.278700132	Medium Risk	0.932803094	Very High Risk	FALSE	10
14	0.912930815	0.10934253	Medium Risk	0.938478291	Very High Risk	FALSE	14
14	0.912930815	0.10934253	Medium Risk	0.945551872	Very High Risk	FALSE	14
17	0.688880684	0.400374526	High Risk	0.929145694	Very High Risk	FALSE	17
13	0.990160845	0.012331864	Medium Risk	0.929145694	Very High Risk	FALSE	13
20	0.489310107	0.691406522	Very High Risk	0.920309842	Very High Risk	TRUE	20
22	0.375925916	0.885427853	Very High Risk	0.920309842	Very High Risk	TRUE	22
20	0.489310107	0.691406522	Very High Risk	0.910877109	Very High Risk	TRUE	20
13	0.990160845	0.012331864	Medium Risk	0.906193435	Very High Risk	FALSE	13
11	0.855826433	-0.181689467	Medium Risk	0.923500896	Very High Risk	FALSE	11
15	0.836515029	0.206353195	High Risk	0.900788307	Very High Risk	FALSE	15
22	0.375925916	0.885427853	Very High Risk	0.880204976	Very High Risk	TRUE	22
23	0.325883858	0.982438518	Very High Risk	0.873216689	Very High Risk	TRUE	23
21	0.430452721	0.788417188	Very High Risk	0.867959201	Very High Risk	TRUE	21
24	0.280387536	1.079449184	Very High Risk	0.85716629	Very High Risk	TRUE	24
35	0.031827809	2.146566503	Very High Risk	0.884118021	Very High Risk	TRUE	35
19	0.552247379	0.594395857	High Risk	0.884118021	Very High Risk	FALSE	19
20	0.489310107	0.691406522	Very High Risk	0.884118021	Very High Risk	TRUE	20
17	0.688880684	0.400374526	High Risk	0.871064007	Very High Risk	FALSE	17
14	0.912930815	0.10934253	Medium Risk	0.849339783	Very High Risk	FALSE	14
17	0.688880684	0.400374526	High Risk	0.852214813	Very High Risk	FALSE	17
18	0.618917446	0.497385191	High Risk	0.848824978	Very High Risk	FALSE	18
16	0.761612584	0.303363861	High Risk	0.874253154	Very High Risk	FALSE	16
8	0.636411912	-0.472721463	Low Risk	0.91338706	Very High Risk	FALSE	8
13	0.990160845	0.012331864	Medium Risk	0.952696443	Very High Risk	FALSE	13
13	0.990160845	0.012331864	Medium Risk	0.952696443	Very High Risk	FALSE	13
13	0.990160845	0.012331864	Medium Risk	0.957376897	Very High Risk	FALSE	13

Continuation of Table B.1

UID	Getis Ord* GI Analysis			Berredo et al. Analysis		Correlation	Count of Hotspots
	P-Value	Z-Score	Risk Class	Risk Value	Risk Class		
7	0.568859396	-0.569732128	Low Risk	0.959825873	Very High Risk	FALSE	7
6	0.504936439	-0.666742794	Low Risk	0.963159561	Very High Risk	FALSE	6
7	0.568859396	-0.569732128	Low Risk	0.963256598	Very High Risk	FALSE	7
6	0.504936439	-0.666742794	Low Risk	0.963718772	Very High Risk	FALSE	6
3	0.338176334	-0.95777479	Low Risk	0.963883996	Very High Risk	FALSE	3
3	0.338176334	-0.95777479	Low Risk	0.963883996	Very High Risk	FALSE	3
5	0.445014177	-0.763753459	Low Risk	0.96230638	Very High Risk	FALSE	5
4	0.389367968	-0.860764124	Low Risk	0.966498613	Very High Risk	FALSE	4
3	0.338176334	-0.95777479	Low Risk	0.966498613	Very High Risk	FALSE	3
2	0.291523458	-1.054785455	Low Risk	0.971036792	Very High Risk	FALSE	2
2	0.291523458	-1.054785455	Low Risk	0.977912426	Very High Risk	FALSE	2
4	0.389367968	-0.860764124	Low Risk	0.974655807	Very High Risk	FALSE	4
4	0.389367968	-0.860764124	Low Risk	0.974655807	Very High Risk	FALSE	4
3	0.338176334	-0.95777479	Low Risk	0.967693031	Very High Risk	FALSE	3
1	0.249404862	-1.151796121	Low Risk	0.973289371	Very High Risk	FALSE	1
0	0.211735751	-1.248806786	Low Risk	0.905102372	Very High Risk	FALSE	0
0	0.211735751	-1.248806786	Low Risk	0.907351136	Very High Risk	FALSE	0
0	0.211735751	-1.248806786	Low Risk	0.907351136	Very High Risk	FALSE	0
0	0.211735751	-1.248806786	Low Risk	0.906172454	Very High Risk	FALSE	0
0	0.211735751	-1.248806786	Low Risk	0.906399846	Very High Risk	FALSE	0
0	0.211735751	-1.248806786	Low Risk	0.906399846	Very High Risk	FALSE	0
0	0.211735751	-1.248806786	Low Risk	0.88997525	Very High Risk	FALSE	0
0	0.211735751	-1.248806786	Low Risk	0.898253083	Very High Risk	FALSE	0
0	0.211735751	-1.248806786	Low Risk	0.898253083	Very High Risk	FALSE	0
0	0.211735751	-1.248806786	Low Risk	0.897456288	Very High Risk	FALSE	0
0	0.211735751	-1.248806786	Low Risk	0.853966892	Very High Risk	FALSE	0
0	0.211735751	-1.248806786	Low Risk	0.851279736	Very High Risk	FALSE	0
0	0.211735751	-1.248806786	Low Risk	0.846378565	Very High Risk	FALSE	0
0	0.211735751	-1.248806786	Low Risk	0.853063583	Very High Risk	FALSE	0
0	0.211735751	-1.248806786	Low Risk	0.86139214	Very High Risk	FALSE	0
0	0.211735751	-1.248806786	Low Risk	0.863594413	Very High Risk	FALSE	0
0	0.211735751	-1.248806786	Low Risk	0.89446497	Very High Risk	FALSE	0
5	0.445014177	-0.763753459	Low Risk	0.93748492	Very High Risk	FALSE	5
21	0.430452721	0.788417188	Very High Risk	0.973853409	Very High Risk	TRUE	21

Continuation of Table B.1

UID	Getis Ord* GI Analysis			Berredo et al. Analysis		Correlation	Count of Hotspots
	P-Value	Z-Score	Risk Class	Risk Value	Risk Class		
22	0.375925916	0.885427853	Very High Risk	0.97457552	Very High Risk	TRUE	22
17	0.688880684	0.400374526	High Risk	0.975330114	Very High Risk	FALSE	17
24	0.280387536	1.079449184	Very High Risk	0.975330114	Very High Risk	TRUE	24
27	0.170536746	1.37048118	Very High Risk	0.974744856	Very High Risk	TRUE	27
22	0.375925916	0.885427853	Very High Risk	0.973615646	Very High Risk	TRUE	22
18	0.618917446	0.497385191	High Risk	0.97163111	Very High Risk	FALSE	18
13	0.990160845	0.012331864	Medium Risk	0.970719814	Very High Risk	FALSE	13
10	0.780474961	-0.278700132	Medium Risk	0.938244939	Very High Risk	FALSE	10
6	0.504936439	-0.666742794	Low Risk	0.926587343	Very High Risk	FALSE	6
15	0.836515029	0.206353195	High Risk	0.916557312	Very High Risk	FALSE	15
22	0.375925916	0.885427853	Very High Risk	0.925494313	Very High Risk	TRUE	22
23	0.325883858	0.982438518	Very High Risk	0.943210125	Very High Risk	TRUE	23
30	0.096610425	1.661513176	Very High Risk	0.969036937	Very High Risk	TRUE	30
26	0.202851129	1.273470515	Very High Risk	0.969036937	Very High Risk	TRUE	26
25	0.239411168	1.176459849	Very High Risk	0.97383827	Very High Risk	TRUE	25
18	0.618917446	0.497385191	High Risk	0.97383827	Very High Risk	FALSE	18
23	0.325883858	0.982438518	Very High Risk	0.970712125	Very High Risk	TRUE	23
36	0.02485962	2.243577169	Very High Risk	0.96937871	Very High Risk	TRUE	36
31	0.078658419	1.758523842	Very High Risk	0.943401456	Very High Risk	TRUE	31
33	0.050873513	1.952545173	Very High Risk	0.961903691	Very High Risk	TRUE	33
43	0.003470644	2.922651827	Very High Risk	0.967798531	Very High Risk	TRUE	43
51	0.000216675	3.69873715	Very High Risk	0.970446944	Very High Risk	TRUE	51
49	0.000457095	3.504715819	Very High Risk	0.970446944	Very High Risk	TRUE	49
44	0.002530565	3.019662492	Very High Risk	0.959063053	Very High Risk	TRUE	44
43	0.003470644	2.922651827	Very High Risk	0.958092749	Very High Risk	TRUE	43
46	0.001310439	3.213683823	Very High Risk	0.958092749	Very High Risk	TRUE	46
47	0.000930648	3.310694488	Very High Risk	0.956986904	Very High Risk	TRUE	47
16	0.761612584	0.303363861	High Risk	0.950965881	Very High Risk	FALSE	16
14	0.912930815	0.10934253	Medium Risk	0.954613805	Very High Risk	FALSE	14
6	0.504936439	-0.666742794	Low Risk	0.954613805	Very High Risk	FALSE	6
6	0.504936439	-0.666742794	Low Risk	0.954546571	Very High Risk	FALSE	6
6	0.504936439	-0.666742794	Low Risk	0.952795506	Very High Risk	FALSE	6
4	0.389367968	-0.860764124	Low Risk	0.951185346	Very High Risk	FALSE	4
12	0.93251675	-0.084678801	Medium Risk	0.94871819	Very High Risk	FALSE	12

Continuation of Table B.1

UID	Getis Ord* GI Analysis			Berredo et al. Analysis		Correlation	Count of Hotspots
	P-Value	Z-Score	Risk Class	Risk Value	Risk Class		
23	0.325883858	0.982438518	Very High Risk	0.925719738	Very High Risk	TRUE	23
23	0.325883858	0.982438518	Very High Risk	0.886652827	Very High Risk	TRUE	23
21	0.430452721	0.788417188	Very High Risk	0.905085206	Very High Risk	TRUE	21
16	0.761612584	0.303363861	High Risk	0.905085206	Very High Risk	FALSE	16
10	0.780474961	-0.278700132	Medium Risk	0.821275055	Very High Risk	FALSE	10
41	0.006359792	2.728630496	Very High Risk	0.966188669	Very High Risk	TRUE	41
37	0.019253409	2.340587834	Very High Risk	0.966188669	Very High Risk	TRUE	37
32	0.063519936	1.855534507	Very High Risk	0.946395993	Very High Risk	TRUE	32
28	0.142242306	1.467491845	Very High Risk	0.941158295	Very High Risk	TRUE	28
26	0.202851129	1.273470515	Very High Risk	0.954409122	Very High Risk	TRUE	26
23	0.325883858	0.982438518	Very High Risk	0.960203767	Very High Risk	TRUE	23
22	0.375925916	0.885427853	Very High Risk	0.889305115	Very High Risk	TRUE	22
14	0.912930815	0.10934253	Medium Risk	0.889305115	Very High Risk	FALSE	14
10	0.780474961	-0.278700132	Medium Risk	0.885562658	Very High Risk	FALSE	10
7	0.568859396	-0.569732128	Low Risk	0.884071231	Very High Risk	FALSE	7
11	0.855826433	-0.181689467	Medium Risk	0.895805657	Very High Risk	FALSE	11
10	0.780474961	-0.278700132	Medium Risk	0.895805657	Very High Risk	FALSE	10
10	0.780474961	-0.278700132	Medium Risk	0.961655557	Very High Risk	FALSE	10
15	0.836515029	0.206353195	High Risk	0.963345885	Very High Risk	FALSE	15
11	0.855826433	-0.181689467	Medium Risk	0.971799552	Very High Risk	FALSE	11
11	0.855826433	-0.181689467	Medium Risk	0.971799552	Very High Risk	FALSE	11
12	0.93251675	-0.084678801	Medium Risk	0.964496255	Very High Risk	FALSE	12
15	0.836515029	0.206353195	High Risk	0.964020252	Very High Risk	FALSE	15
13	0.990160845	0.012331864	Medium Risk	0.964400768	Very High Risk	FALSE	13
16	0.761612584	0.303363861	High Risk	0.964400768	Very High Risk	FALSE	16
13	0.990160845	0.012331864	Medium Risk	0.962023854	Very High Risk	FALSE	13
5	0.445014177	-0.763753459	Low Risk	0.962023854	Very High Risk	FALSE	5
4	0.389367968	-0.860764124	Low Risk	0.959507465	Very High Risk	FALSE	4
7	0.568859396	-0.569732128	Low Risk	0.958222747	Very High Risk	FALSE	7
6	0.504936439	-0.666742794	Low Risk	0.958743215	Very High Risk	FALSE	6
11	0.855826433	-0.181689467	Medium Risk	0.973830521	Very High Risk	FALSE	11
13	0.990160845	0.012331864	Medium Risk	0.97804451	Very High Risk	FALSE	13
11	0.855826433	-0.181689467	Medium Risk	0.97804451	Very High Risk	FALSE	11
11	0.855826433	-0.181689467	Medium Risk	0.969786882	Very High Risk	FALSE	11

Continuation of Table B.1

UID	Getis Ord* GI Analysis			Berredo et al. Analysis		Correlation	Count of Hotspots
	P-Value	Z-Score	Risk Class	Risk Value	Risk Class		
8	0.636411912	-0.472721463	Low Risk	0.969673574	Very High Risk	FALSE	8
4	0.389367968	-0.860764124	Low Risk	0.980063379	Very High Risk	FALSE	4
4	0.389367968	-0.860764124	Low Risk	0.978550375	Very High Risk	FALSE	4
6	0.504936439	-0.666742794	Low Risk	0.963943303	Very High Risk	FALSE	6
12	0.93251675	-0.084678801	Medium Risk	0.97862947	Very High Risk	FALSE	12
22	0.375925916	0.885427853	Very High Risk	0.956385672	Very High Risk	TRUE	22
17	0.688880684	0.400374526	High Risk	0.941519022	Very High Risk	FALSE	17
8	0.636411912	-0.472721463	Low Risk	0.920011044	Very High Risk	FALSE	8
10	0.780474961	-0.278700132	Medium Risk	0.8343786	Very High Risk	FALSE	10
10	0.780474961	-0.278700132	Medium Risk	0.847765803	Very High Risk	FALSE	10
8	0.636411912	-0.472721463	Low Risk	0.847765803	Very High Risk	FALSE	8
7	0.568859396	-0.569732128	Low Risk	0.847765803	Very High Risk	FALSE	7
13	0.990160845	0.012331864	Medium Risk	0.830701411	Very High Risk	FALSE	13
27	0.170536746	1.37048118	Very High Risk	0.924737155	Very High Risk	TRUE	27
24	0.280387536	1.079449184	Very High Risk	0.867063284	Very High Risk	TRUE	24
27	0.170536746	1.37048118	Very High Risk	0.876151919	Very High Risk	TRUE	27
24	0.280387536	1.079449184	Very High Risk	0.893146813	Very High Risk	TRUE	24
22	0.375925916	0.885427853	Very High Risk	0.91009593	Very High Risk	TRUE	22
18	0.618917446	0.497385191	High Risk	0.89331305	Very High Risk	FALSE	18
11	0.855826433	-0.181689467	Medium Risk	0.901396394	Very High Risk	FALSE	11
8	0.636411912	-0.472721463	Low Risk	0.948157251	Very High Risk	FALSE	8
8	0.636411912	-0.472721463	Low Risk	0.931208134	Very High Risk	FALSE	8
12	0.93251675	-0.084678801	Medium Risk	0.888367712	Very High Risk	FALSE	12
11	0.855826433	-0.181689467	Medium Risk	0.888367712	Very High Risk	FALSE	11
11	0.855826433	-0.181689467	Medium Risk	0.880904973	Very High Risk	FALSE	11
17	0.688880684	0.400374526	High Risk	0.879826069	Very High Risk	FALSE	17
14	0.912930815	0.10934253	Medium Risk	0.879826069	Very High Risk	FALSE	14
8	0.636411912	-0.472721463	Low Risk	0.871363997	Very High Risk	FALSE	8
9	0.70713191	-0.375710797	Low Risk	0.888425052	Very High Risk	FALSE	9
12	0.93251675	-0.084678801	Medium Risk	0.953069389	Very High Risk	FALSE	12
10	0.780474961	-0.278700132	Medium Risk	0.953069389	Very High Risk	FALSE	10
12	0.93251675	-0.084678801	Medium Risk	0.938942075	Very High Risk	FALSE	12
20	0.489310107	0.691406522	Very High Risk	0.934262276	Very High Risk	TRUE	20
22	0.375925916	0.885427853	Very High Risk	0.912899852	Very High Risk	TRUE	22

Continuation of Table B.1							
UID	Getis Ord* GI Analysis			Berredo et al. Analysis		Correlation	Count of Hotspots
	P-Value	Z-Score	Risk Class	Risk Value	Risk Class		
27	0.170536746	1.37048118	Very High Risk	0.894279063	Very High Risk	TRUE	27
26	0.202851129	1.273470515	Very High Risk	0.918403864	Very High Risk	TRUE	26
10	0.780474961	-0.278700132	Medium Risk	0.918403864	Very High Risk	FALSE	10
8	0.636411912	-0.472721463	Low Risk	0.918624103	Very High Risk	FALSE	8
10	0.780474961	-0.278700132	Medium Risk	0.911446929	Very High Risk	FALSE	10
9	0.70713191	-0.375710797	Low Risk	0.908004761	Very High Risk	FALSE	9
9	0.70713191	-0.375710797	Low Risk	0.90783298	Very High Risk	FALSE	9
11	0.855826433	-0.181689467	Medium Risk	0.928804994	Very High Risk	FALSE	11
11	0.855826433	-0.181689467	Medium Risk	0.949230671	Very High Risk	FALSE	11
8	0.636411912	-0.472721463	Low Risk	0.949230671	Very High Risk	FALSE	8
8	0.636411912	-0.472721463	Low Risk	0.947772622	Very High Risk	FALSE	8
10	0.780474961	-0.278700132	Medium Risk	0.949155867	Very High Risk	FALSE	10
14	0.912930815	0.10934253	Medium Risk	0.949155867	Very High Risk	FALSE	14
15	0.836515029	0.206353195	High Risk	0.95696938	Very High Risk	FALSE	15
12	0.93251675	-0.084678801	Medium Risk	0.95696938	Very High Risk	FALSE	12
7	0.568859396	-0.569732128	Low Risk	0.955866933	Very High Risk	FALSE	7
7	0.568859396	-0.569732128	Low Risk	0.952890754	Very High Risk	FALSE	7
5	0.445014177	-0.763753459	Low Risk	0.956818044	Very High Risk	FALSE	5
6	0.504936439	-0.666742794	Low Risk	0.963767767	Very High Risk	FALSE	6
8	0.636411912	-0.472721463	Low Risk	0.963767767	Very High Risk	FALSE	8
13	0.990160845	0.012331864	Medium Risk	0.963767767	Very High Risk	FALSE	13
8	0.636411912	-0.472721463	Low Risk	0.821275055	Very High Risk	FALSE	8
6	0.504936439	-0.666742794	Low Risk	0.769010901	High Risk	FALSE	6
5	0.445014177	-0.763753459	Low Risk	0.769010901	High Risk	FALSE	5
4	0.389367968	-0.860764124	Low Risk	0.732485592	High Risk	FALSE	4
5	0.445014177	-0.763753459	Low Risk	0.718446255	High Risk	FALSE	5
8	0.636411912	-0.472721463	Low Risk	0.735395432	High Risk	FALSE	8
11	0.855826433	-0.181689467	Medium Risk	0.703132033	High Risk	FALSE	11
7	0.568859396	-0.569732128	Low Risk	0.69451201	High Risk	FALSE	7
7	0.568859396	-0.569732128	Low Risk	0.748794675	High Risk	FALSE	7
11	0.855826433	-0.181689467	Medium Risk	0.754815698	High Risk	FALSE	11
10	0.780474961	-0.278700132	Medium Risk	0.771764874	High Risk	FALSE	10
2	0.291523458	-1.054785455	Low Risk	0.761700571	High Risk	FALSE	2
1	0.249404862	-1.151796121	Low Risk	0.754520655	High Risk	FALSE	1

Continuation of Table B.1

UID	Getis Ord* GI Analysis			Berredo et al. Analysis		Correlation	Count of Hotspots
	P-Value	Z-Score	Risk Class	Risk Value	Risk Class		
1	0.249404862	-1.151796121	Low Risk	0.761761487	High Risk	FALSE	1
1	0.249404862	-1.151796121	Low Risk	0.761761487	High Risk	FALSE	1
6	0.504936439	-0.666742794	Low Risk	0.738198519	High Risk	FALSE	6
11	0.855826433	-0.181689467	Medium Risk	0.738442779	High Risk	FALSE	11
7	0.568859396	-0.569732128	Low Risk	0.728441775	High Risk	FALSE	7
3	0.338176334	-0.95777479	Low Risk	0.73884958	High Risk	FALSE	3
4	0.389367968	-0.860764124	Low Risk	0.740635693	High Risk	FALSE	4
4	0.389367968	-0.860764124	Low Risk	0.740635693	High Risk	FALSE	4
8	0.636411912	-0.472721463	Low Risk	0.721376777	High Risk	FALSE	8
14	0.912930815	0.10934253	Medium Risk	0.721025646	High Risk	FALSE	14
14	0.912930815	0.10934253	Medium Risk	0.721025646	High Risk	FALSE	14
10	0.780474961	-0.278700132	Medium Risk	0.713773131	High Risk	FALSE	10
8	0.636411912	-0.472721463	Low Risk	0.716136575	High Risk	FALSE	8
16	0.761612584	0.303363861	High Risk	0.809074938	Very High Risk	FALSE	16
19	0.552247379	0.594395857	High Risk	0.809074938	Very High Risk	FALSE	19
18	0.618917446	0.497385191	High Risk	0.75633502	High Risk	TRUE	18
24	0.280387536	1.079449184	Very High Risk	0.752945185	High Risk	FALSE	24
19	0.552247379	0.594395857	High Risk	0.751698494	High Risk	TRUE	19
11	0.855826433	-0.181689467	Medium Risk	0.744811654	High Risk	FALSE	11
4	0.389367968	-0.860764124	Low Risk	0.722035825	High Risk	FALSE	4
1	0.249404862	-1.151796121	Low Risk	0.700564504	High Risk	FALSE	1
3	0.338176334	-0.95777479	Low Risk	0.693288445	High Risk	FALSE	3
13	0.990160845	0.012331864	Medium Risk	0.717371643	High Risk	FALSE	13
16	0.761612584	0.303363861	High Risk	0.717371643	High Risk	TRUE	16
11	0.855826433	-0.181689467	Medium Risk	0.726538599	High Risk	FALSE	11
12	0.93251675	-0.084678801	Medium Risk	0.726538599	High Risk	FALSE	12
7	0.568859396	-0.569732128	Low Risk	0.69639349	High Risk	FALSE	7
8	0.636411912	-0.472721463	Low Risk	0.69639349	High Risk	FALSE	8
8	0.636411912	-0.472721463	Low Risk	0.673230708	High Risk	FALSE	8
4	0.389367968	-0.860764124	Low Risk	0.672338724	High Risk	FALSE	4
4	0.389367968	-0.860764124	Low Risk	0.669346213	High Risk	FALSE	4
14	0.912930815	0.10934253	Medium Risk	0.69184339	High Risk	FALSE	14
10	0.780474961	-0.278700132	Medium Risk	0.694709837	High Risk	FALSE	10
0	0.211735751	-1.248806786	Low Risk	0.682925761	High Risk	FALSE	0

Continuation of Table B.1

UID	Getis Ord* GI Analysis			Berredo et al. Analysis		Correlation	Count of Hotspots
	P-Value	Z-Score	Risk Class	Risk Value	Risk Class		
0	0.211735751	-1.248806786	Low Risk	0.662995458	High Risk	FALSE	0
0	0.211735751	-1.248806786	Low Risk	0.647820532	High Risk	FALSE	0
0	0.211735751	-1.248806786	Low Risk	0.644148052	High Risk	FALSE	0
0	0.211735751	-1.248806786	Low Risk	0.635557652	High Risk	FALSE	0
1	0.249404862	-1.151796121	Low Risk	0.621404588	High Risk	FALSE	1
2	0.291523458	-1.054785455	Low Risk	0.652690887	High Risk	FALSE	2
2	0.291523458	-1.054785455	Low Risk	0.65777564	High Risk	FALSE	2
1	0.249404862	-1.151796121	Low Risk	0.528218746	Medium Risk	FALSE	1
5	0.445014177	-0.763753459	Low Risk	0.505572021	Medium Risk	FALSE	5
10	0.780474961	-0.278700132	Medium Risk	0.52276814	Medium Risk	TRUE	10
14	0.912930815	0.10934253	Medium Risk	0.327118635	Low Risk	FALSE	14
9	0.70713191	-0.375710797	Low Risk	0.327118635	Low Risk	TRUE	9
3	0.338176334	-0.95777479	Low Risk	0.327118635	Low Risk	TRUE	3
5	0.445014177	-0.763753459	Low Risk	0.327118635	Low Risk	TRUE	5
3	0.338176334	-0.95777479	Low Risk	0.327118635	Low Risk	TRUE	3
0	0.211735751	-1.248806786	Low Risk	0.327118635	Low Risk	TRUE	0
2	0.291523458	-1.054785455	Low Risk	0.330508471	Low Risk	TRUE	2
11	0.855826433	-0.181689467	Medium Risk	0.330508471	Low Risk	FALSE	11
15	0.836515029	0.206353195	High Risk	0.330508471	Low Risk	FALSE	15
15	0.836515029	0.206353195	High Risk	0.330508471	Low Risk	FALSE	15
10	0.780474961	-0.278700132	Medium Risk	0.330508471	Low Risk	FALSE	10
5	0.445014177	-0.763753459	Low Risk	0.6947878	High Risk	FALSE	5
6	0.504936439	-0.666742794	Low Risk	0.717727423	High Risk	FALSE	6
7	0.568859396	-0.569732128	Low Risk	0.737710476	High Risk	FALSE	7
6	0.504936439	-0.666742794	Low Risk	0.788029313	High Risk	FALSE	6
10	0.780474961	-0.278700132	Medium Risk	0.843818188	Very High Risk	FALSE	10
9	0.70713191	-0.375710797	Low Risk	0.841094732	Very High Risk	FALSE	9
10	0.780474961	-0.278700132	Medium Risk	0.841094732	Very High Risk	FALSE	10
13	0.990160845	0.012331864	Medium Risk	0.836412132	Very High Risk	FALSE	13
9	0.70713191	-0.375710797	Low Risk	0.816073179	Very High Risk	FALSE	9
5	0.445014177	-0.763753459	Low Risk	0.774567842	High Risk	FALSE	5
5	0.445014177	-0.763753459	Low Risk	0.774567842	High Risk	FALSE	5
6	0.504936439	-0.666742794	Low Risk	0.330508471	Low Risk	TRUE	6
3	0.338176334	-0.95777479	Low Risk	0.330508471	Low Risk	TRUE	3

Continuation of Table B.1

UID	Getis Ord* GI Analysis			Berredo et al. Analysis		Correlation	Count of Hotspots
	P-Value	Z-Score	Risk Class	Risk Value	Risk Class		
3	0.338176334	-0.95777479	Low Risk	0.330508471	Low Risk	TRUE	3
9	0.70713191	-0.375710797	Low Risk	0.330508471	Low Risk	TRUE	9
23	0.325883858	0.982438518	Very High Risk	0.330508471	Low Risk	FALSE	23
29	0.117699604	1.564502511	Very High Risk	0.330508471	Low Risk	FALSE	29
25	0.239411168	1.176459849	Very High Risk	0.330508471	Low Risk	FALSE	25
24	0.280387536	1.079449184	Very High Risk	0.330508471	Low Risk	FALSE	24
29	0.117699604	1.564502511	Very High Risk	0.330508471	Low Risk	FALSE	29
27	0.170536746	1.37048118	Very High Risk	0.330508471	Low Risk	FALSE	27
23	0.325883858	0.982438518	Very High Risk	0.330508471	Low Risk	FALSE	23
29	0.117699604	1.564502511	Very High Risk	0.330508471	Low Risk	FALSE	29
24	0.280387536	1.079449184	Very High Risk	0.415254235	Medium Risk	FALSE	24
19	0.552247379	0.594395857	High Risk	0.415254235	Medium Risk	FALSE	19
26	0.202851129	1.273470515	Very High Risk	0.330508471	Low Risk	FALSE	26
38	0.014785186	2.437598499	Very High Risk	0.330508471	Low Risk	FALSE	38
54	6.61E-05	3.989769146	Very High Risk	0.330508471	Low Risk	FALSE	54
42	0.004718609	2.825641161	Very High Risk	0.330508471	Low Risk	FALSE	42
54	6.61E-05	3.989769146	Very High Risk	0.330508471	Low Risk	FALSE	54
31	0.078658419	1.758523842	Very High Risk	0.330508471	Low Risk	FALSE	31
6	0.504936439	-0.666742794	Low Risk	0.415254235	Medium Risk	FALSE	6
5	0.445014177	-0.763753459	Low Risk	0.5	Medium Risk	FALSE	5
2	0.291523458	-1.054785455	Low Risk	0.483050853	Medium Risk	FALSE	2
0	0.211735751	-1.248806786	Low Risk	0.415254235	Medium Risk	FALSE	0
0	0.211735751	-1.248806786	Low Risk	0.3898305	Low Risk	TRUE	0
0	0.211735751	-1.248806786	Low Risk	0.415254235	Medium Risk	FALSE	0
1	0.249404862	-1.151796121	Low Risk	0.415254235	Medium Risk	FALSE	1
0	0.211735751	-1.248806786	Low Risk	0.567533612	Medium Risk	FALSE	0
0	0.211735751	-1.248806786	Low Risk	0.585709393	Medium Risk	FALSE	0
0	0.211735751	-1.248806786	Low Risk	0.58794558	Medium Risk	FALSE	0
2	0.291523458	-1.054785455	Low Risk	0.58794558	Medium Risk	FALSE	2
6	0.504936439	-0.666742794	Low Risk	0.570996404	Medium Risk	FALSE	6
9	0.70713191	-0.375710797	Low Risk	0.415254235	Medium Risk	FALSE	9
11	0.855826433	-0.181689467	Medium Risk	0.415254235	Medium Risk	TRUE	11
7	0.568859396	-0.569732128	Low Risk	0.415254235	Medium Risk	FALSE	7
9	0.70713191	-0.375710797	Low Risk	0.415254235	Medium Risk	FALSE	9

Continuation of Table B.1

UID	Getis Ord* GI Analysis			Berredo et al. Analysis		Correlation	Count of Hotspots
	P-Value	Z-Score	Risk Class	Risk Value	Risk Class		
9	0.70713191	-0.375710797	Low Risk	0.415254235	Medium Risk	FALSE	9
12	0.93251675	-0.084678801	Medium Risk	0.415254235	Medium Risk	TRUE	12
11	0.855826433	-0.181689467	Medium Risk	0.415254235	Medium Risk	TRUE	11
15	0.836515029	0.206353195	High Risk	0.415254235	Medium Risk	FALSE	15
15	0.836515029	0.206353195	High Risk	0.542791009	Medium Risk	FALSE	15
16	0.761612584	0.303363861	High Risk	0.586364508	Medium Risk	FALSE	16
16	0.761612584	0.303363861	High Risk	0.563061714	Medium Risk	FALSE	16
16	0.761612584	0.303363861	High Risk	0.653278947	High Risk	TRUE	16
12	0.93251675	-0.084678801	Medium Risk	0.730036139	High Risk	FALSE	12
18	0.618917446	0.497385191	High Risk	0.69300276	High Risk	TRUE	18
15	0.836515029	0.206353195	High Risk	0.710065365	High Risk	TRUE	15
19	0.552247379	0.594395857	High Risk	0.714762807	High Risk	TRUE	19
22	0.375925916	0.885427853	Very High Risk	0.70089072	High Risk	FALSE	22
12	0.93251675	-0.084678801	Medium Risk	0.722433329	High Risk	FALSE	12
7	0.568859396	-0.569732128	Low Risk	0.723950207	High Risk	FALSE	7
6	0.504936439	-0.666742794	Low Risk	0.759972334	High Risk	FALSE	6
19	0.552247379	0.594395857	High Risk	0.681257248	High Risk	TRUE	19
16	0.761612584	0.303363861	High Risk	0.682716489	High Risk	TRUE	16
16	0.761612584	0.303363861	High Risk	0.715661526	High Risk	TRUE	16
12	0.93251675	-0.084678801	Medium Risk	0.698712349	High Risk	FALSE	12
5	0.445014177	-0.763753459	Low Risk	0.706378937	High Risk	FALSE	5
2	0.291523458	-1.054785455	Low Risk	0.6665681	High Risk	FALSE	2
4	0.389367968	-0.860764124	Low Risk	0.795673668	High Risk	FALSE	4
16	0.761612584	0.303363861	High Risk	0.634656727	High Risk	TRUE	16
18	0.618917446	0.497385191	High Risk	0.61770761	High Risk	TRUE	18
10	0.780474961	-0.278700132	Medium Risk	0.537597001	Medium Risk	TRUE	10
18	0.618917446	0.497385191	High Risk	0.544706345	Medium Risk	FALSE	18
22	0.375925916	0.885427853	Very High Risk	0.539210141	Medium Risk	FALSE	22
21	0.430452721	0.788417188	Very High Risk	0.560189009	Medium Risk	FALSE	21
17	0.688880684	0.400374526	High Risk	0.568921447	Medium Risk	FALSE	17
5	0.445014177	-0.763753459	Low Risk	0.575709999	Medium Risk	FALSE	5
1	0.249404862	-1.151796121	Low Risk	0.575709999	Medium Risk	FALSE	1
0	0.211735751	-1.248806786	Low Risk	0.579470098	Medium Risk	FALSE	0
5	0.445014177	-0.763753459	Low Risk	0.579470098	Medium Risk	FALSE	5

Continuation of Table B.1

UID	Getis Ord* GI Analysis			Berredo et al. Analysis		Correlation	Count of Hotspots
	P-Value	Z-Score	Risk Class	Risk Value	Risk Class		
13	0.990160845	0.012331864	Medium Risk	0.567229152	Medium Risk	TRUE	13
17	0.688880684	0.400374526	High Risk	0.726062238	High Risk	TRUE	17
27	0.170536746	1.37048118	Very High Risk	0.634003818	High Risk	FALSE	27
33	0.050873513	1.952545173	Very High Risk	0.615294456	High Risk	FALSE	33
6	0.504936439	-0.666742794	Low Risk	0.759972334	High Risk	FALSE	6
12	0.93251675	-0.084678801	Medium Risk	0.705997527	High Risk	FALSE	12
15	0.836515029	0.206353195	High Risk	0.695086241	High Risk	TRUE	15
14	0.912930815	0.10934253	Medium Risk	0.675561309	High Risk	FALSE	14
19	0.552247379	0.594395857	High Risk	0.692088604	High Risk	TRUE	19
28	0.142242306	1.467491845	Very High Risk	0.692088604	High Risk	FALSE	28
30	0.096610425	1.661513176	Very High Risk	0.694370925	High Risk	FALSE	30
25	0.239411168	1.176459849	Very High Risk	0.711320043	High Risk	FALSE	25
6	0.504936439	-0.666742794	Low Risk	0.955206215	Very High Risk	FALSE	6
5	0.445014177	-0.763753459	Low Risk	0.955206215	Very High Risk	FALSE	5
10	0.780474961	-0.278700132	Medium Risk	0.940683126	Very High Risk	FALSE	10
16	0.761612584	0.303363861	High Risk	0.94757241	Very High Risk	FALSE	16

End of Table

APPENDIX C: RESULTS OF VULNERABILITY TO WILDFIRE-INDUCED FLASHOVER

This appendix section provides the results of vulnerability to wildfire-induced flashovers for the OHTL 500kV Ribeiro Gonçalves - São João do Piauí by line span in Table C.1.

Table C.1: Results of Vulnerability to Wildfire-Induced Flashover

Begin of Table C.1				
Span	**Clearance**	**Enhanced Berredo Vulnerability**	**Berredo Vulnerability**	**Vulnerability Correlation**
80	10.97	High	High	TRUE
81	17.48	Low	Medium	FALSE
82	10.95	High	High	TRUE
83	12.45	Medium	High	FALSE
84	10.21	High	High	TRUE
85	11.69	Medium	High	FALSE
86	10.53	High	High	TRUE
87	10.3	High	High	TRUE
88	10.15	High	High	TRUE
89	10.29	High	High	TRUE
90	10.23	High	High	TRUE
91	10.15	High	High	TRUE
92	10.09	High	High	TRUE
93	10.64	High	High	TRUE
94	19.51	Low	Low	TRUE
95	14.9	Low	Medium	FALSE
96	12.07	Medium	High	FALSE
97	10.09	High	High	TRUE
98	13.02	Low	High	FALSE
99	12.4	Medium	High	FALSE
100	14.89	Low	Medium	FALSE
101	10.57	High	High	TRUE
102	16.57	Low	Medium	FALSE
103	33.05	Low	Low	TRUE
104	15.99	Low	Medium	FALSE
105	10.29	High	High	TRUE
106	10.33	High	High	TRUE
107	10.55	High	High	TRUE
108	10.26	High	High	TRUE
109	10.41	High	High	TRUE
110	10.23	High	High	TRUE
111	10.22	High	High	TRUE
112	10.34	High	High	TRUE
113	10.31	High	High	TRUE
114	10.3	High	High	TRUE
115	10.22	High	High	TRUE
116	10.51	High	High	TRUE
117	10.72	High	High	TRUE
118	10.87	High	High	TRUE
119	10.71	High	High	TRUE

Continuation of Table C.1				
Span	**Clearance**	**Enhanced Berredo Vulnerability**	**Berredo Vulnerability**	**Vulnerability Correlation**
120	10.3	High	High	TRUE
121	10.14	High	High	TRUE
122	10.38	High	High	TRUE
123	10.62	High	High	TRUE
124	10.71	High	High	TRUE
125	10.38	High	High	TRUE
126	10.52	High	High	TRUE
127	10.81	High	High	TRUE
128	10.85	High	High	TRUE
129	10.4	High	High	TRUE
130	11.35	High	Medium	FALSE
131	11.25	High	High	TRUE
132	10.35	High	High	TRUE
133	10.39	High	High	TRUE
134	10.43	High	High	TRUE
135	10.46	High	High	TRUE
136	10.45	High	High	TRUE
137	10.57	High	High	TRUE
138	10.53	High	High	TRUE
139	10.63	High	High	TRUE
140	10.36	High	High	TRUE
141	10.53	High	High	TRUE
142	10.29	High	High	TRUE
143	12.73	Low	High	FALSE
144	10.39	High	High	TRUE
145	10.3	High	High	TRUE
146	10.34	High	High	TRUE
147	10.27	High	High	TRUE
148	10.37	High	High	TRUE
149	10.22	High	High	TRUE
150	10.18	High	High	TRUE
151	10.64	High	High	TRUE
152	13.42	Low	High	FALSE
153	10.46	High	High	TRUE
154	10.67	High	High	TRUE
155	12.29	Medium	High	FALSE
156	10.22	High	High	TRUE
157	10.21	High	High	TRUE
158	25.69	Low	Low	TRUE
159	10.39	High	High	TRUE
160	10.81	High	High	TRUE
161	10.65	High	High	TRUE
162	13.7	Low	High	FALSE
163	10.07	High	High	TRUE
164	10.34	High	High	TRUE
165	10.29	High	High	TRUE
166	10.2	High	High	TRUE
167	12.14	Medium	High	FALSE
168	10.35	High	High	TRUE
169	10.32	High	High	TRUE
170	10.3	High	High	TRUE

Continuation of Table C.1				
Span	**Clearance**	**Enhanced Berredo Vulnerability**	**Berredo Vulnerability**	**Vulnerability Correlation**
171	10.32	High	High	TRUE
172	10.29	High	High	TRUE
173	10.33	High	High	TRUE
174	10.36	High	High	TRUE
175	10.38	High	High	TRUE
176	10.48	High	High	TRUE
177	10.25	High	High	TRUE
178	10.29	High	High	TRUE
179	10.31	High	High	TRUE
180	10.29	High	High	TRUE
181	10.36	High	High	TRUE
182	12.41	Medium	Medium	TRUE
183	10.31	High	High	TRUE
184	10.23	High	High	TRUE
185	10.36	High	High	TRUE
186	10.35	High	High	TRUE
187	10.26	High	High	TRUE
188	10.29	High	High	TRUE
189	12.33	Medium	High	FALSE
190	10.28	High	High	TRUE
191	10.23	High	High	TRUE
192	10.31	High	High	TRUE
193	10.28	High	High	TRUE
194	10.35	High	High	TRUE
195	10.36	High	High	TRUE
196	10.27	High	High	TRUE
197	10.42	High	High	TRUE
198	10.37	High	High	TRUE
199	10.3	High	High	TRUE
200	10.88	High	High	TRUE
201	10.95	High	High	TRUE
202	10.36	High	High	TRUE
203	10.76	High	High	TRUE
204	10.32	High	High	TRUE
205	10.75	High	High	TRUE
206	10.62	High	High	TRUE
207	10.45	High	High	TRUE
208	10.58	High	High	TRUE
209	10.63	High	High	TRUE
210	10.41	High	High	TRUE
211	10.53	High	High	TRUE
212	18.65	Low	Medium	FALSE
213	15.56	Low	High	FALSE
214	19.96	Low	Low	TRUE
215	10.93	High	High	TRUE
216	14.19	Low	High	FALSE
217	12.87	Low	High	FALSE
218	11.56	High	High	TRUE
219	12.74	Low	High	FALSE
220	27.73	Low	Low	TRUE
221	11.59	High	High	TRUE

Continuation of Table C.1				
Span	Clearance	Enhanced Berredo Vulnerability	Berredo Vulnerability	Vulnerability Correlation
222	9.91	High	High	TRUE
223	9.88	High	High	TRUE
224	11.39	High	High	TRUE
225	10.5	High	High	TRUE
226	12.24	Medium	High	FALSE
227	10.09	High	High	TRUE
228	10.28	High	High	TRUE
229	10.29	High	High	TRUE
230	10.9	High	High	TRUE
231	10.31	High	High	TRUE
232	10.26	High	High	TRUE
233	10.55	High	High	TRUE
234	10.58	High	High	TRUE
235	10.27	High	High	TRUE
236	10.48	High	High	TRUE
237	10.6	High	High	TRUE
238	10.3	High	High	TRUE
239	10.3	High	High	TRUE
240	10.24	High	High	TRUE
241	10.66	High	High	TRUE
242	10.46	High	High	TRUE
243	10.25	High	High	TRUE
244	10.43	High	High	TRUE
245	10.28	High	High	TRUE
246	10.36	High	High	TRUE
247	10.36	High	High	TRUE
248	12.28	Medium	High	FALSE
249	10.28	High	High	TRUE
250	10.22	High	High	TRUE
251	10.18	High	High	TRUE
252	10.23	High	High	TRUE
253	10.23	High	High	TRUE
254	10.26	High	High	TRUE
255	10.27	High	High	TRUE
256	10.25	High	High	TRUE
257	10.31	High	High	TRUE
258	10.22	High	High	TRUE
259	10.43	High	High	TRUE
260	10.96	High	High	TRUE
261	10.38	High	High	TRUE
262	10.17	High	High	TRUE
263	10.29	High	High	TRUE
264	10.29	High	High	TRUE
265	10.33	High	High	TRUE
266	10.28	High	High	TRUE
267	10.27	High	High	TRUE
268	12.17	Medium	High	FALSE
269	10.77	High	High	TRUE
270	9.64	High	High	TRUE
271	10.34	High	High	TRUE
272	10.78	High	High	TRUE

Continuation of Table C.1				
Span	**Clearance**	**Enhanced Berredo Vulnerability**	**Berredo Vulnerability**	**Vulnerability Correlation**
273	10.57	High	High	TRUE
274	10.17	High	High	TRUE
275	10.92	High	High	TRUE
276	17.46	Low	Medium	FALSE
277	24.53	Low	High	FALSE
278	17.26	Low	High	FALSE
279	10.33	High	High	TRUE
280	10.38	High	High	TRUE
281	10.32	High	High	TRUE
282	11.71	Medium	High	FALSE
283	12.38	Medium	High	FALSE
284	13.52	Low	High	FALSE
285	10.34	High	High	TRUE
286	10.2	High	High	TRUE
287	10.52	High	High	TRUE
288	16.18	Low	Medium	FALSE
289	15.56	Low	Medium	FALSE
290	9.7	High	High	TRUE
291	16.32	Low	Medium	FALSE
292	12.45	Medium	High	FALSE
293	10.42	High	High	TRUE
294	10.5	High	High	TRUE
295	10.45	High	High	TRUE
296	10.52	High	High	TRUE
297	12.42	Medium	High	FALSE
298	10.26	High	High	TRUE
299	10.24	High	High	TRUE
300	10.41	High	High	TRUE
301	10.8	High	High	TRUE
302	13.52	Low	High	FALSE
303	10.36	High	High	TRUE
304	10.46	High	High	TRUE
305	14.47	Low	Medium	FALSE
306	10.41	High	High	TRUE
307	10.5	High	High	TRUE
308	12.25	Medium	High	FALSE
309	10.83	High	High	TRUE
310	15.24	Low	Medium	FALSE
311	14.17	Low	Medium	FALSE
312	12.13	Medium	Medium	TRUE
313	9.02	High	High	TRUE
314	10.22	High	High	TRUE
315	10.44	High	High	TRUE
316	10.86	High	High	TRUE
317	10.49	High	High	TRUE
318	10.45	High	High	TRUE
319	10.23	High	High	TRUE
320	10.37	High	High	TRUE
321	10.29	High	High	TRUE
322	10.35	High	High	TRUE
323	10.38	High	High	TRUE

Continuation of Table C.1				
Span	**Clearance**	**Enhanced Berredo Vulnerability**	**Berredo Vulnerability**	**Vulnerability Correlation**
324	10.28	High	High	TRUE
325	10.42	High	High	TRUE
326	15.24	Low	Low	TRUE
327	13.31	Low	Medium	FALSE
328	12.16	Medium	Medium	TRUE
329	22.48	Low	Low	TRUE
330	15.68	Low	Medium	FALSE
331	20.21	Low	Low	TRUE
332	14.05	Low	Medium	FALSE
333	11.36	High	High	TRUE
334	10.12	High	High	TRUE
335	10.46	High	High	TRUE
336	10.52	High	High	TRUE
337	10.47	High	High	TRUE
338	10.5	High	High	TRUE
339	10.5	High	High	TRUE
340	10.1	High	High	TRUE
341	10.24	High	High	TRUE
342	10.42	High	High	TRUE
343	10.21	High	High	TRUE
344	10.3	High	High	TRUE
345	10.4	High	High	TRUE
346	10.58	High	High	TRUE
347	10.47	High	High	TRUE
348	10.3	High	High	TRUE
349	17.75	Low	Low	TRUE
350	10.71	High	High	TRUE
351	11.62	High	High	TRUE
352	10.1	High	High	TRUE
353	10.36	High	High	TRUE
354	10.4	High	High	TRUE
355	9.96	High	High	TRUE
356	11.46	High	High	TRUE
357	10.09	High	High	TRUE
358	10.22	High	High	TRUE
359	10.35	High	High	TRUE
360	10.32	High	High	TRUE
361	9.86	High	High	TRUE
362	10.28	High	High	TRUE
363	10.46	High	High	TRUE
364	9.9	High	High	TRUE
365	10.01	High	High	TRUE
366	11.65	High	High	TRUE
367	18.26	Low	Low	TRUE
368	20.56	Low	Low	TRUE
369	13.14	Low	Medium	FALSE
370	9.71	High	High	TRUE
371	10.33	High	High	TRUE
372	10.03	High	High	TRUE
373	17.05	Low	Low	TRUE
374	10.48	High	High	TRUE

Continuation of Table C.1				
Span	**Clearance**	**Enhanced Berredo Vulnerability**	**Berredo Vulnerability**	**Vulnerability Correlation**
375	12.57	Low	High	FALSE
376	13.53	Low	Medium	FALSE
377	10.57	High	High	TRUE
378	11.6	High	Medium	FALSE
379	11.53	High	High	TRUE
380	13.63	Low	Medium	FALSE
381	14.39	Low	Medium	FALSE
382	22.07	Low	Low	TRUE
383	10.88	High	High	TRUE
384	10.66	High	High	TRUE
385	10.32	High	High	TRUE
386	11.67	High	High	TRUE
387	10.19	High	High	TRUE
388	24.9	Low	Low	TRUE
389	9.79	High	High	TRUE
390	18.07	Low	Low	TRUE
391	17.46	Low	Low	TRUE
392	10	High	High	TRUE
393	11.4	High	High	TRUE
394	11.32	High	High	TRUE
395	10.67	High	High	TRUE
396	10.25	High	High	TRUE
397	10.2	High	High	TRUE
398	11.01	High	High	TRUE
399	10.36	High	High	TRUE
400	10.15	High	High	TRUE
401	11.35	High	High	TRUE
402	11.48	High	High	TRUE
403	10.42	High	High	TRUE
404	10.41	High	High	TRUE
405	10.68	High	High	TRUE
406	10.79	High	High	TRUE
407	10.15	High	High	TRUE
408	10.11	High	High	TRUE
409	12.05	Medium	High	FALSE
410	12.08	Medium	High	FALSE
411	14.27	Low	High	FALSE
412	12.32	Medium	High	FALSE
413	10.28	High	High	TRUE
414	10.39	High	High	TRUE
415	10.35	High	High	TRUE
416	10.62	High	High	TRUE
417	11.57	High	High	TRUE
418	10.38	High	High	TRUE
419	11.26	High	High	TRUE
420	11.64	High	High	TRUE
421	10.8	High	High	TRUE
422	10.21	High	High	TRUE
423	9.56	High	High	TRUE
424	16.88	Low	Low	TRUE
425	9.79	High	High	TRUE

Continuation of Table C.1				
Span	**Clearance**	**Enhanced Berredo Vulnerability**	**Berredo Vulnerability**	**Vulnerability Correlation**
426	10.28	High	High	TRUE
427	11.19	High	High	TRUE
428	16.92	Low	Low	TRUE
429	13.02	Low	Medium	FALSE
430	11.09	High	High	TRUE
431	10.22	High	High	TRUE
432	10.77	High	High	TRUE
433	11.29	High	High	TRUE
End of Table				

APPENDIX D: RESULTS OF CRITICALITY OF OUTAGE

This appendix section provides the results of criticality of outage for the OHTL 500kV Ribeiro Gonçalves - São João do Piauí by line span in Table D.1.

Table D.1: Results of Criticality to Outage

Begin of Table D.1										
Span	Clearance	Risk of Wildfire			Vulnerability			Criticality		
		z-score	p-value	Wildfire	Enhanced Berredo Vulnerability	Berredo Vulnerability	Vulnerability Correlation	Enhanced Berredo Criticality	Berredo Criticality	Criticality Correlation
80	10.97	0.400374526	0.688880684	High Risk	High	High	TRUE	High	High	TRUE
81	17.48	0.012331864	0.990160845	Medium Risk	Low	Medium	FALSE	Low	High	FALSE
82	10.95	0.691406522	0.489310107	Very High Risk	High	High	TRUE	High	High	TRUE
83	12.45	0.885427853	0.375925916	Very High Risk	Medium	High	FALSE	High	High	TRUE
84	10.21	0.691406522	0.489310107	Very High Risk	High	High	TRUE	High	High	TRUE
85	11.69	0.012331864	0.990160845	Medium Risk	Medium	High	FALSE	Medium	High	FALSE
86	10.53	-0.181689467	0.855826433	Medium Risk	High	High	TRUE	High	High	TRUE
87	10.3	0.206353195	0.836515029	High Risk	High	High	TRUE	High	High	TRUE
88	10.15	0.885427853	0.375925916	Very High Risk	High	High	TRUE	High	High	TRUE
89	10.29	0.982438518	0.325883858	Very High Risk	High	High	TRUE	High	High	TRUE
90	10.23	0.788417188	0.430452721	Very High Risk	High	High	TRUE	High	High	TRUE
91	10.15	1.079449184	0.280387536	Very High Risk	High	High	TRUE	High	High	TRUE
92	10.09	2.146566503	0.031827809	Very High Risk	High	High	TRUE	High	High	TRUE
93	10.64	0.594395857	0.552247379	High Risk	High	High	TRUE	High	High	TRUE
94	19.51	0.691406522	0.489310107	Very High Risk	Low	Low	TRUE	Medium	High	FALSE
95	14.9	0.400374526	0.688880684	High Risk	Low	Medium	FALSE	Low	High	FALSE
96	12.07	0.10934253	0.912930815	Medium Risk	Medium	High	FALSE	Medium	High	FALSE
97	10.09	0.400374526	0.688880684	High Risk	High	High	TRUE	High	High	TRUE
98	13.02	0.497385191	0.618917446	High Risk	Low	High	FALSE	Low	High	FALSE
99	12.4	0.303363861	0.761612584	High Risk	Medium	High	FALSE	Medium	High	FALSE
100	14.89	-0.472721463	0.636411912	Low Risk	Low	Medium	FALSE	Low	High	FALSE
101	10.57	-0.666742794	0.504936439	Low Risk	High	High	TRUE	Medium	High	FALSE
102	16.57	-0.763753459	0.445014177	Low Risk	Low	Medium	FALSE	Low	High	FALSE
103	33.05	-0.278700132	0.780474961	Medium Risk	Low	Low	TRUE	Low	High	FALSE
104	15.99	0.303363861	0.761612584	High Risk	Low	Medium	FALSE	Low	High	FALSE
105	10.29	0.012331864	0.990160845	Medium Risk	High	High	TRUE	High	High	TRUE
106	10.33	0.012331864	0.990160845	Medium Risk	High	High	TRUE	High	High	TRUE
107	10.55	0.012331864	0.990160845	Medium Risk	High	High	TRUE	High	High	TRUE
108	10.26	-0.569732128	0.568859396	Low Risk	High	High	TRUE	Medium	High	FALSE

Continuation of Table D.1

Span	Clearance	Risk of Wildfire			Vulnerability			Criticality		
		z-score	p-value	Wildfire	Enhanced Berredo Vulnerability	Berredo Vulnerability	Vulnerability Correlation	Enhanced Berredo Criticality	Berredo Criticality	Criticality Correlation
109	10.41	-0.666742794	0.504936439	Low Risk	High	High	TRUE	Medium	High	FALSE
110	10.23	-0.569732128	0.568859396	Low Risk	High	High	TRUE	Medium	High	FALSE
111	10.22	-0.666742794	0.504936439	Low Risk	High	High	TRUE	Medium	High	FALSE
112	10.34	-0.95777479	0.338176334	Low Risk	High	High	TRUE	Medium	High	FALSE
113	10.31	-0.95777479	0.338176334	Low Risk	High	High	TRUE	Medium	High	FALSE
114	10.3	-0.763753459	0.445014177	Low Risk	High	High	TRUE	Medium	High	FALSE
115	10.22	-0.860764125	0.389367968	Low Risk	High	High	TRUE	Medium	High	FALSE
116	10.51	-0.95777479	0.338176334	Low Risk	High	High	TRUE	Medium	High	FALSE
117	10.72	-1.054785455	0.291523458	Low Risk	High	High	TRUE	Medium	High	FALSE
118	10.87	-1.054785455	0.291523458	Low Risk	High	High	TRUE	Medium	High	FALSE
119	10.71	-0.860764125	0.389367968	Low Risk	High	High	TRUE	Medium	High	FALSE
120	10.3	-0.860764125	0.389367968	Low Risk	High	High	TRUE	Medium	High	FALSE
121	10.14	-0.95777479	0.338176334	Low Risk	High	High	TRUE	Medium	High	FALSE
122	10.38	-1.151796121	0.249404862	Low Risk	High	High	TRUE	Medium	High	FALSE
123	10.62	-1.248806786	0.211735751	Low Risk	High	High	TRUE	Medium	High	FALSE
124	10.71	-1.248806786	0.211735751	Low Risk	High	High	TRUE	Medium	High	FALSE
125	10.38	-1.248806786	0.211735751	Low Risk	High	High	TRUE	Medium	High	FALSE
126	10.52	-1.248806786	0.211735751	Low Risk	High	High	TRUE	Medium	High	FALSE
127	10.81	-1.248806786	0.211735751	Low Risk	High	High	TRUE	Medium	High	FALSE
128	10.85	-1.248806786	0.211735751	Low Risk	High	High	TRUE	Medium	High	FALSE
129	10.4	-1.248806786	0.211735751	Low Risk	High	High	TRUE	Medium	High	FALSE
130	11.35	-1.248806786	0.211735751	Low Risk	High	Medium	FALSE	Medium	High	FALSE
131	11.25	-1.248806786	0.211735751	Low Risk	High	High	TRUE	Medium	High	FALSE
132	10.35	-1.248806786	0.211735751	Low Risk	High	High	TRUE	Medium	High	FALSE
133	10.39	-1.248806786	0.211735751	Low Risk	High	High	TRUE	Medium	High	FALSE
134	10.43	-1.248806786	0.211735751	Low Risk	High	High	TRUE	Medium	High	FALSE
135	10.46	-1.248806786	0.211735751	Low Risk	High	High	TRUE	Medium	High	FALSE
136	10.45	-1.248806786	0.211735751	Low Risk	High	High	TRUE	Medium	High	FALSE
137	10.57	-1.248806786	0.211735751	Low Risk	High	High	TRUE	Medium	High	FALSE
138	10.53	-1.248806786	0.211735751	Low Risk	High	High	TRUE	Medium	High	FALSE
139	10.63	-1.248806786	0.211735751	Low Risk	High	High	TRUE	Medium	High	FALSE

Continuation of Table D.1										
Span	Clearance	Risk of Wildfire			Vulnerability			Criticality		
		z-score	p-value	Wildfire	Enhanced Berredo Vulnerability	Berredo Vulnerability	Vulnerability Correlation	Enhanced Berredo Criticality	Berredo Criticality	Criticality Correlation
140	10.36	-0.763753459	0.445014177	Low Risk	High	High	TRUE	Medium	High	FALSE
141	10.53	0.788417188	0.430452721	Very High Risk	High	High	TRUE	High	High	TRUE
142	10.29	0.885427853	0.375925916	Very High Risk	High	High	TRUE	High	High	TRUE
143	12.73	0.400374526	0.688880684	High Risk	Low	High	FALSE	Low	High	FALSE
144	10.39	1.079449184	0.280387536	Very High Risk	High	High	TRUE	High	High	TRUE
145	10.3	1.37048118	0.170536746	Very High Risk	High	High	TRUE	High	High	TRUE
146	10.34	0.885427853	0.375925916	Very High Risk	High	High	TRUE	High	High	TRUE
147	10.27	0.497385191	0.618917446	High Risk	High	High	TRUE	High	High	TRUE
148	10.37	0.012331864	0.990160845	Medium Risk	High	High	TRUE	High	High	TRUE
149	10.22	0.206353195	0.836515029	High Risk	High	High	TRUE	High	High	TRUE
150	10.18	0.497385191	0.618917446	High Risk	High	High	TRUE	High	High	TRUE
151	10.64	0.788417188	0.430452721	Very High Risk	High	High	TRUE	High	High	TRUE
152	13.42	0.497385191	0.618917446	High Risk	Low	High	FALSE	Low	High	FALSE
153	10.46	-0.278700132	0.780474961	Medium Risk	High	High	TRUE	High	High	TRUE
154	10.67	-0.278700132	0.780474961	Medium Risk	High	High	TRUE	High	High	TRUE
155	12.29	0.10934253	0.912930815	Medium Risk	Medium	High	FALSE	Medium	High	FALSE
156	10.22	0.10934253	0.912930815	Medium Risk	High	High	TRUE	High	High	TRUE
157	10.21	-0.278700132	0.780474961	Medium Risk	High	High	TRUE	High	High	TRUE
158	25.69	-0.666742794	0.504936439	Low Risk	Low	Low	TRUE	Low	High	FALSE
159	10.39	0.206353195	0.836515029	High Risk	High	High	TRUE	High	High	TRUE
160	10.81	0.885427853	0.375925916	Very High Risk	High	High	TRUE	High	High	TRUE
161	10.65	0.982438518	0.325883858	Very High Risk	High	High	TRUE	High	High	TRUE
162	13.7	1.661513176	0.096610425	Very High Risk	Low	High	FALSE	Medium	High	FALSE
163	10.07	1.273470515	0.202851129	Very High Risk	High	High	TRUE	High	High	TRUE
164	10.34	1.176459849	0.239411168	Very High Risk	High	High	TRUE	High	High	TRUE
165	10.29	0.497385191	0.618917446	High Risk	High	High	TRUE	High	High	TRUE
166	10.2	0.982438518	0.325883858	Very High Risk	High	High	TRUE	High	High	TRUE
167	12.14	2.243577169	0.02485962	Very High Risk	Medium	High	FALSE	High	High	TRUE
168	10.35	1.758523842	0.078658419	Very High Risk	High	High	TRUE	High	High	TRUE
169	10.32	1.952545173	0.050873513	Very High Risk	High	High	TRUE	High	High	TRUE
170	10.3	2.922651827	0.003470644	Very High Risk	High	High	TRUE	High	High	TRUE

Continuation of Table D.1

Span	Clearance	Risk of Wildfire			Vulnerability			Criticality		
		z-score	p-value	Wildfire	Enhanced Berredo Vulnerability	Berredo Vulnerability	Vulnerability Correlation	Enhanced Berredo Criticality	Berredo Criticality	Criticality Correlation
171	10.32	3.69873715	0.000216675	Very High Risk	High	High	TRUE	High	High	TRUE
172	10.29	3.504715819	0.000457095	Very High Risk	High	High	TRUE	High	High	TRUE
173	10.33	3.019662492	0.002530565	Very High Risk	High	High	TRUE	High	High	TRUE
174	10.36	2.922651827	0.003470644	Very High Risk	High	High	TRUE	High	High	TRUE
175	10.38	3.213683823	0.001310439	Very High Risk	High	High	TRUE	High	High	TRUE
176	10.48	3.310694488	0.000930648	Very High Risk	High	High	TRUE	High	High	TRUE
177	10.25	2.728630496	0.006359792	Very High Risk	High	High	TRUE	High	High	TRUE
178	10.29	2.340587834	0.019253409	Very High Risk	High	High	TRUE	High	High	TRUE
179	10.31	1.855534507	0.063519936	Very High Risk	High	High	TRUE	High	High	TRUE
180	10.29	1.467491845	0.142242306	Very High Risk	High	High	TRUE	High	High	TRUE
181	10.36	1.273470515	0.202851129	Very High Risk	High	High	TRUE	High	High	TRUE
182	12.41	0.982438518	0.325883858	Very High Risk	Medium	Medium	TRUE	High	High	TRUE
183	10.31	0.885427853	0.375925916	Very High Risk	High	High	TRUE	High	High	TRUE
184	10.23	0.10934253	0.912930815	Medium Risk	High	High	TRUE	High	High	TRUE
185	10.36	-0.278700132	0.780474961	Medium Risk	High	High	TRUE	High	High	TRUE
186	10.35	-0.569732128	0.568859396	Low Risk	High	High	TRUE	Medium	High	FALSE
187	10.26	-0.181689467	0.855826433	Medium Risk	High	High	TRUE	High	High	TRUE
188	10.29	-0.278700132	0.780474961	Medium Risk	High	High	TRUE	High	High	TRUE
189	12.33	-0.278700132	0.780474961	Medium Risk	Medium	High	FALSE	Medium	High	FALSE
190	10.28	0.206353195	0.836515029	High Risk	High	High	TRUE	High	High	TRUE
191	10.23	-0.181689467	0.855826433	Medium Risk	High	High	TRUE	High	High	TRUE
192	10.31	-0.181689467	0.855826433	Medium Risk	High	High	TRUE	High	High	TRUE
193	10.28	-0.084678801	0.93251675	Medium Risk	High	High	TRUE	High	High	TRUE
194	10.35	0.206353195	0.836515029	High Risk	High	High	TRUE	High	High	TRUE
195	10.36	0.012331864	0.990160845	Medium Risk	High	High	TRUE	High	High	TRUE
196	10.27	0.303363861	0.761612584	High Risk	High	High	TRUE	High	High	TRUE
197	10.42	0.012331864	0.990160845	Medium Risk	High	High	TRUE	High	High	TRUE
198	10.37	-0.763753459	0.445014177	Low Risk	High	High	TRUE	Medium	High	FALSE
199	10.3	-0.860764125	0.389367968	Low Risk	High	High	TRUE	Medium	High	FALSE
200	10.88	-0.569732128	0.568859396	Low Risk	High	High	TRUE	Medium	High	FALSE
201	10.95	-0.666742794	0.504936439	Low Risk	High	High	TRUE	Medium	High	FALSE

Continuation of Table D.1

Span	Clearance	Risk of Wildfire			Vulnerability			Criticality		
		z-score	p-value	Wildfire	Enhanced Berredo Vulnerability	Berredo Vulnerability	Vulnerability Correlation	Enhanced Berredo Criticality	Berredo Criticality	Criticality Correlation
202	10.36	-0.181689467	0.855826433	Medium Risk	High	High	TRUE	High	High	TRUE
203	10.76	0.012331864	0.990160845	Medium Risk	High	High	TRUE	High	High	TRUE
204	10.32	-0.181689467	0.855826433	Medium Risk	High	High	TRUE	High	High	TRUE
205	10.75	-0.181689467	0.855826433	Medium Risk	High	High	TRUE	High	High	TRUE
206	10.62	-0.472721463	0.636411912	Low Risk	High	High	TRUE	Medium	High	FALSE
207	10.45	-0.860764125	0.389367968	Low Risk	High	High	TRUE	Medium	High	FALSE
208	10.58	-0.860764125	0.389367968	Low Risk	High	High	TRUE	Medium	High	FALSE
209	10.63	-0.666742794	0.504936439	Low Risk	High	High	TRUE	Medium	High	FALSE
210	10.41	-0.084678801	0.93251675	Medium Risk	High	High	TRUE	High	High	TRUE
211	10.53	0.885427853	0.375925916	Very High Risk	High	High	TRUE	High	High	TRUE
212	18.65	0.400374526	0.688880684	High Risk	Low	Medium	FALSE	Low	Medium	FALSE
213	15.56	-0.472721463	0.636411912	Low Risk	Low	High	FALSE	Low	High	FALSE
214	19.96	-0.278700132	0.780474961	Medium Risk	Low	Low	TRUE	Low	High	FALSE
215	10.93	-0.278700132	0.780474961	Medium Risk	High	High	TRUE	High	High	TRUE
216	14.19	-0.472721463	0.636411912	Low Risk	Low	High	FALSE	Low	High	FALSE
217	12.87	-0.569732128	0.568859396	Low Risk	Low	High	FALSE	Low	High	FALSE
218	11.56	0.012331864	0.990160845	Medium Risk	High	High	TRUE	High	High	TRUE
219	12.74	1.37048118	0.170536746	Very High Risk	Low	High	FALSE	Medium	High	FALSE
220	27.73	1.079449184	0.280387536	Very High Risk	Low	Low	TRUE	Medium	High	FALSE
221	11.59	1.37048118	0.170536746	Very High Risk	High	High	TRUE	High	High	TRUE
222	9.91	1.079449184	0.280387536	Very High Risk	High	High	TRUE	High	High	TRUE
223	9.88	0.885427853	0.375925916	Very High Risk	High	High	TRUE	High	High	TRUE
224	11.39	0.497385191	0.618917446	High Risk	High	High	TRUE	High	High	TRUE
225	10.5	-0.181689467	0.855826433	Medium Risk	High	High	TRUE	High	High	TRUE
226	12.24	-0.472721463	0.636411912	Low Risk	Medium	High	FALSE	Low	High	FALSE
227	10.09	-0.472721463	0.636411912	Low Risk	High	High	TRUE	Medium	High	FALSE
228	10.28	-0.084678801	0.93251675	Medium Risk	High	High	TRUE	High	High	TRUE
229	10.29	-0.181689467	0.855826433	Medium Risk	High	High	TRUE	High	High	TRUE
230	10.9	-0.181689467	0.855826433	Medium Risk	High	High	TRUE	High	High	TRUE
231	10.31	0.400374526	0.688880684	High Risk	High	High	TRUE	High	High	TRUE
232	10.26	0.10934253	0.912930815	Medium Risk	High	High	TRUE	High	High	TRUE

Continuation of Table D.1

Span	Clearance	Risk of Wildfire			Vulnerability			Criticality		
		z-score	p-value	Wildfire	Enhanced Berredo Vulnerability	Berredo Vulnerability	Vulnerability Correlation	Enhanced Berredo Criticality	Berredo Criticality	Criticality Correlation
233	10.55	-0.472721463	0.636411912	Low Risk	High	High	TRUE	Medium	High	FALSE
234	10.58	-0.375710797	0.70713191	Low Risk	High	High	TRUE	Medium	High	FALSE
235	10.27	-0.084678801	0.93251675	Medium Risk	High	High	TRUE	High	High	TRUE
236	10.48	-0.278700132	0.780474961	Medium Risk	High	High	TRUE	High	High	TRUE
237	10.6	-0.084678801	0.93251675	Medium Risk	High	High	TRUE	High	High	TRUE
238	10.3	0.691406522	0.489310107	Very High Risk	High	High	TRUE	High	High	TRUE
239	10.3	0.885427853	0.375925916	Very High Risk	High	High	TRUE	High	High	TRUE
240	10.24	1.37048118	0.170536746	Very High Risk	High	High	TRUE	High	High	TRUE
241	10.66	1.273470515	0.202851129	Very High Risk	High	High	TRUE	High	High	TRUE
242	10.46	-0.278700132	0.780474961	Medium Risk	High	High	TRUE	High	High	TRUE
243	10.25	-0.472721463	0.636411912	Low Risk	High	High	TRUE	Medium	High	FALSE
244	10.43	-0.278700132	0.780474961	Medium Risk	High	High	TRUE	High	High	TRUE
245	10.28	-0.375710797	0.70713191	Low Risk	High	High	TRUE	Medium	High	FALSE
246	10.36	-0.375710797	0.70713191	Low Risk	High	High	TRUE	Medium	High	FALSE
247	10.36	-0.181689467	0.855826433	Medium Risk	High	High	TRUE	High	High	TRUE
248	12.28	-0.181689467	0.855826433	Medium Risk	Medium	High	FALSE	Medium	High	FALSE
249	10.28	-0.472721463	0.636411912	Low Risk	High	High	TRUE	Medium	High	FALSE
250	10.22	-0.472721463	0.636411912	Low Risk	High	High	TRUE	Medium	High	FALSE
251	10.18	-0.278700132	0.780474961	Medium Risk	High	High	TRUE	High	High	TRUE
252	10.23	0.10934253	0.912930815	Medium Risk	High	High	TRUE	High	High	TRUE
253	10.23	0.206353195	0.836515029	High Risk	High	High	TRUE	High	High	TRUE
254	10.26	-0.084678801	0.93251675	Medium Risk	High	High	TRUE	High	High	TRUE
255	10.27	-0.569732128	0.568859396	Low Risk	High	High	TRUE	Medium	High	FALSE
256	10.25	-0.569732128	0.568859396	Low Risk	High	High	TRUE	Medium	High	FALSE
257	10.31	-0.763753459	0.445014177	Low Risk	High	High	TRUE	Medium	High	FALSE
258	10.22	-0.666742794	0.504936439	Low Risk	High	High	TRUE	Medium	High	FALSE
259	10.43	-0.472721463	0.636411912	Low Risk	High	High	TRUE	Medium	High	FALSE
260	10.96	0.012331864	0.990160845	Medium Risk	High	High	TRUE	High	High	TRUE
261	10.38	0.303363861	0.761612584	High Risk	High	High	TRUE	High	High	TRUE
262	10.17	0.10934253	0.912930815	Medium Risk	High	High	TRUE	High	High	TRUE
263	10.29	-0.666742794	0.504936439	Low Risk	High	High	TRUE	Medium	High	FALSE

Continuation of Table D.1

Span	Clearance	Risk of Wildfire			Vulnerability			Criticality		
		z-score	p-value	Wildfire	Enhanced Berredo Vulnerability	Berredo Vulnerability	Vulnerability Correlation	Enhanced Berredo Criticality	Berredo Criticality	Criticality Correlation
264	10.29	-0.666742794	0.504936439	Low Risk	High	High	TRUE	Medium	High	FALSE
265	10.33	-0.666742794	0.504936439	Low Risk	High	High	TRUE	Medium	High	FALSE
266	10.28	-0.860764125	0.389367968	Low Risk	High	High	TRUE	Medium	High	FALSE
267	10.27	-0.084678801	0.93251675	Medium Risk	High	High	TRUE	High	High	TRUE
268	12.17	0.982438518	0.325883858	Very High Risk	Medium	High	FALSE	High	High	TRUE
269	10.77	0.982438518	0.325883858	Very High Risk	High	High	TRUE	High	High	TRUE
270	9.64	0.788417188	0.430452721	Very High Risk	High	High	TRUE	High	High	TRUE
271	10.34	0.303363861	0.761612584	High Risk	High	High	TRUE	High	High	TRUE
272	10.78	-0.278700132	0.780474961	Medium Risk	High	High	TRUE	High	High	TRUE
273	10.57	-0.472721463	0.636411912	Low Risk	High	High	TRUE	Medium	High	FALSE
274	10.17	-0.666742794	0.504936439	Low Risk	High	High	TRUE	Medium	High	FALSE
275	10.92	-0.763753459	0.445014177	Low Risk	High	High	TRUE	Medium	High	FALSE
276	17.46	-0.860764125	0.389367968	Low Risk	Low	Medium	FALSE	Low	High	FALSE
277	24.53	-0.763753459	0.445014177	Low Risk	Low	High	FALSE	Low	High	FALSE
278	17.26	-0.472721463	0.636411912	Low Risk	Low	High	FALSE	Low	High	FALSE
279	10.33	-0.181689467	0.855826433	Medium Risk	High	High	TRUE	High	High	TRUE
280	10.38	-0.569732128	0.568859396	Low Risk	High	High	TRUE	Medium	High	FALSE
281	10.32	-0.569732128	0.568859396	Low Risk	High	High	TRUE	Medium	High	FALSE
282	11.71	-0.181689467	0.855826433	Medium Risk	Medium	High	FALSE	Medium	High	FALSE
283	12.38	-0.278700132	0.780474961	Medium Risk	Medium	High	FALSE	Medium	High	FALSE
284	13.52	-1.054785455	0.291523458	Low Risk	Low	High	FALSE	Low	High	FALSE
285	10.34	-1.151796121	0.249404862	Low Risk	High	High	TRUE	Medium	High	FALSE
286	10.2	-1.151796121	0.249404862	Low Risk	High	High	TRUE	Medium	High	FALSE
287	10.52	-1.151796121	0.249404862	Low Risk	High	High	TRUE	Medium	High	FALSE
288	16.18	-0.666742794	0.504936439	Low Risk	Low	Medium	FALSE	Low	High	FALSE
289	15.56	-0.181689467	0.855826433	Medium Risk	Low	Medium	FALSE	Low	High	FALSE
290	9.7	-0.569732128	0.568859396	Low Risk	High	High	TRUE	Medium	High	FALSE
291	16.32	-0.95777479	0.338176334	Low Risk	Low	Medium	FALSE	Low	High	FALSE
292	12.45	-0.860764125	0.389367968	Low Risk	Medium	High	FALSE	Low	High	FALSE
293	10.42	-0.860764125	0.389367968	Low Risk	High	High	TRUE	Medium	High	FALSE
294	10.5	-0.472721463	0.636411912	Low Risk	High	High	TRUE	Medium	High	FALSE

Continuation of Table D.1										
Span	Clearance	Risk of Wildfire			Vulnerability			Criticality		
		z-score	p-value	Wildfire	Enhanced Berredo Vulnerability	Berredo Vulnerability	Vulnerability Correlation	Enhanced Berredo Criticality	Berredo Criticality	Criticality Correlation
295	10.45	0.10934253	0.912930815	Medium Risk	High	High	TRUE	High	High	TRUE
296	10.52	0.10934253	0.912930815	Medium Risk	High	High	TRUE	High	High	TRUE
297	12.42	-0.278700132	0.780474961	Medium Risk	Medium	High	FALSE	Medium	High	FALSE
298	10.26	-0.472721463	0.636411912	Low Risk	High	High	TRUE	Medium	High	FALSE
299	10.24	0.303363861	0.761612584	High Risk	High	High	TRUE	High	High	TRUE
300	10.41	0.594395857	0.552247379	High Risk	High	High	TRUE	High	High	TRUE
301	10.8	0.497385191	0.618917446	High Risk	High	High	TRUE	High	High	TRUE
302	13.52	1.079449184	0.280387536	Very High Risk	Low	High	FALSE	Medium	High	FALSE
303	10.36	0.594395857	0.552247379	High Risk	High	High	TRUE	High	High	TRUE
304	10.46	-0.181689467	0.855826433	Medium Risk	High	High	TRUE	High	High	TRUE
305	14.47	-0.860764125	0.389367968	Low Risk	Low	Medium	FALSE	Low	High	FALSE
306	10.41	-1.151796121	0.249404862	Low Risk	High	High	TRUE	Medium	High	FALSE
307	10.5	-0.95777479	0.338176334	Low Risk	High	High	TRUE	Medium	High	FALSE
308	12.25	0.012331864	0.990160845	Medium Risk	Medium	High	FALSE	Medium	High	FALSE
309	10.83	0.303363861	0.761612584	High Risk	High	High	TRUE	High	High	TRUE
310	15.24	-0.181689467	0.855826433	Medium Risk	Low	Medium	FALSE	Low	High	FALSE
311	14.17	-0.084678801	0.93251675	Medium Risk	Low	Medium	FALSE	Low	High	FALSE
312	12.13	-0.569732128	0.568859396	Low Risk	Medium	Medium	TRUE	Low	High	FALSE
313	9.02	-0.472721463	0.636411912	Low Risk	High	High	TRUE	Medium	High	FALSE
314	10.22	-0.472721463	0.636411912	Low Risk	High	High	TRUE	Medium	High	FALSE
315	10.44	-0.860764125	0.389367968	Low Risk	High	High	TRUE	Medium	High	FALSE
316	10.86	-0.860764125	0.389367968	Low Risk	High	High	TRUE	Medium	High	FALSE
317	10.49	0.10934253	0.912930815	Medium Risk	High	High	TRUE	High	High	TRUE
318	10.45	-0.278700132	0.780474961	Medium Risk	High	High	TRUE	High	High	TRUE
319	10.23	-1.248806786	0.211735751	Low Risk	High	High	TRUE	Medium	High	FALSE
320	10.37	-1.248806786	0.211735751	Low Risk	High	High	TRUE	Medium	High	FALSE
321	10.29	-1.248806786	0.211735751	Low Risk	High	High	TRUE	Medium	High	FALSE
322	10.35	-1.248806786	0.211735751	Low Risk	High	High	TRUE	Medium	High	FALSE
323	10.38	-1.248806786	0.211735751	Low Risk	High	High	TRUE	Medium	High	FALSE
324	10.28	-1.151796121	0.249404862	Low Risk	High	High	TRUE	Medium	High	FALSE
325	10.42	-1.054785455	0.291523458	Low Risk	High	High	TRUE	Medium	Medium	TRUE

Continuation of Table D.1										
Span	Clearance	Risk of Wildfire			Vulnerability			Criticality		
		z-score	p-value	Wildfire	Enhanced Berredo Vulnerability	Berredo Vulnerability	Vulnerability Correlation	Enhanced Berredo Criticality	Berredo Criticality	Criticality Correlation
326	15.24	-1.054785455	0.291523458	Low Risk	Low	Low	TRUE	Low	Medium	FALSE
327	13.31	-1.151796121	0.249404862	Low Risk	Low	Medium	FALSE	Low	Medium	FALSE
328	12.16	-0.763753459	0.445014177	Low Risk	Medium	Medium	TRUE	Low	Medium	FALSE
329	22.48	-0.278700132	0.780474961	Medium Risk	Low	Low	TRUE	Low	Medium	FALSE
330	15.68	0.10934253	0.912930815	Medium Risk	Low	Medium	FALSE	Low	Medium	FALSE
331	20.21	-0.375710797	0.70713191	Low Risk	Low	Low	TRUE	Low	Medium	FALSE
332	14.05	-0.95777479	0.338176334	Low Risk	Low	Medium	FALSE	Low	Medium	FALSE
333	11.36	-0.763753459	0.445014177	Low Risk	High	High	TRUE	Medium	Medium	TRUE
334	10.12	-0.95777479	0.338176334	Low Risk	High	High	TRUE	Medium	Medium	TRUE
335	10.46	-1.248806786	0.211735751	Low Risk	High	High	TRUE	Medium	Medium	TRUE
336	10.52	-1.054785455	0.291523458	Low Risk	High	High	TRUE	Medium	Medium	TRUE
337	10.47	-0.181689467	0.855826433	Medium Risk	High	High	TRUE	High	Medium	FALSE
338	10.5	0.206353195	0.836515029	High Risk	High	High	TRUE	High	Medium	FALSE
339	10.5	0.206353195	0.836515029	High Risk	High	High	TRUE	High	Medium	FALSE
340	10.1	-0.278700132	0.780474961	Medium Risk	High	High	TRUE	High	Medium	FALSE
341	10.24	-0.763753459	0.445014177	Low Risk	High	High	TRUE	Medium	Medium	TRUE
342	10.42	-0.666742794	0.504936439	Low Risk	High	High	TRUE	Medium	Medium	TRUE
343	10.21	-0.569732128	0.568859396	Low Risk	High	High	TRUE	Medium	Medium	TRUE
344	10.3	-0.666742794	0.504936439	Low Risk	High	High	TRUE	Medium	High	FALSE
345	10.4	-0.278700132	0.780474961	Medium Risk	High	High	TRUE	High	Medium	FALSE
346	10.58	-0.375710797	0.70713191	Low Risk	High	High	TRUE	Medium	Medium	TRUE
347	10.47	-0.278700132	0.780474961	Medium Risk	High	High	TRUE	High	High	TRUE
348	10.3	0.012331864	0.990160845	Medium Risk	High	High	TRUE	High	High	TRUE
349	17.75	-0.375710797	0.70713191	Low Risk	Low	Low	TRUE	Low	High	FALSE
350	10.71	-0.763753459	0.445014177	Low Risk	High	High	TRUE	Medium	High	FALSE
351	11.62	-0.763753459	0.445014177	Low Risk	High	High	TRUE	Medium	High	FALSE
352	10.1	-0.666742794	0.504936439	Low Risk	High	High	TRUE	Medium	Medium	TRUE
353	10.36	-0.95777479	0.338176334	Low Risk	High	High	TRUE	Medium	Medium	TRUE
354	10.4	-0.95777479	0.338176334	Low Risk	High	High	TRUE	Medium	Medium	TRUE
355	9.96	-0.375710797	0.70713191	Low Risk	High	High	TRUE	Medium	Medium	TRUE
356	11.46	0.982438518	0.325883858	Very High Risk	High	High	TRUE	High	Medium	FALSE

Continuation of Table D.1

Span	Clearance	Risk of Wildfire			Vulnerability			Criticality		
		z-score	p-value	Wildfire	Enhanced Berredo Vulnerability	Berredo Vulnerability	Vulnerability Correlation	Enhanced Berredo Criticality	Berredo Criticality	Criticality Correlation
357	10.09	1.564502511	0.117699604	Very High Risk	High	High	TRUE	High	Medium	FALSE
358	10.22	1.176459849	0.239411168	Very High Risk	High	High	TRUE	High	Medium	FALSE
359	10.35	1.079449184	0.280387536	Very High Risk	High	High	TRUE	High	Medium	FALSE
360	10.32	1.564502511	0.117699604	Very High Risk	High	High	TRUE	High	Medium	FALSE
361	9.86	1.37048118	0.170536746	Very High Risk	High	High	TRUE	High	Medium	FALSE
362	10.28	0.982438518	0.325883858	Very High Risk	High	High	TRUE	High	Medium	FALSE
363	10.46	1.564502511	0.117699604	Very High Risk	High	High	TRUE	High	Medium	FALSE
364	9.9	1.079449184	0.280387536	Very High Risk	High	High	TRUE	High	Medium	FALSE
365	10.01	0.594395857	0.552247379	High Risk	High	High	TRUE	High	Medium	FALSE
366	11.65	1.273470515	0.202851129	Very High Risk	High	High	TRUE	High	Medium	FALSE
367	18.26	2.4375985	0.014785186	Very High Risk	Low	Low	TRUE	Medium	Medium	TRUE
368	20.56	3.989769146	6.61E-05	Very High Risk	Low	Low	TRUE	Medium	Medium	TRUE
369	13.14	2.825641161	0.004718609	Very High Risk	Low	Medium	FALSE	Medium	Medium	TRUE
370	9.71	3.989769146	6.61E-05	Very High Risk	High	High	TRUE	High	Medium	FALSE
371	10.33	1.758523842	0.078658419	Very High Risk	High	High	TRUE	High	Medium	FALSE
372	10.03	-0.666742794	0.504936439	Low Risk	High	High	TRUE	Medium	Medium	TRUE
373	17.05	-0.763753459	0.445014177	Low Risk	Low	Low	TRUE	Low	Medium	FALSE
374	10.48	-1.054785455	0.291523458	Low Risk	High	High	TRUE	Medium	Medium	TRUE
375	12.57	-1.248806786	0.211735751	Low Risk	Low	High	FALSE	Low	High	FALSE
376	13.53	-1.248806786	0.211735751	Low Risk	Low	Medium	FALSE	Low	Medium	FALSE
377	10.57	-1.248806786	0.211735751	Low Risk	High	High	TRUE	Medium	High	FALSE
378	11.6	-1.151796121	0.249404862	Low Risk	High	Medium	FALSE	Medium	High	FALSE
379	11.53	-1.248806786	0.211735751	Low Risk	High	High	TRUE	Medium	High	FALSE
380	13.63	-1.248806786	0.211735751	Low Risk	Low	Medium	FALSE	Low	High	FALSE
381	14.39	-1.248806786	0.211735751	Low Risk	Low	Medium	FALSE	Low	Medium	FALSE
382	22.07	-1.054785455	0.291523458	Low Risk	Low	Low	TRUE	Low	High	FALSE
383	10.88	-0.666742794	0.504936439	Low Risk	High	High	TRUE	Medium	Medium	TRUE
384	10.66	-0.375710797	0.70713191	Low Risk	High	High	TRUE	Medium	Medium	TRUE
385	10.32	-0.181689467	0.855826433	Medium Risk	High	High	TRUE	High	Medium	FALSE
386	11.67	-0.569732128	0.568859396	Low Risk	High	High	TRUE	Medium	Medium	TRUE
387	10.19	-0.375710797	0.70713191	Low Risk	High	High	TRUE	Medium	Medium	TRUE

Continuation of Table D.1										
Span	Clearance	Risk of Wildfire			Vulnerability			Criticality		
		z-score	p-value	Wildfire	Enhanced Berredo Vulnerability	Berredo Vulnerability	Vulnerability Correlation	Enhanced Berredo Criticality	Berredo Criticality	Criticality Correlation
388	24.9	-0.375710797	0.70713191	Low Risk	Low	Low	TRUE	Low	High	FALSE
389	9.79	-0.084678801	0.93251675	Medium Risk	High	High	TRUE	High	High	TRUE
390	18.07	-0.181689467	0.855826433	Medium Risk	Low	Low	TRUE	Low	High	FALSE
391	17.46	0.206353195	0.836515029	High Risk	Low	Low	TRUE	Low	Medium	FALSE
392	10	0.206353195	0.836515029	High Risk	High	High	TRUE	High	Medium	FALSE
393	11.4	0.303363861	0.761612584	High Risk	High	High	TRUE	High	High	TRUE
394	11.32	0.303363861	0.761612584	High Risk	High	High	TRUE	High	High	TRUE
395	10.67	0.303363861	0.761612584	High Risk	High	High	TRUE	High	High	TRUE
396	10.25	-0.084678801	0.93251675	Medium Risk	High	High	TRUE	High	High	TRUE
397	10.2	0.497385191	0.618917446	High Risk	High	High	TRUE	High	High	TRUE
398	11.01	0.206353195	0.836515029	High Risk	High	High	TRUE	High	High	TRUE
399	10.36	0.594395857	0.552247379	High Risk	High	High	TRUE	High	High	TRUE
400	10.15	0.885427853	0.375925916	Very High Risk	High	High	TRUE	High	High	TRUE
401	11.35	-0.084678801	0.93251675	Medium Risk	High	High	TRUE	High	High	TRUE
402	11.48	-0.569732128	0.568859396	Low Risk	High	High	TRUE	Medium	High	FALSE
403	10.42	-0.666742794	0.504936439	Low Risk	High	High	TRUE	Medium	High	FALSE
404	10.41	-0.666742794	0.504936439	Low Risk	High	High	TRUE	Medium	High	FALSE
405	10.68	-0.084678801	0.93251675	Medium Risk	High	High	TRUE	High	High	TRUE
406	10.79	0.206353195	0.836515029	High Risk	High	High	TRUE	High	High	TRUE
407	10.15	0.10934253	0.912930815	Medium Risk	High	High	TRUE	High	High	TRUE
408	10.11	0.594395857	0.552247379	High Risk	High	High	TRUE	High	High	TRUE
409	12.05	1.467491845	0.142242306	Very High Risk	Medium	High	FALSE	High	High	TRUE
410	12.08	1.661513176	0.096610425	Very High Risk	Medium	High	FALSE	High	High	TRUE
411	14.27	1.176459849	0.239411168	Very High Risk	Low	High	FALSE	Medium	High	FALSE
412	12.32	0.594395857	0.552247379	High Risk	Medium	High	FALSE	Medium	High	FALSE
413	10.28	0.303363861	0.761612584	High Risk	High	High	TRUE	High	High	TRUE
414	10.39	0.303363861	0.761612584	High Risk	High	High	TRUE	High	High	TRUE
415	10.35	-0.084678801	0.93251675	Medium Risk	High	High	TRUE	High	High	TRUE
416	10.62	-0.763753459	0.445014177	Low Risk	High	High	TRUE	Medium	High	FALSE
417	11.57	-1.054785455	0.291523458	Low Risk	High	High	TRUE	Medium	High	FALSE
418	10.38	-0.860764125	0.389367968	Low Risk	High	High	TRUE	Medium	High	FALSE

Continuation of Table D.1

Span	Clearance	Risk of Wildfire			Vulnerability			Criticality		
		z-score	p-value	Wildfire	Enhanced Berredo Vulnerability	Berredo Vulnerability	Vulnerability Correlation	Enhanced Berredo Criticality	Berredo Criticality	Criticality Correlation
419	11.26	0.303363861	0.761612584	High Risk	High	High	TRUE	High	High	TRUE
420	11.64	0.497385191	0.618917446	High Risk	High	High	TRUE	High	Medium	FALSE
421	10.8	-0.278700132	0.780474961	Medium Risk	High	High	TRUE	High	High	TRUE
422	10.21	0.497385191	0.618917446	High Risk	High	High	TRUE	High	High	TRUE
423	9.56	0.885427853	0.375925916	Very High Risk	High	High	TRUE	High	High	TRUE
424	16.88	0.788417188	0.430452721	Very High Risk	Low	Low	TRUE	Medium	Medium	TRUE
425	9.79	0.400374526	0.688880684	High Risk	High	High	TRUE	High	Medium	FALSE
426	10.28	-0.763753459	0.445014177	Low Risk	High	High	TRUE	Medium	High	FALSE
427	11.19	-1.151796121	0.249404862	Low Risk	High	High	TRUE	Medium	High	FALSE
428	16.92	-1.248806786	0.211735751	Low Risk	Low	Low	TRUE	Low	High	FALSE
429	13.02	-0.763753459	0.445014177	Low Risk	Low	Medium	FALSE	Low	High	FALSE
430	11.09	0.012331864	0.990160845	Medium Risk	High	High	TRUE	High	High	TRUE
431	10.22	0.400374526	0.688880684	High Risk	High	High	TRUE	High	Medium	FALSE
432	10.77	1.37048118	0.170536746	Very High Risk	High	High	TRUE	High	Medium	FALSE
433	11.29	1.952545173	0.050873513	Very High Risk	High	High	TRUE	High	Medium	FALSE

End of Table